A MODELING STUDY OF COAL PYROLYSIS

Thesis by

Paul How-Kei Cheong

In Partial Fulfillment of the Requirements

for the Degree of

Doctor of Philosophy

California Institute of Technology

Pasadena, California

1977

(Submitted September 16, 1976)

To Anna,

for your patience

and encouragement.

ACKNOWLEDGEMENTS

My deepest gratitude goes to my research advisor, Professor George Gavalas, for his guidance, inspiration and encouragement during the course of this work.

I am also thankful to my colleagues Dr. M. Oka and Ravi Jain for providing experimental data from their own work, to Hsueh Chia Chang and Richard Larson for their assistance in the computer programming, and to Sharon ViGario and Kathy Lewis for their help in typing my thesis.

This project was funded by the National Science Foundation, and personal support was provided by the California Institute of Technology in the form of graduate teaching and research assistantships. Both institutions are gratefully acknowledged.

Finally, I would like to thank my father and mother for all that they have sacrificed to make this possible.

ABSTRACT

A model of coal pyrolysis is developed with the elements of : (i) structure, (ii) chemical reactions, and (iii) transport.

(i) The chemical structure of coal is modeled as aromatic clusters bearing aliphatic side chains, bridges, and phenolic functional groups, consistent with various spectroscopic data and known chemical behavior.

(ii) A detailed scheme of thermal free radical reactions leading to the formation of tar, gases and deactivated char is postulated. State variables are defined as concentrations of the participating functional groups to describe the stoichiometry and rates of these reactions.

(iii) Macropores and transitional pores partition the coal particle into smaller subunits in which transport of tarry and gaseous products is by means of activated diffusion. The transport model postulates an active surface region of the subunits and a process of renewal of that region. A counting procedure is devised to predict the amount of aromatic fragments that escape from the subunits.

The physicochemical processes are translated into a system of ordinary differential equations in the state variables, parametrized by the initial conditions and appropriate rate parameters. Numerical simulation is performed for two case studies where the necessary parameters are deduced from available pyrolysis and structural data and from additional assumptions.

The model is applicable within the range of primary pyrolysis ($<650^{o}C$) and predicts the ultimate weight loss as well as the

distribution of products as a function of temperature and coal type. A supplementary model is also formulated for the reaction and transport of volatile materials in the macropores. This model takes into account the effects of the external pressure and the particle size on the evolution of products.

LIST OF FIGURES

LIST OF TABLES

NOMENCLATURE

Symbols and constants that are defined and used locally are not included here.

a	ratio of H_α to H_β or pore radius (cm.)
A_i	amount of gas species i generated (moles i/ℓ-original bulk phase)
A_j	Arrhenius factors for reaction j (ℓ-mole/sec or sec^{-1})
b	ratio of H_{ar} to H_{al}
b_1	concentration of methylene bridges (moles/ℓ bulk phase)
b_2	concentration of ethylene bridges (moles/ℓ bulk phase)
b_3	concentration of longer bridges (moles/ℓ bulk phase)
$b_{2\cdot}$	concentration of ethylene bridge radicals (moles/ℓ bulk phase)
$b_{3\cdot}$	concentration of longer bridge radicals (moles/ℓ bulk phase)
$b_{2=}$	concentration of $\Phi\dot{C}=\dot{C}\Phi'$ bridges (moles/ℓ bulk phase)
$b_{3=}$	concentration of $\Phi\dot{C}=R\dot{C}\Phi'$ bridges (moles/ℓ bulk phase)
b_0	concentration of phenyl type bridges (moles/ℓ bulk phase)
c_1	concentration of methyl chains (moles/ℓ bulk phase)
c_2	concentration of longer alkyl chains (moles/ℓ bulk phase)
$c_{1=}$	concentration of $\Phi\dot{C}=CH_2$ groups (moles/ℓ bulk phase)
$c_{2=}$	concentration of $\Phi\dot{C}=R$ groups (moles/ℓ bulk phase)
c_{ar}	number of aromatic carbon atoms in an average cluster
C	sum of C_{ar} and C_{al}
C_1	defined in equation (VI-39)

C_2	defined in equation (VI-39)
C_{al}	concentration of aliphatic carbon atoms (moles/ℓ bulk phase)
C_{ar}	concentration of aromatic carbon atoms (moles/ℓ bulk phase)
C_{α}	concentration of α-carbon atoms (moles/ℓ bulk phase)
C_{β}	concentration of β-carbon atoms (moles/ℓ bulk phase)
D_1	diffusivity of tarry materials in the macropores (cm^2/sec)
$D_{1,e}$	effective diffusivity of tarry materials in the coal particle (cm^2/sec)
D_2	diffusivity of gaseous products in the macropores (cm^2/sec)
f_1	probability that a singly bonded α-carbon substituent is not next to a double bond
f_2	probability that an α hydrogen atom is not next to a bridge
f_3	probability that an α-carbon substituent is a hydrogen atom
f_a	aromaticity
g_1	corrective factor for the gel effect in hydrogen abstraction reactions
g_2	corrective factor for the gel effect in recombination reactions
h_{aru}	number of peripheral sites in an average cluster
H	concentration of hydrogen atoms (moles/ℓ bulk phase)
H_{al}	concentration of aliphatic hydrogen atoms (moles/ℓ bulk phase)
H_{ar}	concentration of aromatic hydrogen atoms (moles/ℓ bulk phase)
H_{α}	concentration of α hydrogen atoms (moles/ℓ bulk phase)
H_{β}	concentration of β hydrogen atoms (moles/ℓ bulk phase)
k	rate constants (ℓ bulk phase-$mole^{-1}sec^{-1}$ or sec^{-1})

ℓ	number of β-carbons in the species c_2 and b_3
m	defined in equation (VI-39)
M	the total concentrations of bridges (moles/ℓ bulk phase)
n	amount of gaseous produce generated (moles/ℓ of original bulk phase) or in Chapter VI, molar flux normal to the coal particle (moles-$cm^{-2}sec^{-1}$)
N_c	concentration of aromatic clusters (moles/ℓ bulk phase)
N_{CH_3}	concentration of CH_3 groups on a peripheral site (moles/ℓ bulk phase)
p	pressure (atm)
P_1	probability that a fragment containing exactly one cluster is released when a connection is broken
P_2	probability that a fragment containing exactly two clusters is released when a connection is broken
r	radial position in a spherical coal particle (cm)
r_b	rate of breaking of the bridges in region I (moles/ℓ of region I-sec)$^{-1}$
R	gas constant (ℓ-atm $mole^{-1}$ $^oK^{-1}$)
R_p	coal particle radius (cm)
s_1	parameter associated with g_1 (Kcal/mole)
s_2	parameter associated with g_2 (Kcal/mole)
S	concentration of peripheral sites (moles/ℓ bulk phase)
t	time (sec)
T	temperature (^oC) or (^oK)
V_I	fractional volume of region I

V_{II} fractional volume of region II

x atomic ratio of H_α to C_α

y atomic ratio of H_β to C_β

y_1 mole fraction of tar in the macropores

y_2 mole fraction of gases in the macropores

y_3 mole fraction of inert component in the macropores

z atomic H/C ratio

Greek Symbols

$\alpha\cdot$ concentration of α radicals (moles/ℓ bulk phase)

$\beta_1\cdot$ concentration of $\Phi CCH_2\cdot$ groups (moles/ℓ bulk phase)

$\beta_2\cdot$ concentration of $\Phi CR\cdot$ groups (moles/ℓ bulk phase)

γ_1 net local rate of generation of tar (moles $cm^{-3}sec^{-1}$)

γ_2 local rate of generation of gases (moles $cm^{-3}sec^{-1}$)

γ_f forward local rate of generation of tar (moles $cm^{-3}sec^{-1}$)

γ_b backward local rate of generation of tar (moles $cm^{-3}sec^{-1}$)

Γ_b backward overall rate of generation of tar (moles $cm^{-3}sec^{-1}$)

δ tortuosity factor

δ_{cage} corrective factor for the cage effect

ε_M porosity of macropores

η viscosity (centipoise)

κ permeability ($gm\text{-}cm\text{-}sec^{-2}atm^{-1}$)

λ average number of species i carried by one cluster

μ probability a connection is destroyed when a bridge breaks

ν_{ij} stoichiometric coefficients

ρ	density (gm/cm^3 particles)
ω_1	first-order rate constant for backward deposition of aromatic fragments in the gas phase ($mole\text{-}cm^{-3}sec^{-1}atm^{-1}$)
ω_2	second-order rate constant for backward deposition of aromatic fragments in the gas phase ($mole\text{-}cm^{-3}sec^{-1}atm^{-2}$)
Ω_1	rate of transport of clusters from region I to the gas phase (moles/ℓ region I-sec)
Ω_2	rate of transport of clusters from region II to region I (moles/ℓ region II-sec)

Subscripts

o	denotes a situation where the cage or gel effect is inapplicable,(in Chapter VI) denotes evaluation at the particle boundary $r=R_p$
I	denotes region I
II	denotes region II
e	effective
eff	effective
i	refers to species
j	refers to reactions

TABLE OF CONTENTS

I INTRODUCTION

It appears to be common knowledge today that petroleum and natural gas reserves have no longer kept pace with the ever-expanding energy demand in this nation, and that it will be well into the next century before nuclear power and solar energy can be expected to bridge the gap, the result being an urgent need to rely heavily on coal as a major source of energy. Indeed, as an organic fossil composed mainly of carbon and hydrogen, coal is a commodity of vast usage potential, not only in terms of its calorific value, but also for a myriad of useful chemicals that can be derived from it.

Traditionally, coal has failed to compete well with petroleum and natural gas in the energy market solely for the economic factor of process and transportation cost. The technology to produce gaseous and liquid fuels and raw materials from coal existed decades ago, but nearly all commercial operations were closed down during the post-war period when large reserves of petroleum and natural gas were then available. The recent surge in oil and gas prices has stimulated a thriving interest in both governmental and industrial sectors to develop cheaper, cleaner ways of coal utilization. Dozens of gasification and liquefaction projects are already in the pilot plant stage, and many are claiming full commercialization by 1980.

The optimal design and implementation of any elaborate process would require the understanding, in the finest possible detail, of its crude materials and products. The need to develop efficient coal utilization as quickly as possible has prompted greatly accelerated basic research in the area of coal science, with efforts chiefly divided between two general

categories: those related respectively to structure and reactivity.

Coal, unlike most other common chemical substances, is a carbonaceous material of quite varying chemical composition depending on where it is mined, its principal elements being carbon, hydrogen, oxygen, and sulfur. As is described in the next section, substantial progress has now been achieved toward understanding the chemical constitution of these elements, for example, the identification of the major organic functional groups. In parallel, much information has also been collected, rather independently, on the behavior of coal under various conditions of treatment, notably, those of pyrolysis and hydrogenation at different temperatures and pressures.

Unfortunately there is, in the author's opinion, a lack of interrelation between the two disciplines. The direct relationship between structure and reactivity, obvious as it must be, has been given much less attention than is really justified. For example, in studies of the thermal behavior of coal, little of the bulk of information available on its structure has been invoked to explain observed phenomena, and worse is the case with hydrogenation. It appears imperative, for a full understanding of the chemistry of coal utilization, that a unifying approach be synthesized and efficient interrelation between structure and reactivity be established.

This work is an attempt in this direction. We focus on the thermal behavior of coal for three main reasons:

1. All known processes of coal conversion involve the application of heat to some extent so that pyrolysis is always an integral part.
2. It is desirable to start with the simplest reaction system,

consisting of coal and nothing else.

3. Among current coal conversion processes,(for example, that used by the Occidental Petroleum Company,)some are exclusively pyrolysis of the coal to produce lighter molecular weight products.

When coal is heated to above a certain temperature, usually between 400^{o} C and 500^{o} C, chemical reactions occur producing various amounts of gases, tar, and coke. The tar and gases are usually referred to as volatiles, although some tar portions may be of molecular weight well over 1000. The relative amounts of these products and their kinetics of evolution all depend on a large number of factors, such as the type of coal, the temperature-time history, the particle size and the total pressure. The complexity of the system has discouraged any rigorous theoretical treatment of the pyrolysis mechanism based on coal structure and fundamental processes. Thus, among previous studies, that of Chermin and Van Krevelen (Chermin, 1957) suggests the following model of three consecutive reactions:

$$\text{I} \qquad \text{Coal} \xrightarrow{k_1} \text{Metaplast}$$

$$\text{II} \qquad \text{Metaplast} \xrightarrow{k_2} \text{Semi-coke} + \text{Primary gas}$$

$$\text{III} \qquad \text{Semi-coke} \xrightarrow{k_3} \text{Coke} + \text{Secondary gas}$$

This relatively simple model, with the flexibility of three rate constants, is used to describe, at least semiquantitatively, the kinetics of weight loss of the coal. But it clearly does not relate these

reactions to the structure of the coal or to any other fundamental chemical processes. The rate constants k_1, k_2, and k_3 must be changed with each different coal and temperature considered.

Among more recent models, that of Anthony, et al. (Anthony, 1974) describes the weight loss by a set of parallel first-order reactions with a normal distribution of activation energies parametrized by its mean and variance. The escape of volatiles is controlled by a backward rate constant and an overall mass transfer coefficient. This model takes into account the effect of pressure (via the diffusion coefficient) in reducing the amount of volatiles evolved and satisfactorily describes the weight loss versus time curves. Again, little reference is made to coal structure or to any actual chemical processes.

In this study we seek a realistic model for pyrolysis that would effectively utilize and combine what we already know about coal structure and its thermal behavior in the framework of organic chemistry and taking into account the principles of transport processes. Based on this information, we propose a physicochemical mechanism for the actual chemical reactions and transport processes that occur within the coal particle during pyrolysis. Mathematical expressions are then formulated to describe these fundamental chemical and physical rate processes. Our ultimate goal is to describe and predict practically important aspects of pyrolysis such as the dependence of product distribution on controllable factors such as the heating rate and the type of coal used.

II BACKGROUND INFORMATION ON COAL STRUCTURE

Chemical Structure

Scope

A fundamental study of the complex processes that occur in coal pyrolysis requires much more information on coal structure than can be obtained from our present state of knowledge. It is a difficult task, if not an impossible one, to reconcile the numerous conflicting conclusions of the most prominent investigators. No attempt is made here to furnish a review of the vast body of literature on this subject, for many good ones are already available (I. G. C. Dryden, 1963). Rather, the generally accepted facts about coal structure are synthesized into a conceptual model for the coal molecule. The model possesses specific properties that are directly related to the coal's reactivity. These properties, when properly parametrized, introduce a realistic system under which coals can be chemically characterized. The molecular model will be the basis of this entire work.

A Molecular Model

It is widely known that coal contains aromatic rings with aliphatic and oxygen substituent groups attached. The size of these ring systems has not been fully established but is believed to range from between two and four rings in lower rank coals up to bituminous, to more than twelve in anthracite (Hirsch, 1958). The major types of substituent groups have been elucidated, to a large extent, by various spectroscopic techniques either directly on coal or on its mild degradation products.

Infrared analysis on solid coal (Brown, 1955) shows that olefinic double bonds and acetylinic triple bonds are both absent. The aliphatic portion of coal structure appears to be mainly saturated. The distribution of oxygen varies greatly among coals of different ranks. The consensus is that most of the oxygen in coal is in the form of carbonyl, hydroxyl (mostly phenolic), and carboxyl groups (I. G. C. Dryden, 1963). The quantitative determination of the various aliphatic and oxygen groups is an area of active research and substantial debate at this time. However, the above information is sufficient for a conceptual picture to be drawn of the structural constitution of all coals based on three major elements: carbon, hydrogen, and oxygen.

The nonaromatic portion of coal must be present in one of four forms according to its chemical bonding with respect to the aromatic rings. If it is not bonded to any aromatic ring at all, it is considered an adsorbed nonaromatic molecule and not strictly part of the coal material. Water and simple alkanes are such examples. The three other forms are side chains (branches), bridges, and nonaromatic (alicyclic) rings, respectively.

If one limits the nature of the oxygen groups (other than heterocyclic) to the three most abundant--phenolic, ketonic, and carboxyl--one can actually construct any coal molecule by the following procedure:

First, lay down the aromatic ring systems and obtain the purely aromatic portion. Proceed with the purely aliphatic substituents limited to alkyl side chains, methylene, ethylene and longer bridges, and alicyclic rings. Finally, replace some of the hydrogens by phenolic

OH, ketonic =O, and carboxylic $\overset{=O}{\underset{OH}{\diagdown}}$, respectively.

The whole process brings out a very important underlying feature of coal structure, that of a predominantly carbon skeleton. It will be seen later that the reactivity of coal is primarily associated with this carbon skeleton, which consists simply of aromatic units bearing alkyl side chains interconnected by a network of bridges. The chemical characterization of coal then translates into the description of the carbon skeleton in terms of the size range of the aromatic rings, the length and abundance of the side chains and bridges, and, very importantly, the nature of the network that joins the aromatic clusters. The notion of a coal molecule being a network of aromatic rings bearing aliphatic branches appears to be helpful in formulating the fundamental processes of pyrolysis.

The Physical Structure

Most coals are found to have significant pore volume with porosities ranging from 4 to 23% (Gan, 1972). The range of pore sizes can be roughly classified into macropores (> 300 Å), transitional pores (12 - 300 Å), and micropores (4 - 12 Å). A peculiar feature common to all coals is that a substantial fraction of the open pore volume can be attributed to pores between 4 and 12 Å. Materials with this property are known to exhibit molecular sieve behavior preferentially allowing the transport of smaller molecules. The relationship between the open pore structure of coal and transport limitation in pyrolysis is discussed in the following chapter.

III THE FUNDAMENTAL PROCESSES OF PYROLYSIS: A QUALITATIVE DESCRIPTION

Scope

In the study of the thermal behavior of coal, we attempt a detailed description of the fundamental physical and chemical processes that take place during coal pyrolysis. Chemical transformation begins with a chain of elementary free radical reactions among the substitutent functional groups of the aromatic clusters. The resulting changes in the structural configuration of the coal molecule (the network) explain the mechanism of volatile product generation. In this chapter, a list of the most significant thermal reactions is compiled, and the two essential transport processes for the products are identified. It is important, before we develop a mathematical model, that we understand the actual chemical reactions and the nature of transport processes that occur within the coal particle. This chapter is an attempt in this direction.

The Chemical Species

For all its highly complex chemical constitution, coal is an organic compound and is expected to behave chemically as such. The thermal decomposition of alkyl aromatic compounds has not been studied as extensively as that of the purely aliphatics; nevertheless, much of the chemistry is understood. Aromatic rings are very stable towards thermal treatment. It is the aliphatic and oxygen functional groups in coal that account for its reactivity during pyrolysis (especially at temperatures below 600^{o} C), and we will focus our attention on the reactions of these functional groups.

The usual notion of a chemical reaction being the transformation of one molecular species into another quickly raises the problem of identifying the molecular species in coal. A more practical and convenient system of chemical species must be employed to describe the chemical changes taking place. In this chapter, the chemical species are not identified as molecules, but instead they are substituent groups of aromatic clusters such as a methyl chain or an ethylene bridge. The general notation for a chemical species is Φ-X, where Φ- represents a peripheral site of an aromatic ring, and X is the functional group attached; for example, a methyl chain is denoted by Φ-CH_3 and an ethylene bridge by $\Phi CH_2CH_2\Phi'$. Here the basic quantity of interest is not the number of molecules but rather the number of functional groups attached to aromatic ring systems.

In the lower temperature range for which this study is designed, not all the functional groups that exist in coal will take part directly in a chemical reaction. In fact, after we examine the possible reactions, we will see that it is possible to describe the primary reactions mainly in terms of the carbon-hydrogen skeleton independent of the oxygen groups. In this case, the carbon-hydrogen skeleton translates into three classes of chemical species: alkyl chains, bridges, and alicyclic rings.

The Chemical Reactions

Our basic tool in postulating the fundamental chemical processes in coal pyrolysis is the extrapolation of available information on the thermal reactions of pure compounds bearing similar structures. Thus,

a methyl group substituted to an aromatic cluster in coal is considered to have a reactivity comparable to the methyl group in toluene. We recognize, of course, that the reactivity of a functional group must be affected by neighboring groups as well as steric constraints and even the size of the aromatic ring. The comparison, therefore, is not meant in the absolute sense but rather the relative reactivity of the functional groups is weighed with respect to each other so as to determine what the most important reactions are. We proceed to survey the reactivity of individual functional groups.

The most vulnerable functional group to react is the carboxylic acid group which readily gives up carbon dioxide at temperatures substantially below that required for the more vigorous pyrolysis reactions ($\sim 300^{o}$ C) (Fitzer, 1971). This reaction can be considered an independent reaction by itself.

Above incipient pyrolysis temperature ($> 400^{o}$ C), some breakage of the weaker bonds occurs, initiating a chain of free radical reactions. These chain reactions primarily affect the carbon-hydrogen skeleton of the coal molecule, and for this reason, we account for them separately as a set of primary reactions. This limits the number of chemical species to those groups containing only carbon and hydrogen. The oxygen functional groups, having another level of reactivity, are considered independently of the set of primary free radical reactions.

The coal molecule is made up of various types of carbon-carbon, carbon-hydrogen, carbon-oxygen, and oxygen-hydrogen bonds. Except for the hydroxyl hydrogen, every atom is bonded to at least one

carbon atom. According to functionality, there are three classes of carbons:

i) aromatic carbons which we denote by C_{ar};

ii) carbons adjacent to an aromatic ring, denoted by C_{α};

iii) the remaining carbons must be β or β^{+} carbons, denoted simply by C_{β}.

One can then enumerate the major types of chemical bonds that exist in coal:

A C_{ar}-C_{ar}, C_{ar}-C_{α}, C_{α}-C_{β}, C_{β}-C_{β}

B C_{ar}-H, C_{α}-H, C_{β}-H

C C_{ar}=O (quinonic), C_{α}=O (carbonyl), C_{β}=O (carbonyl), C_{ar}-O (phenolic)

D -O-H (phenolic)

Of the four categories, the organic chemist recognizes that the σ-carbon-carbon bonds are, in general, much weaker than those bonds in categories B, C, and D. Moreover, in considering bond strengths, the resonance contribution from an aromatic ring system has a large effect. A comparison of some carbon-carbon bond energies serves as an illustration (Benson, 1968) (Table III-1).

Table III-1. Dissociation Energies of Some σ Carbon-carbon Bonds.

Type of Bond	Example	Bond Energy (Kcal/mole)
C_{ar}-C_{α}	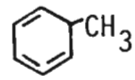	102
C_{ar}-C_{α}	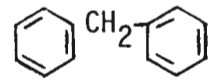	78.5
C_{α}-C_{β}	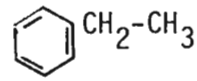	73
C_{α}-C_{β}	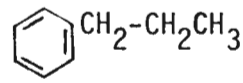	68.6
C_{α}-C_{α}	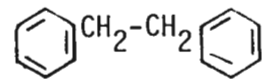	56.8

Because of resonance effects, bonds linked to an α-carbon are the most susceptible to direct fission which releases what we will call an α-radical. The set of primary reactions of coal pyrolysis can now be classified into six categories, as follows:

i) Bond Dissociation

The breakage of alkyl chains and bridges occurs at the α position producing various radicals including α-radicals, β-radicals, free alkyl radicals and phenyl-type radicals. Typical examples are:

1. $\Phi CH_2CH_3 \longrightarrow \Phi CH_2\cdot + CH_3\cdot$

2. $\Phi CH_2CH_2\Phi' \longrightarrow \Phi CH_2\cdot + \Phi' CH_2\cdot$

3. $\Phi CH_2CH_2CH_2\Phi' \longrightarrow \Phi CH_2CH_2\cdot + \Phi'CH_2\cdot$

4. $\Phi CH_2\Phi' \longrightarrow \Phi CH_2\cdot + \Phi'\cdot$

These radicals are highly reactive species which will take part in further reactions, notably:

ii) Hydrogen Abstraction

Alkyl radicals such as $CH_3\cdot$, β-radicals such as $\Phi CH_2CH_2\cdot$, and phenyl-type radicals $\Phi\cdot$ can rapidly participate in a series of hydrogen abstractions from a neighboring hydrogen-rich environment. In contrast, α-radicals such as $\Phi CH_2\cdot$ are resonance stabilized and will hardly abstract any β or aromatic hydrogen. Because hydrogen exchanges are generally very fast compared to the other reactions, this virtually creates a thermodynamically controlled situation in which the amount of α-radicals will become very large compared to the β or alkyl radicals. Some new radical species are generated through these hydrogen exchanges. These include ethylene and longer bridge radicals such as $\Phi CH_2\dot{C}H\Phi'$ and $\Phi CH_2CH_2\dot{C}H\Phi'$.

iii) β-scission of Longer Chain and Bridge Radicals

When a radical position occurs on a longer chain or bridge, the β-scission is a common reaction resulting in a shorter chain radical and a double bond. For example,

$$\Phi CH_2CH_2CH_2\cdot \longrightarrow \Phi CH_2\cdot + C_2H_4$$

$$\Phi CH_2CH_2\dot{C}H\Phi' \longrightarrow \Phi CH_2\cdot + \Phi'CH{=}CH_2$$

iv) Hydrogen Elimination

Radicals are capable of eliminating a hydrogen atom to form a

double bond. For example,

$$\Phi CH_2CH_2\cdot \longrightarrow \Phi CH{=}CH_2 + H\cdot$$

$$\Phi CH_2\dot{C}H\Phi' \longrightarrow \Phi CH{=}CH\Phi' + H\cdot$$

$$\Phi CH_2CH_2\dot{C}H\Phi' \longrightarrow \Phi CH_2CH{=}CH\Phi' + H\cdot$$

v) Addition

As double bonds are generated by β-scission or hydrogen elimination, they are vulnerable for attack by surrounding free radicals. For example,

$$CH_3\cdot + \Phi CH{=}CH_2 \longrightarrow \Phi\dot{C}HCH_2CH_3$$

vi) Recombination

Because of the vast difference in reactivity between α-radicals and the others, hydrogen exchanges create a much higher concentration of the α-radicals, so that the most important radical recombination reaction by far is that between two α-radicals to form an ethylene bridge.

The above categories of radical reactions are common to most organic free radicals and are believed to be the principal reactions affecting the carbon-hydrogen skeleton. The radicals are not known to attack carbonyl or phenolic groups directly. Of course, this relatively simple scheme of reactions can be considered satisfactory only in the lower temperature range in which the stronger bonds remain intact and 700^{o} C is probably an upper limit for this range.

Generation of Products

Whereas the chemical reactions involve substituent functional groups of aromatic clusters, the observed products of pyrolysis, commonly

referred to as tar and gases, are complete molecules derived from the original coal material. The underlying mechanism of their formation hinges on the molecular configuration of coal being a network of substituted aromatic clusters. Breakage of side chains releases smaller molecules commensurate with the length of the chains themselves. For example, the reaction $\Phi CH_2CH_3 \rightarrow \Phi CH_2\cdot + CH_3\cdot$ releases a methyl radical which quickly abstracts a neighboring hydrogen and leaves as methane. The formation of tar is related to the disruption of the cluster network. When a bridge breaks, the network is cut at some point. Depending on the exact location of scission within the network, the resulting fragments may contain one, several, or many aromatic clusters. This is illustrated in Figure III-1 for a hypothetical molecule, where the circles represent aromatic clusters and the lines represent bridges joining them.

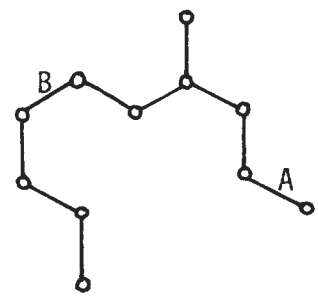

Figure III-1. A hypothetical network of aromatic clusters.

Breakage of a bridge at position A releases an aromatic fragment that contains only one cluster. This fragment may be considered volatile since it probably has sufficient vapor pressure to distill off at the

temperature of pyrolysis. A much heavier molecule resembling the original structure is also obtained which, having a high molecular weight, must remain in the char residue. If a bridge is broken at position B, however, the resulting fragments will both be too heavy to distill as tar products. Generally speaking, the disruption of side chains leads to light hydrocarbon gases, and the breaking of bridges in favorable configurations causes the liberation of tar molecules.

The evolution of carbon oxides and water is very substantial for coals of high oxygen content such as subbituminous coals. Carbon dioxide originates from carboxylic acid groups which decompose rather easily, for example,

$$\Phi COOH \longrightarrow \Phi H + CO_2$$

The carboxylic acid groups can also condense to yield an anhydride. For example,

$$\Phi COOH + \Phi' COOH \longrightarrow \Phi C(=O)OC(=O)\Phi' + H_2O$$

The primary source of carbon monoxide is most likely the carbonyl groups. A possible decarbonylation mechanism is:

$$\Phi COCH_2\cdot \longrightarrow \Phi CH_2\cdot + CO$$

the reactant radical being first formed by hydrogen abstraction. As for the phenolic groups which are relatively stable, some condensation may still occur at higher temperature.

$$\Phi OH + \Phi' OH \longrightarrow \Phi O\Phi' + H_2O$$

or $$\Phi OH + \Phi' H \longrightarrow \Phi\text{-}\Phi' + H_2O$$

These reactions are considered to be the most important chemical processes that involve oxygen functional groups directly. Two features of the reactions of oxygen-containing groups are worth noticing: their progress does not affect the functional groups in the carbon-hydrogen skeleton and, except for the α-radicals produced by decarbonylation, all other products do not take part in further reactions. These two features make it possible to consider the chemistry of pyrolysis as having two independent components, the reactions among the oxygen functional groups, and the free radical reactions continuously restructuring the carbon-hydrogen skeleton.

Transport Limitations in Pyrolysis

The Subunit

The actual evolution of any volatile product in pyrolysis is limited by its transport out of the coal particle. The chemical engineer is familiar with mass transfer processes in solid-gas reactions such as those occurring in heterogeneous catalysis or solid combustion. However, there is a fundamental difference in the treatment of the transport processes in coal pyrolysis, namely, that chemical reaction is not confined to taking place on the solid surfaces. It occurs throughout the bulk phase. Nevertheless, volatile species generated in the interior of the particle can escape only by way of a series of pores that lead to the outside.

Most coals and chars possess a very wide pore size distribution, a substantial fraction of which is in the molecular range 4 to 12 Å. A very important distinction stands out between the transport processes

in these ultrafine pores and in the larger ones. When the size of the ultrafine pores closely approaches that of the transported product molecules, the diffusing species cannot be regarded as a separate phase. It is the dispersive interaction between those molecules and the pores which determines the rate of mass transport. This regime of transport, commonly referred to as activated diffusion, has been studied by Walker (Walker, 1966). In general, the rate is very slow compared to ordinary Knudsen or molecular diffusion. The rate also depends critically on the size of the diffusing molecules, so much so that microporous media demonstrate molecular sieve behavior allowing passage only of molecules below a certain kinetic diameter.

The macropores (> 300 Å) and transitional pores (> 12 Å), hereafter referred to collectively as macropores, can be thought of as a partition of the coal particle into two phases: the bulk phase and the pore phase. During pyrolysis, the macropores entail a gas phase consisting of volatile products being transported by ordinary diffusion or hydrodynamic flow. The bulk phase containing the micropores is a condensed phase where the volatile products are generated and where transport is by means of activated diffusion.

Consider now a volatile molecule generated in the interior of the coal particle. To escape outwards, it needs to undergo two transport processes in series: first, from the bulk phase to the pores and then along the pores outwards. The key point is that these processes occur in series. There are inherently two characteristic path lengths which the volatile products have to travel. The first one is characterized

by the average distance between two neighboring macropores within the bulk phase; the other is characterized by the particle radius. We can now associate with the reaction phase (bulk phase) a characteristic dimension given by the distance between neighboring macropores. This is equivalent to saying that the coal particle is partitioned into smaller units of this characteristic dimension. We shall refer to these smaller units as "subunits."

The concept of subunits has been first introduced by Nandi and Walker (Nandi, 1970). In their study of the unsteady state diffusion of methane in coal, they concluded that the characteristic time for diffusion r_o^2/D corresponds to a much smaller path length r_o than the coal particle size. They also found that the diffusion coefficient D exhibits an Arrhenious-type temperature dependence, indicating a regime of activated diffusion. As a result, they proposed that the larger pores divide the particle into smaller units, and it is the size of these smaller units, penetrated by micropores alone, that controls the activated diffusion process.

The fundamental processes of coal pyrolysis that lead to the generation of volatile products can now be enumerated based on the concept of the subunits.

i) Thermal reactions of the functional groups in the subunits, generating volatile products. This has been discussed previously.

ii) Transport of volatiles from the subunits to the macropores in parallel with the chemical reactions in i) above.

iii) Transport and reaction of the volatile materials in the macropores.

Transport in the Subunits

The size of a subunit d_s may be estimated from detailed pore size distribution data. However, a rough estimate of $d_s = 10\ d_t$ where d_t is the average diameter of the transitional pores, ($d_t \sim$ 30-50 Å) may be sufficient for our purpose. This rough estimate is supported by some microscopy studies (McCartney, 1966). Smaller gaseous molecules such as CH_4, CO_2 are able to diffuse through a distance of several hundred angstroms within the subunit, the molecular size of CO_2 being about 3.7 Å. The tarry material consisting of one or more clusters must be so severely limited in mobility that only those molecules very near the surface of the subunit can diffuse into the gas phase. The subunit, therefore, is separated into two regions: a surface region where the tar material is in direct contact with the macropores, and an internal region where the aromatic clusters are trapped in a state of continual chemical reaction during pyrolysis. A very crude estimate of the thickness of the surface region may be 10-20 Å commensurate with the size of tar molecules. The surface region, moreover, is not a stationary or stagnant layer. The escape of tar into the gas phase creates vacancies which are filled up by the movement of aromatic clusters from the internal region, or rather, the porous external region collapses on the interior, with a continuous compaction effect. This replenishment of material constitutes a renewal process which will maintain the size of the surface region.

Transport and Reactions in the Gas Phase

When the volatile molecules reach the macropores, they are subject

to further, though less severe, transport limitations. Transport is facilitated by the familiar mechanism of Knudsen or molecular diffusion in the smaller pores and by hydrodynamic forced flow in conjunction with continuous diffusion in the larger pores. If a sufficiently high pressure gradient is developed through the rapid generation of products, the hydrodynamic contribution may be the predominant one.

The volatile products originate from the breakage of side chains and bridges. A broken side chain becomes a very reactive alkyl free radical which, most likely, will abstract a hydrogen atom before it reaches the gas phase. Saturated gaseous molecules such as CH_4, H_2, CO, and CO_2 will most likely undergo no further reactions in the macropores. The aromatic free radical fragments that can get to the gas phase are those which are formed in the surface region in direct contact with the gas phase. After entering the gas phase in the macropores, these fragments, carrying free radical sites, can recombine with each other or with the free radical sites that exist in the surface region. The residence time of these volatile materials in the macropores is evidently a factor limiting the total amount of products that eventually leaves the coal particle.

An Overall View of the Pyrolysis Processes

For a long time, it has been recognized that the thermal treatment of coal involves two basic phenomena: devolatilization and carbonization. Along with the generation of the volatile tar and gas products, the remaining material becomes more carbonaceous and less reactive in nature. Unmistakably, devolatilization and carbonization occur

simultaneously and in competition with each other. This is demonstrated by the fact that the relative amounts of gas, tar, and char obtained from pyrolysis of the same coal vary considerably with reaction conditions such as the temperature-time history, the particle size, and the ambient pressure. The above description of pyrolysis in terms of a series of fundamental processes enables the understanding of the competition among the various possible products and hopefully allows one to find the optimal reaction conditions to maximize the product distribution, which is of the utmost importance from the practical standpoint.

The principal mechanism of coal devolatilization has been discussed in the previous sections. Among the many free radical reactions outlined for the carbon-hydrogen skeleton, many contribute directly to the transformation of coal to a less reactive solid residue, char. Foremost among these reactions is the formation of double bonds which are thermally very stable. For example, the reactions

$$\Phi CH_2 \dot{C}H\Phi' \longrightarrow \Phi CH{=}CH\Phi' + H\cdot$$

and

$$\Phi\dot{C}HCH_3 \longrightarrow \Phi CH{=}CH_2 + H\cdot$$

result in the formation of "unbreakable" bridges and chains in the coal molecule. Radical recombination between aromatic fragments will increase the overall size of the coal molecule reducing the number of volatile fragments. Transport processes also play a role. The tar molecules unable to escape fast enough recombine with the bulk phase and become permanently retained in the char residue.

In chemical kinetics, a deeper understanding of the competition

among parallel reactions automatically translates into a comparison of rates. We have surveyed the basic processes that are expected to occur at temperatures below 700^{o} C, utilizing available information on the structure of coal. The quantitative description of the individual rates of these processes is the key to further progress, a task we shall attempt in the next chapter.

IV. DESCRIBING THE PYROLYSIS PROCESSES: MATHEMATICAL MODELING

PART I: THE STATE VARIABLES

General Philosophy

In the last chapter, we identified the fundamental processes in coal pyrolysis and briefly described the competing reactions that determine the relative amounts of char, tar and gas products. Further progress depends on our ability to translate this description into mathematical language. To achieve this, we propose the following framework:

1. Introduce a set of "state variables" to which numerical values can be assigned. These state variables should adequately characterize the reactivity of coal under pyrolysis conditions.
2. The fundamental processes are identified as specific changes in time of the state variables. These changes proceed with rates that will be expressed mathematically in terms of the state variables and other relevant parameters, such as the reaction temperature.
3. The system of chemical and physical events can then be represented as (differential) equations in time involving the state variables and relevant reaction parameters.
4. The original structure of the coal, when described in terms of the state variables, specifies the initial conditions for the equations.
5. The resulting initial value problem is eventually solved to simulate the overall pyrolysis process.

Such are the steps that we must undertake; so the methodology becomes the key issue. In the course of this mathematical formulation, we are faced with basically two kinds of difficulties: limitation of

information available and limitation of our resources to handle large systems of equations. Ideally, we desire a complete understanding of the structure of the particular coal of interest and the rate of each fundamental process such as the distribution of cluster sizes, the distribution of chains and bridges, the rate constant of each elementary chemical reaction, the volatility and diffusivity of each product species and a system of equations that describe all the processes. In reality, most of the information we need is derived from experimental measurements and, unfortunately, until now, many of the very important aspects of pyrolysis either cannot be or have not been studied experimentally. For instance, we can at present make some assessment of the proportions of aromatic and aliphatic carbon and hydrogen in coal. We can further estimate the amount of α hydrogens in these groups. But we have yet no method to determine the relative amounts of bridges and chains, which are definitely of primary importance from the point of view of product generation.

Evidently, to understand the mechanism of coal pyrolysis in terms of the fundamental processes, we need a complementary well-designed program of experiments. A major objective of this work is headed in this direction. In the modeling efforts, a piece of missing information will find itself either as an assumption or an undetermined parameter.

We employ three criteria in formulating our model:

1. Incorporate all the important fundamental processes, even if we must do it crudely due to lack of information. A process is important if it contributes significantly to the overall thermal behavior.

2. Minimize the number of undetermined parameters. This can be accomplished by appropriate parameter lumping and by making reasonable assumptions that will simplify a mathematical expression.
3. Minimize the number of state variables. The number of state variables is directly related to the number of equations in our system and hence the labor required for their solution. We seek the smallest set of variables that yields adequate information on the structure of the coal and char during pyrolysis.

With this brief introduction, we proceed to describe the modeling strategy.

The State Variables

Two parallel mechanisms have been proposed for the chemistry of coal pyrolysis: the interaction of oxygen functional groups to release carbon oxides and water, and the free radical reactions within the carbon-hydrogen skeleton. The former can be described by a relatively straightforward set of state variables, namely, the amount of each oxygen functional group that remains in the coal at any time. Included in the set are the carboxylic acid group -COOH, the carbonyl group C=O and the phenolic group Φ-OH. The free radical reactions, however, affect skeletal structures of considerable complexity, and the choice of the appropriate state variables that describe these changes is not trivial.

The building block of the carbon-hydrogen skeleton is the aromatic cluster. A cluster consists of a system of aromatic rings which are directly linked together and includes all their substituent groups other

than aliphatic bridges. Aromatic rings are directly linked together if they are fused or are connected by biphenyl type bridges (Φ-Φ'). This is illustrated in figure IV - 1 where two clusters are enclosed in rectangles.

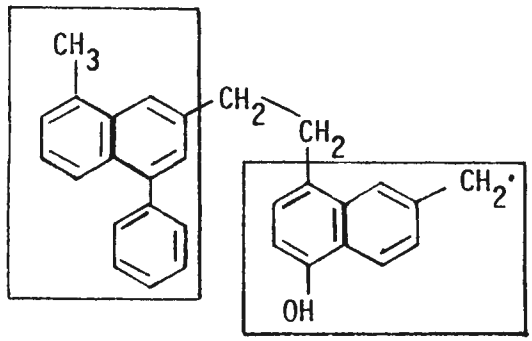

Figure (IV - 1): Structural examples of aromatic clusters

To be completely rigorous, we would define as state variables a distribution corresponding to the number of aromatic clusters having a certain ring size. But then we would have to describe the substituents to individual size group of clusters thereby introducing an enormous number of state variables. Alternatively, we choose three quantities to describe the aromatic clusters:

i) the total number of aromatic clusters regardless of size in a unit volume of subunits (bulk phase) denoted by N_c,

ii) the total number of aromatic carbons in a unit volume of subunits, denoted by C_{ar}, and

iii) the number of peripheral sites of aromatic clusters in a unit volume of subunits, denoted by S .

These three quantities suggest the notion of an "average" cluster which is characterized by two parameters.

$$\left.\begin{aligned} c_{ar} &\equiv C_{ar}/N_c \\ h_{aru} &\equiv S/N_c \end{aligned}\right\} \quad (IV - 1)$$

We make our first simplifying assumption: all aromatic clusters in coal have c_{ar} aromatic carbons and h_{aru} sites. We denote the total number of clusters by N_c.

In the lower temperature range, the aromatic ring systems are stable towards chemical disruption so that c_{ar} and h_{aru} will be fixed parameters once they are defined.

We consider the carbon-hydrogen skeleton as an aggregate of aromatic clusters containing purely aliphatic side chains and connected by bridges, plus some other permanent linkages which may be formed when the coal is heated. The classification of the functional groups into side chains and bridges introduces certain difficulty with alicyclic rings because they possess the stoichiometry of a bridge without actually linking two clusters together. Nevertheless, alicyclic rings will be treated as bridges because both undergo the same reactions. The result is an overestimation of the total number of bridges which we neglect in view of the fact that the number of bridges is an adjustable parameter.

The state variables must then describe the purely aliphatic portion of the coal molecule -- the side chains and the bridges.

One possible way of describing the side chains is to label them as methyl, ethyl, propyl or butyl groups, etc. But this is convenient only if they are all straight chains. The numerous possibilities of branched chain isomers will probably make this system obsolete. A similar problem

occurs with the bridges if they are structurally identified as methylene, ethylene, propylene or butylene, etc. Again the possibilities of secondary or tertiary branching are many. The real difficulty, moreover, lies in the description of the changes that these substituents undergo. There are so many structural possibilities that a much simplified system must be developed. We start this development with a closer observation of the properties of aromatic-aliphatic structures.

The aromatic cluster has h_{aru} number of peripheral sites. Each site can accommodate only one substituent atom, thus branching can never occur at an aromatic carbon. The substituent atom may be a hydrogen, a phenolic oxygen or an α carbon. The α carbon must in turn be linked by three other bonds to other substituent groups. We have discovered that we would have a much more convenient and efficient system by defining as state variables the various substituent groups of these α carbons, without loss of any retrievable information.

Just like the substituent to an aromatic edge site, the substituents to α carbons can be classified into chains or bridges depending on whether they are eventually linked to another cluster or not. To describe the aromatic-aliphatic skeleton of coal structure, we propose the following distinction of α-carbon substituents:

1. α hydrogen (H_α) 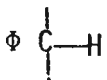
2. methyl chain (c_1) 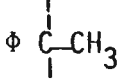
3. longer chain (c_2) 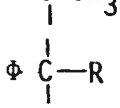

where R stands for any purely paraffinic alkyl groups besides methyl.

4. methylene bridge (b_1) 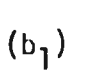

5. ethylene bridge (b_2) 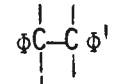

6. longer bridge (b_3) 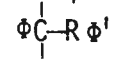

where R again represents any purely paraffinic grouping except $-CH_2-$. As state variables, the quantities H_α, c_1, c_2 etc. must be expressed as concentrations of the respective functional groups per unit volume of subunits. Moreover, in the case of the bridges b_2 and b_3, the same substituent group must occur twice on different α-carbons. As an illustration, an ethylene bridge 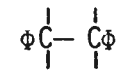 must take up two α-carbon substituent positions (so must any longer bridge), so that the concentration of α-carbons (C_α) will follow the equality

$$C_\alpha = \frac{H_\alpha + c_1 + c_2 + b_1 + 2b_2 + 2b_3}{3} \qquad (IV-2)$$

As we observe, the transformation of the α- carbon substituents is intimately related with the set of free radical chain reactions described in chapter III. As dissociation, hydrogen abstraction, and recombination take place, new species of α-carbon substituents will emerge. Like other chemical reactions, these changes obey their own pattern of stoichiometry and rates. In fact, the most important advantage of choosing α-carbon substituents as state variables is the convenience with which the stoichiometry of functional group changes can be described. The new state variables that emerge from the free radical chain reactions are:

1. α radicals ($\alpha\cdot$)

2. β radicals ($\beta_1\cdot$) 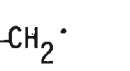

3. β radicals ($\beta_2\cdot$) 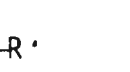

where R· is an alkyl radical

4. ethylene bridge radicals ($b_2^{\cdot}$) 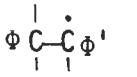

5. longer bridge radicals ($b_3^{\cdot}$) 

where R is an alkyl group

6. chains with double bonds ($c_1=$) 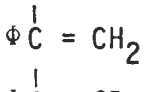

7. chains with double bonds ($c_2=$) 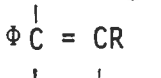

8. bridges with double bonds ($b_2=$) 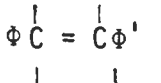

9. bridges with double bonds ($b_3=$) 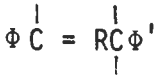

where R is an alkyl group.

Moreover, there will be new species generated which are not α-carbon substituents. For example, dissociation of a chain generates an alkyl free radical which is not attached to any aromatic cluster. These new species may react further with the α-carbon substituents in the bulk phase and their concentrations must therefore be monitored. They include:

10. $CH_3^{\cdot}$, free methyl radicals
11. $R^{\cdot}$, free alkyl radicals besides methyl
12. $H^{\cdot}$, free hydrogen atoms
13. $\Phi^{\cdot}$, phenyl type radicals (this is not an α-carbon substituent)
14. CH_4 , methane
15. RH , saturated (non-radical) paraffins
16. R= , light olefins
17. H_2 , hydrogen gas.

Stoichiometry and Rates

The chemical reactions among various functional groups have been divided into classes such as dissociation, hydrogen abstraction, recombi-

nation, etc. In terms of our state variables which are α-carbon substituents, these reactions translate into certain stoichiometric relationships among the different substituents. For example, the dissociation reaction

$$\Phi\dot{C}(\Phi')-CH_3 \rightarrow \Phi\dot{C}(\Phi') + CH_3\cdot$$

which involves only one α-substituent can be written as

$$c_1 \rightarrow \alpha\cdot + CH_3\cdot$$

A more complicated stoichiometric relationship is seen in

$$CH_3\cdot + \Phi\dot{C}(H)-C(\Phi')\Phi' \rightarrow CH_4 + \Phi\dot{C}(\Phi')-C(\Phi')\Phi'$$

The variables involved are $CH_3\cdot$, b_2, H_α, CH_4 and $b_2\cdot$ the stoichiometry is

$$CH_3\cdot + b_2 + H_\alpha \rightarrow CH_4 + b_2\cdot$$

In our representation, b_2 indicates a structure like $\Phi\dot{C}(\Phi')-C(\Phi')\Phi'$ with four α-carbon substituents unspecified, so it accounts for two α positions. However, $b_2\cdot$ is the structure $\Phi\dot{C}(\Phi')-C(\Phi')\Phi'$ with only three α positions unspecified. Therefore, in this process one α hydrogen is lost and the stoichiometry above results. One specific rule of the stoichiometry is apparent, namely the total number of α-carbon substituents on the left hand side must be exactly balanced by that on the right hand side, with the exception of only one reaction

$$\Phi CH_3 + H\cdot \rightarrow \Phi H + CH_3\cdot$$

which is translated as

$$3H_\alpha + H\cdot \rightarrow CH_3\cdot$$

with a loss of three α positions because there is a loss of one α carbon in the process. In other words, each species accounts for a specific

number of α-carbon positions indicated as follows:

	Structure	Species	Number of α positions
1.	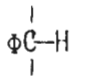	H_α	1
2.	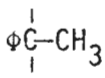	c_1	1
3.	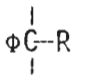	c_2	1
4.	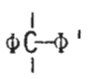	b_1	1
5.	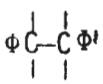	b_2	2
6.	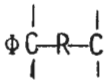	b_3	2
7.	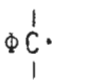	$\alpha\cdot$	1
8.	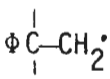	$\beta_1\cdot$	1
9.	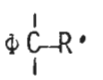	$\beta_2\cdot$	1
10.	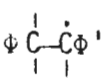	$b_2\cdot$	3
11.	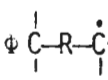	$b_3\cdot$	3
12.	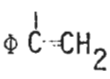	$c_1^=$	2
13.	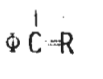	$c_2^=$	2
14.	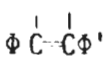	$b_2^=$	4
15.	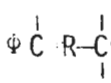	$b_3^=$	3

	Structure	Species	Number of α positions
16.	$CH_3\cdot$	$CH_3\cdot$	0
17.	R·	R·	0
18.	H·	H·	0
19.	Φ·	Φ·	0
20.	CH_4	CH_4	0
21.	RH	RH	0
22.	R=	R =	0
23.	H_2	H_2	0

The stoichiometry of the pyrolysis reactions involving the carbon-hydrogen skeleton is given in the following table together with the expressions that describe their rates. Explanation of this table follows immediately.

TABLE IV-1

Stoichiometry and Rates of Free Radical Reactions

	Reactions	Stoichiometry	Rates
	Bond Dissociation		
1.	$\Phi\dot{C}\Phi' \rightarrow \Phi\dot{C}\cdot + \Phi'\cdot$	$b_1 \rightarrow \alpha\cdot + \Phi\cdot$	$f_1 k_1 b_1$
2.	$\Phi\dot{C}\dot{C}\Phi' \rightarrow \Phi\dot{C}\cdot + \Phi'\dot{C}\cdot$	$b_2 \rightarrow \alpha\cdot + \alpha\cdot$	$f_1 k_2 b_2$
3.	$\Phi\dot{C}R\dot{C}\Phi' \rightarrow \Phi\dot{C}\text{-}R\cdot + \Phi'\dot{C}\cdot$	$b_3 \rightarrow \alpha\cdot + \beta_2^{\cdot}$	$f_1 k_3 b_3$
4.	$\Phi\dot{C}CH_3 \rightarrow \Phi\dot{C}\cdot + CH_3^{\cdot}$	$c_1 \rightarrow \alpha\cdot + CH_3^{\cdot}$	$f_1 k_4 c_1$
5.	$\Phi\dot{C}R \rightarrow \Phi\dot{C}\cdot + R\cdot$	$c_2 \rightarrow \alpha\cdot + R\cdot$	$f_1 k_5 c_2$
	Hydrogen Abstraction		
6.	$\Phi\dot{C}R\dot{C}\Phi' + \Phi\dot{C}\text{-}H \rightarrow \Phi CRC\Phi' + \Phi\dot{C}\cdot$	$b_3^{\cdot} + H_\alpha \rightarrow b_3 + \alpha\cdot$	$g_1 f_1 f_2 k_6 b_3^{\cdot}[H_\alpha]$
7.	$CH_3^{\cdot} + \Phi\dot{C}H \rightarrow CH_4 + \Phi\dot{C}\cdot$	$CH_3^{\cdot} + H_\alpha \rightarrow CH_4 + \alpha\cdot$	$f_1 f_2 k_7 [CH_3^{\cdot}][H_\alpha]$
8.	$R\cdot + \Phi\dot{C}H \rightarrow RH + \Phi\dot{C}\cdot$	$R\cdot + H_\alpha \rightarrow RH + \alpha\cdot$	$f_1 f_2 k_8 [R\cdot]\ [H_\alpha]$
9.	$\Phi\cdot + \Phi'\dot{C}H \rightarrow \Phi H + \Phi'\dot{C}\cdot$	$\Phi\cdot + H_\alpha \rightarrow \alpha\cdot$	$g_1 f_1 f_2 k_9 [\Phi\cdot][H_\alpha]$

	Reactions	Stoichiometry	Rates
10.	$H\cdot + \Phi\dot{C}H \rightarrow H_2 + \Phi\dot{C}\cdot$	$H\cdot + H_\alpha \rightarrow H_2 + \alpha\cdot$	$f_1 f_2 k_{10}[H\cdot][H_\alpha]$
11.	$\Phi\dot{C}R\cdot + \Phi\dot{C}H \rightarrow \Phi\dot{C}R + \Phi\dot{C}\cdot$	$\beta_2^{\cdot} + H_\alpha \rightarrow c_2 + \alpha\cdot$	$g_1 f_1 f_2 k_{11}\beta_2^{\cdot}[H_\alpha]$
12.	$\Phi\dot{C}CH_2^{\cdot} + \Phi\dot{C}H \rightarrow \Phi\dot{C}CH_3 + \Phi\dot{C}\cdot$	$\beta_1^{\cdot} + H_\alpha \rightarrow c_1 + \alpha\cdot$	$g_1 f_1 f_2 k_{12}\beta_1^{\cdot}[H_\alpha]$
13.	$\Phi\dot{C}\dot{C}\Phi' + \Phi\dot{C}H \rightarrow \Phi C(H)C\,\Phi' + \Phi\dot{C}\cdot$	$b_2^{\cdot} \rightarrow b_2 + \alpha\cdot$	$g_1 f_1 f_2 k_{13} b_2^{\cdot}[H_\alpha]$
14.	$CH_3^{\cdot} + \Phi\dot{C}CH_3 \rightarrow CH_4 + \Phi\dot{C}CH_2^{\cdot}$	$CH_3^{\cdot} + c_1 \rightarrow CH_4 + \beta_1\cdot$	$k_{14}[CH_3]c_1$
15.	$H\cdot + \Phi\dot{C}CH_3 \rightarrow H_2 + \Phi\dot{C}CH_2^{\cdot}$	$H\cdot + c_1 \rightarrow H_2 + \beta_1\cdot$	$k_{15}[H\cdot]c_1$
16.	$R\cdot + \Phi\dot{C}CH_3 \rightarrow RH + \Phi\dot{C}CH_2^{\cdot}$	$R\cdot + c_1 \rightarrow RH + \beta_1\cdot$	$k_{16}[R\cdot]c_1$
17.	$\Phi\cdot + \Phi\dot{C}CH_3 \rightarrow \Phi H + \Phi\dot{C}CH_2^{\cdot}$	$\Phi\cdot + c_1 \rightarrow \beta_1\cdot$	$g_1 k_{17}[\Phi\cdot]c_1$
18.	$CH_3^{\cdot} + \Phi\dot{C}R \rightarrow CH_4 + \Phi\dot{C}R\cdot$	$CH_3^{\cdot} + c_2 \rightarrow CH_4 + \beta_2^{\cdot}$	$k_{18}[CH_3^{\cdot}]c_2$
19.	$H\cdot + \Phi\dot{C}R \rightarrow H_2 + \Phi\dot{C}R\cdot$	$H\cdot + c_2 \rightarrow H_2 + \beta_2^{\cdot}$	$k_{19}[H\cdot]c_2$
20.	$R\cdot + \Phi\dot{C}R \rightarrow RH + \Phi\dot{C}R\cdot$	$R\cdot + c_2 \rightarrow RH + \beta_2^{\cdot}$	$k_{20}[R\cdot]c_2$

	Reactions	Stoichiometry	Rates
21.	$\Phi\cdot + \Phi'\overset{|}{\underset{|}{C}}R \rightarrow \Phi H + \Phi'\overset{|}{\underset{|}{C}}R\cdot$	$\Phi\cdot + c_2 \rightarrow \beta_2^{\cdot}$	$g_1 k_{21}[\Phi\cdot]c_2$
22.	$CH_3^{\cdot} + \Phi\overset{|}{\underset{|}{C}}\overset{H}{\underset{|}{C}}\Phi' \rightarrow CH_4 + \Phi\overset{|}{\underset{|}{C}}\overset{\cdot}{\underset{|}{C}}\Phi'$	$CH_3^{\cdot} + b_2 + H_\alpha \rightarrow CH_4 + b_2^{\cdot}$	$(1-f_2)k_{22}\frac{b_2}{b_2+b_3}[CH_3^{\cdot}][H_\alpha]$
23.	$H\cdot + \Phi\overset{|}{\underset{|}{C}}\overset{H}{\underset{|}{C}}\Phi' \rightarrow H_2 + \Phi\overset{|}{\underset{|}{C}}\overset{\cdot}{\underset{|}{C}}\Phi'$	$H\cdot + b_2 + H_\alpha \rightarrow H_2 + b_2^{\cdot}$	$(1-f_2)k_{23}\frac{b_2}{b_2+b_3}[H\cdot][H_\alpha]$
24.	$R\cdot + \Phi\overset{|}{\underset{|}{C}}\overset{H}{\underset{|}{C}}\Phi' \rightarrow RH + \Phi\overset{|}{\underset{|}{C}}\overset{\cdot}{\underset{|}{C}}\Phi'$	$R\cdot + b_2 + H_\alpha \rightarrow RH + b_2^{\cdot}$	$(1-f_2)\frac{b_2}{b_2+b_3}k_{24}[R\cdot][H_\alpha]$
25.	$\Phi\cdot + \Phi\overset{|}{\underset{|}{C}}\overset{H}{\underset{|}{C}}\Phi' \rightarrow \Phi H + \Phi\overset{|}{\underset{|}{C}}\overset{\cdot}{\underset{|}{C}}\Phi'$	$\Phi\cdot + b_2 + H_\alpha \rightarrow b_2^{\cdot}$	$g_1(1-f_2)\frac{b_2}{b_2+b_3}k_{25}[\Phi\cdot][H_\alpha]$
26.	$\Phi\overset{|}{\underset{|}{C}}CH_2^{\cdot} + \Phi\overset{|}{\underset{|}{C}}\overset{H}{\underset{|}{C}}\Phi' \rightarrow \Phi\overset{|}{\underset{|}{C}}CH_3 + \Phi\overset{|}{\underset{|}{C}}\overset{\cdot}{\underset{|}{C}}\Phi'$	$\beta_1\cdot + b_2 + H_\alpha \rightarrow c_1 + b_2^{\cdot}$	$g_1(1-f_2)\frac{b_2}{b_2+b_3}k_{26}\beta_1\cdot[H_\alpha]$
27.	$\Phi\overset{|}{\underset{|}{C}}R\cdot + \Phi\overset{|}{\underset{|}{C}}\overset{H}{\underset{|}{C}}\Phi' \rightarrow \Phi\overset{|}{\underset{|}{C}}R + \Phi\overset{|}{\underset{|}{C}}\overset{\cdot}{\underset{|}{C}}\Phi'$	$\beta_2^{\cdot} + b_2 + H_\alpha \rightarrow c_2 + b_2^{\cdot}$	$g_1(1-f_2)\frac{b_2}{b_2+b_3}k_{27}\beta_2^{\cdot}[H_\alpha]$
28.	$\Phi\overset{H}{\underset{|}{C}}\overset{|}{\underset{|}{R}}\overset{|}{\underset{|}{C}}\Phi' + \Phi\overset{|}{\underset{|}{C}}\cdot \rightarrow \Phi\overset{\cdot}{\underset{|}{C}}\overset{|}{\underset{|}{R}}\overset{|}{\underset{|}{C}}\Phi' + \Phi\overset{|}{\underset{|}{C}}H$	$b_3 + \alpha\cdot \rightarrow b_3^{\cdot} + H_\alpha$	$g_1(1-f_2)\frac{b_3}{b_2+b_3}k_{28}\alpha\cdot[H_\alpha]$
29.	$\Phi\overset{|}{\underset{|}{C}}\cdot + \Phi\overset{|}{\underset{|}{C}}\overset{H}{\underset{|}{C}}\Phi' \rightarrow \Phi\overset{|}{\underset{|}{C}}H + \Phi\overset{|}{\underset{|}{C}}\overset{\cdot}{\underset{|}{C}}\Phi'$	$b_2 + \alpha\cdot \rightarrow b_2^{\cdot}$	$g_1(1-f_2)\frac{b_2}{b_2+b_3}k_{29}\alpha\cdot[H_\alpha]$

	Reactions	Stoichiometry	Rates
30.	$CH_3^{\cdot} + \Phi\overset{H}{\underset{}{C}}R\overset{}{\underset{}{C}}\Phi' \rightarrow CH_4 + \Phi\dot{C}RC\Phi'$	$H_\alpha + CH_3^{\cdot} + b_3 \rightarrow CH_4 + b_3^{\cdot}$	$(1-f_2)\frac{b_3}{b_2+b_3}k_{30}[CH_3^{\cdot}][H_\alpha]$
31.	$H^{\cdot} + \Phi\overset{H}{\underset{}{C}}R\overset{}{\underset{}{C}}\Phi' \rightarrow H_2 + \Phi\dot{C}RC\Phi'$	$H_\alpha + H^{\cdot} + b_3 \rightarrow H_2 + b_3^{\cdot}$	$(1-f_2)\frac{b_3}{b_2+b_3}k_{31}[H^{\cdot}][H_\alpha]$
32.	$R^{\cdot} + \Phi\overset{H}{\underset{}{C}}R\overset{}{\underset{}{C}}\Phi' \rightarrow RH + \Phi\dot{C}RC\Phi'$	$H_\alpha + R^{\cdot} + b_3 \rightarrow RH + b_3^{\cdot}$	$(1-f_2)\frac{b_3}{b_2+b_3}k_{32}[R^{\cdot}][H_\alpha]$
33.	$\Phi^{\cdot} + \Phi\overset{H}{\underset{}{C}}R\overset{}{\underset{}{C}}\Phi' \rightarrow \Phi H + \Phi\dot{C}RC\Phi'$	$H_\alpha + \Phi^{\cdot} + b_3 \rightarrow b_3^{\cdot}$	$g_1(1-f_2)\frac{b_3}{b_2+b_3}k_{33}[\Phi^{\cdot}][H_\alpha]$
34.	$\Phi\overset{}{\underset{}{C}}CH_2^{\cdot} + \Phi\overset{H}{\underset{}{C}}R\overset{}{\underset{}{C}}\Phi' \rightarrow \Phi\overset{}{\underset{}{C}}CH_3 + \Phi\dot{C}RC\Phi'$	$H_\alpha + \beta_1^{\cdot} + b_3 \rightarrow c_1 + b_3^{\cdot}$	$g_1(1-f_2)\frac{b_3}{b_2+b_3}k_{34}\beta_1^{\cdot}[H_\alpha]$
35.	$\Phi\overset{}{\underset{}{C}}R^{\cdot} + \Phi\overset{H}{\underset{}{C}}R\overset{}{\underset{}{C}}\Phi' \rightarrow \Phi\overset{}{\underset{}{C}}R + \Phi\dot{C}RC\Phi'$	$H_\alpha + \beta_2^{\cdot} + b_3 \rightarrow c_2 + b_3^{\cdot}$	$g_1(1-f_2)\frac{b_3}{b_2+b_3}k_{35}\beta_2^{\cdot}[H_\alpha]$
	Hydrogen Elimination		
36.	$\Phi\overset{H}{\underset{}{C}}CH_2^{\cdot} \rightarrow \Phi\overset{}{\underset{}{C}}=C + H^{\cdot}$	$\beta_1^{\cdot} + H_\alpha \rightarrow c_1{=} + H^{\cdot}$	$f_3k_{36}\beta_1^{\cdot}$
37.	$\Phi\overset{H}{\underset{}{C}}R^{\cdot} \rightarrow \Phi\overset{}{\underset{}{C}}=R + H^{\cdot}$	$\beta_2^{\cdot} + H_\alpha \rightarrow c_2{=} + H^{\cdot}$	$f_3k_{37}\beta_2^{\cdot}$

	Reactions	Stoichiometry	Rates
38.	$\Phi\dot{C}C\Phi' \rightarrow \Phi C{=}C\Phi' + H\cdot$	$b_2^{\cdot} + H_\alpha \rightarrow b_2{=} + H\cdot$	$f_3 k_{38} b_2^{\cdot}$
39.	$\Phi\dot{C}RC\Phi' \rightarrow \Phi C{=}RC\Phi' + H\cdot$	$b_3^{\cdot} \rightarrow b_3{=} + H\cdot$	$k_{39} b_3^{\cdot}$
40.	$\Phi\dot{C}CH_3 \rightarrow \Phi C{=}CH_2 + H\cdot$	$\alpha\cdot + c_1 \rightarrow c_1{=} + H\cdot$	$k_{40}\frac{2c_1\alpha\cdot}{3C_\alpha}$
41.	$\Phi\dot{C}R \rightarrow \Phi C{=}R + H\cdot$	$\alpha\cdot + c_2 \rightarrow c_2{=} + H\cdot$	$k_{41}\frac{2c_2\alpha\cdot}{3C_\alpha}$
	β - scission		
42.	$\Phi\dot{C}RC\Phi' \rightarrow \Phi C{=}R + \Phi'\dot{C}\cdot$	$b_3^{\cdot} \rightarrow c_2{=} + \alpha\cdot$	$k_{42} b_3^{\cdot}$
43.	$\Phi\dot{C}R\cdot \rightarrow \Phi\dot{C}\cdot$ + olefin	$\beta_2^{\cdot} \rightarrow \alpha\cdot + R{=}$	$k_{43}\beta_2^{\cdot}$
	Addition		
44.	$H\cdot + \Phi CH_3 \rightarrow \Phi H + CH_3^{\cdot}$	$3H_\alpha + H\cdot \rightarrow CH_3^{\cdot}$	$k_{44} N_{CH_3}[H\cdot]$

	Reactions	Stoichiometry	Rates
45.	$CH_3^{\cdot} + \Phi\dot{C}{=}R \rightarrow \Phi\dot{C}RCH_3$	$CH_3^{\cdot} + c_2{=} \rightarrow \alpha\cdot + c_2$	$k_{45}[CH_3^{\cdot}]c_2{=}$
46.	$R'\cdot + \Phi\dot{C}{=}R \rightarrow \Phi\dot{C}RR'$	$R\cdot + c_2{=} \rightarrow \alpha\cdot + c_2$	$k_{46}[R\cdot]c_2{=}$
47.	$H\cdot + \Phi\dot{C}{=}R \rightarrow \Phi\dot{C}RH$	$H\cdot + c_2{=} \rightarrow \alpha\cdot + c_2$	$k_{47}[H\cdot]c_2{=}$
48.	$H\cdot + \Phi\dot{C}{=}CH_2 \rightarrow \Phi\dot{C}CH_3$	$H\cdot + c_1{=} \rightarrow \alpha\cdot + c_1$	$k_{48}[H\cdot]c_1{=}$
49.	$CH_3^{\cdot} + \Phi\dot{C}{=}CH_2 \rightarrow \Phi\dot{C}CH_2CH_3$	$CH_3^{\cdot} + c_1{=} \rightarrow \alpha\cdot + c_2$	$k_{49}[CH_3^{\cdot}]c_1{=}$
50.	$R\cdot + \Phi\dot{C}{=}CH_2 \rightarrow \Phi\dot{C}CH_2R$	$R\cdot + c_1{=} \rightarrow \alpha\cdot + c_2$	$k_{50}[R\cdot]c_1{=}$
	Recombination		
51.	$\Phi\dot{C}\cdot + \Phi'\dot{C}\cdot \rightarrow \Phi C(=C)\Phi'$	$\alpha\cdot + \alpha\cdot \rightarrow b_2$	$g_2k_{51}\alpha^{\cdot 2}$
52.	$\Phi\dot{C}\cdot + \Phi'\dot{C}R\cdot \rightarrow \Phi CRC\Phi'$	$\alpha\cdot + \beta_2^{\cdot} \rightarrow b_3$	$g_2k_{52}\alpha\cdot\beta_2^{\cdot}$

Reactions	Stoichiometry	Rates
53. $\Phi\dot{C}\cdot + \Phi\dot{C}CH_2\cdot \rightarrow \Phi CRC\Phi'$	$\alpha\cdot + \beta_1\cdot \rightarrow b_3$	$g_2k_{53}\alpha\cdot\beta_1\cdot$
54. $\Phi\dot{C}\cdot + CH_3\cdot \rightarrow \Phi\dot{C}CH_3$	$\alpha\cdot + CH_3\cdot \rightarrow c_1$	$k_{54}\alpha\cdot[CH_3\cdot]$
55. $\Phi\dot{C}\cdot + R\cdot \rightarrow \Phi\dot{C}R$	$\alpha\cdot + R\cdot \rightarrow c_2$	$k_{55}\alpha\cdot[R\cdot]$
56. $\Phi\dot{C}\cdot + H\cdot \rightarrow \Phi\dot{C}H$	$\alpha\cdot + H\cdot \rightarrow H_\alpha$	$k_{56}\alpha\cdot[H\cdot]$

The chemical symbols c_1, c_2, $\alpha\cdot$, etc. denote chemical species when used to describe reactions, and they represent concentrations of those species when used to describe rates. Since the context of stoichiometry or rates is generally obvious, no attempt is made to provide different notation for each of them.

The quantities f_1 through f_3, g_1 and g_2 are rate adjustment factors. N_{CH_3} is the concentration of α-methyl groups which exists at the particular time. We proceed with the derivation of these quantities and with specific comments on each reaction with regards to the stoichiometry and rates.

It has long been recognized, and will be assumed here, that free radical chain reactions such as those listed above belong to the class of elementary reactions for which the rate can be expressed as the product of a rate constant and the concentration(s) of the participating reactant(s). Because many of our chemical species are not independent molecules but functional groups attached to aromatic units, we make two general assumptions:

(1) that the α-carbon substituents are randomly situated among the aromatic units and

(2) that all identical functional groups can be treated as possessing the same reactivities independent of their precise location.

These assumptions are necessary in order to make the accounting of functional groups mathematically tractable. They are reasonable insofar as we have no indication from our present knowledge that the functional groups in coal should take on any preferential arrangements or patterns.

We do, however, recognize that the progress of many reactions is affected by specific neighboring groups and by the physical environment of the chemical species. This leads us to introduce rate adjustment factors such as f_1 through f_3, g_1 and g_2, which modify the rates to correct for these neighboring group or environment effects.

The rates of elementary reactions between molecular species can generally be expressed as

$$r = k \prod_i c_i \qquad \text{(IV-3)}$$

where r is the reaction rate per unit volume, k is a rate constant and c_i represents the concentration of the molecules of participating species i. k has an Arrhenius dependence on the temperature T.

$$k = Ae^{-E/RT} \qquad \text{(IV-4)}$$

where A is the frequency factor, E an activation energy and R the universal gas constant. We apply this same general principle to the reactions among functional groups, assuming that

$$r_j = k_j \prod_i c_{ij} \qquad \text{(IV-5)}$$

where j is an index for reactions and i for the participating reactants. Because of parameter lumping a chemical species would include functional groups of varying reactivities due to substituent effects. This is well illustrated in the following example.

The rate of the dissociation reaction

4. 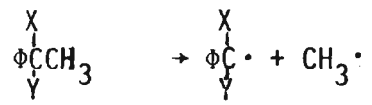

or

$$c_1 \rightarrow \alpha\cdot + CH_3\cdot$$

depends on X and Y, so that when we assume that identical functional groups have the same reactivities, we must interpret reaction rates as averages. In particular, if X and Y happen to be a double bond, a species like $\overset{\bullet}{C}=R$ will be generated with the dissociation, which is not a likely process. We should therefore discount those methyl groups that are next to a double bond in our rate expression for this process. Hence, we adjust the rate by a factor f_1 and write

$$r_4 = f_1 k_4 c_1 \qquad \text{(IV-6)}$$

where f_1 is the probability that any singly bonded α carbon substituent is not next to a double bond. f_1 is, of course, a function of the values of the state variables at the particular time, which can be calculated as follows:

The number of α-double bond attachments in the system is $2b_2^= + b_3^= + c_1^= + c_2^=$. This is also equal to the number of singly bonded substituents next to a double bond. The total number of singly bonded substituents, however, is $3C_\alpha - (4b_2^= + 2b_3^= + 2c_1^= + 2c_2^=)$, where $3C_\alpha$ is the total number of α carbon substituent positions. The probability f_1 is therefore

$$f_1 = 1 - \frac{2b_2^= + b_3^= + c_1^= + c_2^=}{3C_\alpha - 2(2b_2^= + b_3^= + c_1^= + c_2^=)} \qquad \text{(IV-7)}$$

Where appropriate, the factor f_1 is used to modify reaction rates which are affected by the presence of a neighboring double bond.

The factor f_2 is used in the context of α hydrogen abstraction. In our reaction scheme, α hydrogen may be abstracted from bridges as well as from chains. As examples we consider reactions 7, 22 and 30.

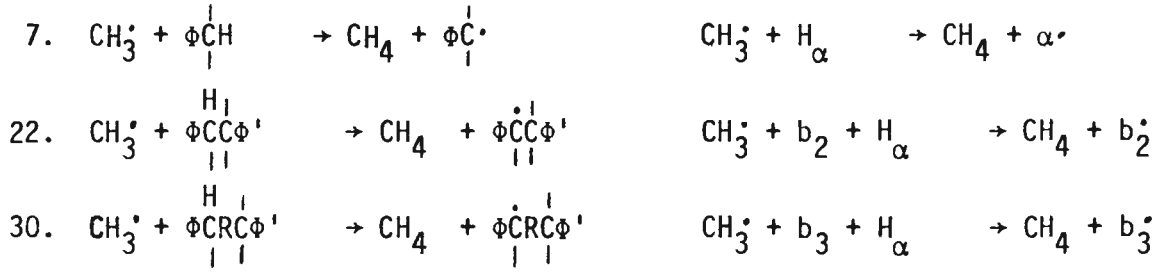

The rates of these reactions are respectively

$$\left.\begin{aligned} r_7 &= f_1 k_7 [CH_3^\bullet] H_{\alpha,c} \\ r_{22} &= k_{22} [CH_3^\bullet] H_{\alpha,b_2} \\ r_{30} &= k_{30} [CH_3^\bullet] H_{\alpha,b_3} \end{aligned}\right\} \quad \text{(IV-8)}$$

where $H_{\alpha,c}$ is the concentration of α hydrogen atoms which do not belong to an ethylene or a longer bridge, H_{α,b_2} is the concentration of α hydrogen atoms on an ethylene bridge and H_{α,b_3} is the concentration of α hydrogen atoms on a longer bridge.

We may define

$$H_{\alpha,c} \equiv f_2 H_\alpha \qquad \text{(IV-9)}$$

whence f_2 can be equated with the probability that an α hydrogen

does not belong to an ethylene or longer bridge. An α carbon has three substituents. Given that one is a hydrogen, the probability that none of the other two is a b_2 or b_3 is

$$f_2 = \left[1 - \frac{2(b_2 + b_3)}{3C_\alpha}\right]^2 \qquad \text{(IV-10)}$$

It is rather straightforward to show that

$$\left.\begin{aligned} H_{\alpha,b_2} &= \frac{b_2}{b_2 + b_3}(1-f_2)H_\alpha \\ \text{and} \\ H_{\alpha,b_3} &= \frac{b_3}{b_2 + b_3}(1-f_2)H_\alpha \end{aligned}\right\} \qquad \text{(IV-11)}$$

so that

$$r_7 = f_2 f_1 k_7 [CH_3^\cdot] H_\alpha$$

$$r_{22} = (1-f_2)k_{22}\frac{b_2}{b_2 + b_3}[CH_3^\cdot]H_\alpha$$

and $$r_{30} = (1-f_2)k_{30}\frac{b_3}{b_2 + b_3}[CH_3^\cdot]H_\alpha$$

The factor f_3 is used in the context of hydrogen elimination, such as reaction 38,

38. $\Phi\overset{\cdot H}{\underset{\|}{C}}C\Phi' \rightarrow \Phi\overset{|}{C}{=}\overset{|}{C}\Phi' + H\cdot$; $b_2\cdot + H_\alpha \rightarrow b_2{=} + H\cdot$

in which case hydrogen can be eliminated only if it is actually present. Here the rate should be

$$r_{38} = f_3 k_{38} b_2 \qquad \text{(IV-12)}$$

where f_3 is the probability that any α-carbon substituent is a hydrogen. Hence

$$f_3 = \frac{H_\alpha}{3C_\alpha} \qquad \text{(IV-13)}$$

The hydrogen elimination reactions 40 and 41

40. $\Phi\dot{C}_{\text{I}}CH_3 \rightarrow \Phi C_{\text{I}}{=}CH_2 + H\cdot$ $\qquad \alpha\cdot + c_1 \rightarrow c_1{=} + H\cdot$

41. $\Phi\dot{C}_{\text{I}}R \rightarrow \Phi C_{\text{I}}{=}R + H\cdot$ $\qquad \alpha\cdot + c_2 \rightarrow c_2{=} + H\cdot$

have rates that are first order in the concentrations of the species $\Phi\dot{C}_{\text{I}}CH_3$ and $\Phi\dot{C}_{\text{I}}R$ respectively. The probability that an α radical is next to a methyl group is $\frac{2c_1}{3C_\alpha}$. This gives

$$r_{40} = k_{40}[\Phi\dot{C}_{\text{I}}CH_3] = k_{40}\left(\frac{2c_1\alpha\cdot}{3c_\alpha}\right)$$

and $\qquad \text{(IV-14)}$

$$r_{41} = k_{41}[\Phi\dot{C}_{\text{I}}R] = k_{41}\left(\frac{2c_2\alpha\cdot}{3C_\alpha}\right)$$

In addition to correcting for neighboring group effects, we note that the physical environment of a functional group can also affect its reactivity, as we now demonstrate.

To describe the chemistry of coal pyrolysis in terms of these elementary reactions, it is essential to obtain reliable estimates of the rate constants and their dependence on temperature. Although aromatic free radical systems have been much less rigorously studied than those originating from small alkane molecules, the organic chemist can still obtain reasonably good estimates of the magnitude of many of these reaction rates, largely through a knowledge of the relevant bond

energies, the theory of thermochemical kinetics (Benson, 1968), and the availability of certain gas phase experimental data. Our major difficulty in the estimation of rate constants lies, therefore, not in our ability to assign frequency factors or activation energies to these reactions, but essentially in the applicability of thermochemical kinetics and gas phase experimental data to reactions that occur in a condensed phase like coal. Granted that our basis of information is a set of rate constants of the form

$$k_j = A_j \exp(-\frac{E_j}{RT}) \qquad \text{(IV-15)}$$

where j is an index for reactions, A and E are the frequency factor and activation energy respectively, R is the gas constant and T the temperature, we need to extrapolate this information to apply to the corresponding reactions in the condensed medium.

To our present knowledge, there does not exist any quantitative theory that adequately relates gas phase kinetics with the rates of the same reaction in a solid phase. Two general phenomena, commonly known as the cage and the gel effects, account for the deviation of condensed phase kinetics from predictions derived from gas phase behavior.

The cage effect is most pronounced in the dissociation of bridges. Consider the scission

2. $\Phi\overset{|}{\underset{|}{C}}\text{-}\overset{|}{\underset{|}{C}}\Phi' \xrightarrow{k_d} \Phi\overset{|}{C}\cdot + \Phi'\overset{|}{C}\cdot$, $b_2 \rightarrow \alpha\cdot + \alpha\cdot$

The resulting α-radicals are free to participate in further reactions only if after the bond rupture the aromatic fragments are able to diffuse apart before recombination occurs. The diffusivity or mobility of the daughter radicals plays the key role here. When this reaction occurs

with the generation of two heavy aromatic radicals in a dense medium the surrounding material tends to prevent true dissociation of the radical species. This means a decrease of the rate of dissociation of the bridges as opposed to the corresponding rate in the gas phase. This cage effect would not apply to the dissociation of chains because of the small size and high mobility of the resulting alkyl radicals.

To examine the cage effect on the dissociation of various types of bridges, we review the processes that lead to tar product formation. When a bridge breaks, two possibilities exist for each resulting fragment radical; if it is of sufficient vapor pressure and is in a surface region, near a transitional or macropore, it will excape as a product fragment, otherwise it will stay in the bulk phase. We postulate that the cage effect is not applicable to the dissociation of any bridge that leads to a product fragment, because the product fragment is volatile and is located near a pore surface. For the other bridges, the rate of dissociation must be reduced. This amounts to a reduction of the frequency factor for dissociation, as the decrease is due to a diffusive process which is not highly dependent on temperature. To this end we write

$$k_d = \delta_{cage}\, k_{d,o} \qquad \text{(IV-16)}$$

where δ_{cage} is a reduction factor, $k_{d,o}$ is the hypothetical rate constant without the cage effect.

The gel effect primarily affects bimolecular reactions involving functional groups belonging to aromatic clusters. Such reactions fall in the categories of hydrogen abstraction and radical recombination to

form a bridge. The chemical structure of coal is visualized as aggregates of aromatic clusters joined by bridges. As the number of these bridges increases the molecular configuration of the coal becomes a tight one. For the hydrogen abstraction reaction:

$$FH + F'\cdot \underset{k_b}{\overset{k_f}{\rightleftharpoons}} F\cdot + F'H$$

where FH, F·, F'H, F'· are functional groups attached to aromatic clusters, and k_f and k_b are the forward and backward rate constants, we consider an oversimplified pathway.

$$FH + F'\cdot \underset{k_1'}{\overset{k_1}{\rightleftharpoons}} (\dot{F}H\dot{F}')^* \underset{k_2'}{\overset{k_2}{\rightleftharpoons}} F\cdot + F'H$$

where $(\dot{F}H\dot{F}')^*$ represents an intermediate configuration when the two functional groups are brought to the vicinity required for reaction. If a pseudosteady state is assumed for this intermediate, then

$$\left.\begin{aligned} k_f &= \frac{k_1 k_2}{k_1' + k_2} \\ \text{and} \qquad k_b &= \frac{k_1' k'_2}{k_1' + k_2} \end{aligned}\right\} \quad \text{(IV-17)}$$

If we represent the abundance of bridges in terms of its ratio to the number of clusters, the gel effect indicates that both k_1 and k_2' above will be reduced by an increase of this M/N_c ratio. We may write

$$\left.\begin{aligned} k_f &= g_1\left(\frac{M}{N_c}\right)k_{f,o} \\ \text{and}\qquad k_b &= g_1\left(\frac{M}{N_c}\right)k_{b,o} \end{aligned}\right\} \qquad \text{(IV-18)}$$

where $g_1 \leq 1$ is a decreasing function of the ratio M/N_c, and $k_{f,o}$ and $k_{b,o}$ are hypothetical rate constants without the gel effect. The factor g_1 would apply to all hydrogen abstraction reactions between functional groups attached to aromatic ring systems.

The gel effect with respect to recombination to form bridges is somewhat different. Whereas in hydrogen abstraction reactions the two functional groups involved need to be brought temporarily within a distance close enough for reaction, in recombination reactions the two radicals involved must combine to form a chemical bond. The restriction imposed on this process by an increased M/N_c ratio must indeed be stronger. Hence, for the recombination

$$F\cdot + F'\cdot \xrightarrow{k_r} FF'$$

we modify k_r as

$$k_r = g_2\left(\frac{M}{N_c}\right)k_{r,o} \qquad \text{(IV-19)}$$

where g_2 is a stronger decreasing function of M/N_c than g_1 and $k_{r,o}$ is the rate constant applicable in the absence of the gel effect.

So far we have examined the cage and gel effects as they apply to our chemical system. The cage effect reduces the frequency factor of the bridge dissociation rate and the gel effect affects the rates of certain bimolecular reactions by factors which depend on the M/N_c ratio.

Admittedly, we do not have even crude information from which to assess quantitatively from theory the magnitude of these factors. They must unfortunately become adjustable parameters whose values we attempt to clarify when we compare computational results with experimental evidence. The strength of the gel effect suggests an increase of the activation energy for the bimolecular reactions affected. We assume

$$g_1 = \exp\left(-\frac{s_1 M/N_c}{RT}\right)$$
$$g_2 = \exp\left(-\frac{s_2 M/N_c}{RT}\right) \qquad \text{(IV-20)}$$

where s_1 and s_2 are proportionality factors treated as adjustable parameters.

To determine completely the chemical kinetics in the bulk phase we require the gas phase rate constants of the fifty-six reactions that we consider. The form

$$k_j = A_j \exp\left(-\frac{E_j}{RT}\right)$$

is assumed for all of them. In Appendix 1, the values of $\log_{10} A_j$ and E_j are tabulated and followed by a listing of the sources from which they are derived.

Having obtained a set of stoichiometric coefficients and rates for the elementary reactions, we proceed to describe, in mathematical terms, the transport of molecular species which is necessary for the generation of material products.

V DESCRIBING THE PYROLYSIS PROCESSES: MATHEMATICAL MODELING

PART 2: THE DIFFERENTIAL EQUATIONS

Transport Processes in the Bulk Phase

The elementary reactions which we have proposed merely describe the interactions among various functional groups. The actual mechanism of material transport must also be considered to complete a material balance on individual species. This mechanism has been discussed qualitatively in section III. Here we present a summary of the theory proposed and the additional assumptions necessary for the mathematical description of the processes involved.

1. The bulk phase in coal pyrolysis consists of an aggregate of subunits separated by the macropores and transitional pores. The subunit itself can be divided into two regions, the surface region (Region I) and the internal region (Region II).
2. Molecular species not attached to aromatic clusters can diffuse from the subunit to the transitional pores without further reactions. They include the species H_2, CH_4, RH, and R=.
3. Small radical species are so reactive that they will either abstract a hydrogen, add to a double bond, or recombine with some other radical species before moving to another region or the gas phase. These include $CH_3\cdot$, H·, and R·.
4. Molecular species containing one or two aromatic clusters will escape to the gas phase instantaneously if they are generated in region I.
5. For every aromatic cluster that escapes from region I to the gas

phase, there is one cluster that will transfer from region II to region I to fill the vacancy.

6. Aromatic clusters are only transferred from region I to the gas phase or from region II to region I. Each cluster that is transferred carries with itself an amount of each functional group proportionate to its (the cluster's) size and to the concentration of that group in the original region at that particular time.
7. The volume of region I and the concentration of clusters in region II stay unchanged.
8. Except for the transport processes mentioned in 5 above, there is no communication between region I and region II. The concentrations of functional groups may be different in these regions.
9. The set of elementary chemical reactions described previously is applicable to both regions.
10. Special assumptions are made of the distribution of bridges and clusters to permit the calculation of volatile fragment generation. They are described in detail as we set up the differential equations for the state variables.

Because of assumption 8 and the different transport mechanisms in regions I and II, the number of functional groups in each region must be accounted for separately. The state variables representing these functional groups are their concentrations based on a unit volume of the appropriate region, I or II. The differential equations, however, must be derived in terms of a material balance. The volumes of these regions, therefore, must be taken into account in the formulation. We

shall use subscripts I and II to describe the surface and the interior regions, respectively. We start with a volume V_b of the bulk phase consisting of V_I of region I and V_{II} of region II. For the gases, we denote species i as any one of CH_4, RH, R= or H_2, and obtain the following equations

$$\text{Region I:} \quad \frac{dn_{iI}}{dt} = \sum_j \nu_{ij} r_{jI} V_I \qquad i = CH_4, \text{ RH, R= and } H_2 \qquad \text{(V-1)}$$

$$\text{Region II:} \quad \frac{dn_{iII}}{dt} = \sum_j \nu_{ij} r_{jII} V_{II}$$

where n_i represents the number of moles of i generated, ν_{ij} is the stoichiometric coefficient of species i with respect to reaction j and V denotes the volume, r_j is the rate of reaction j in terms of the concentrations of the reactants, and t is time.

For the small radicals, i = $CH_3\cdot$, R· and H·, we have

$$\frac{d(c_{iI}V_I)}{dt} = \sum_j \nu_{ij} r_j V_I - \sigma_{iI} c_{iI} V_I + \sigma_{iII} c_{iII} V_{II} \qquad \text{(V-2)}$$

$$\frac{d(c_{iII}V_{II})}{dt} = \sum_j \nu_{ij} r_j V_{II} - \sigma_{iII} c_{iII} V_{II}$$

where the terms involving σ_i's represent the diffusive transport of the radicals into or out of the respective regions, and the σ_i's can be interpreted as characteristic diffusion times. Using assumption 3, we propose that diffusive transport of the radicals can be neglected when compared with the reaction terms and write

$$\frac{d(c_{iI}V_I)}{dt} = \sum_j \nu_{ij} r_j V_I \qquad \text{(V-3)}$$

and $$\frac{d(c_{iII}V_{II})}{dt} = \sum_j \nu_{ij} r_j V_{II}$$

From assumption 7, V_I is constant. The derivative in the second equation can be broken up into $(V_{II}\frac{dc_{iII}}{dt} + c_{iII}\frac{dV_{II}}{dt})$ so that

$$\frac{dc_{iI}}{dt} = \sum_j \nu_{ij} r_{jI} \qquad i = CH_3^{\cdot}, R^{\cdot} \text{ and } H^{\cdot}$$

and $$\frac{dc_{iII}}{dt} = \sum_j \nu_{ij} r_{jII} - \frac{c_{iII}}{V_{II}} \frac{dV_{II}}{dt} \qquad \text{(V-4)}$$

We proceed to derive an expression for $\frac{dV_{II}}{dt}$. For the other chemical species and the aromatic clusters, the material balance involves both chemical kinetics and transport terms. The concentration of aromatic clusters and the volume of both regions must be known before these terms can be determined. From assumptions 5 and 7, the concentration of aromatic clusters must both be unchanged. Since aromatic clusters are not created or destroyed in any chemical reaction, we have

$$\frac{d(N_c V_I)}{dt} = 0 = -\Omega_1 V_I + \Omega_2 V_{II}$$

$$\frac{d(N_c V_{II})}{dt} = N_c \frac{dV_{II}}{dt} = -\Omega_2 V_{II} \qquad \text{(V-5)}$$

where Ω_1 is the rate of transport of clusters from region I to the gas phase per unit volume of region I. Ω_1 is related to the rate of generation of volatile fragments. Under appropriate assumptions, it can be expressed as a function of the concentrations of bridges and

clusters in region I. Ω_2 is the rate of transport of clusters from region II to region I per unit volume of region II. We have then

$$\Omega_2 = \frac{\Omega_1 V_I}{V_{II}} \tag{V-6}$$

and

$$\frac{dV_{II}}{dt} = - \frac{\Omega_1 V_I}{N_c} \tag{V-7}$$

For each substituent functional group attached to an aromatic cluster, we have

$$\begin{aligned} \frac{d(c_{iI} V_I)}{dt} &= \sum_j \nu_{ij} r_{jI} V_I - \lambda_{iI} \Omega_1 V_I + \lambda_{iII} \Omega_2 V_{II} \\ \frac{d(c_{iII} V_{II})}{dt} &= \sum_j \nu_{ij} r_{jII} V_{II} - \lambda_{iII} \Omega_2 V_{II} \end{aligned} \tag{V-8}$$

where c_i denotes the concentration of species i in a particular region and λ_i denotes the number of functional groups i carried by each cluster from a particular region. λ_{iI} is a rather complex function of the state variables in region I. However, under assumption 6, we assert that

$$\lambda_{iII} = \frac{c_{iII}}{N_c} \tag{V-9}$$

A few rearrangements of equations (V-6) to (V-9) eventually yield

$$\begin{aligned} \frac{dc_{iI}}{dt} &= \sum_j \nu_{ij} r_{jI} - \Omega_1 (\lambda_{iI} - \lambda_{iII}) \\ \frac{dc_{iII}}{dt} &= \sum_j \nu_{ij} r_{jII} \end{aligned} \tag{V-10}$$

Equations (V-1), (V-4), (V-7), and (V-10), which are of rather simple forms, are the working equations for the state variables. The terms on the right-hand sides must all be expressed in terms of the independent variables in the differential equations. Such is the case with the rate terms r_j, which are functions of the functional group concentrations. Obviously, the functional forms of Ω_1 and λ_{iI} are required to determine the differential equations system completely.

The derivation of the rate at which volatile fragments become completely dissociated requires a rather subtle counting procedure and additional assumptions about the arrangements of bridges and clusters in the bulk phase. We propose the following model.

10a. The aromatic clusters in coal are arranged in a regular honeycomb pattern as in Figure V-1.

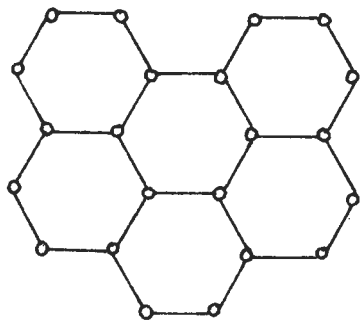

Figure V-1. A honeycomb arrangement for aromatic clusters.

They are connected by bridges much as the open circles are joined by the solid lines.

10b. For a system of N_c clusters and M bridges, the bridges are randomly joining the clusters subject to three constraints of:

(i) no more than two bridges between any two clusters;

(ii) each cluster being directly connected to at most three neighboring ones; and

(iii) no free fragments that contain only one or two clusters.

This arrangement limits the number of connections among N_c clusters to at most $3N_c/2$. Each connection may have either one or two bridges. Now for a system of N_c clusters and M bridges, we can calculate the expected number $\bar{n}$ of connections that have two bridges. The problem is identical to that of randomly putting M balls into $3N_c/2$ boxes, each box having no more than two balls. Here the balls correspond to the bridges and the boxes, the possible locations for a connection. We ask the probability ρ_k that exactly k boxes contain two balls each. This can be expressed as a ratio of binomial coefficients:

$$\rho_k = \frac{\text{number of favorable configurations}}{\text{total number of configurations}}$$

$$= \frac{\binom{3N_c/2}{k}\binom{3N_c/2 - k}{M - 2k}\, 2^{M-2k}}{\binom{3N_c}{M}}$$

$$= \frac{(3N_c/2)!\ \ M!\ \ (3N_c - M)!\ \ 2^{M-2k}}{k!\ (M - 2k)!\ (3N_c/2 - M + k)!(3N_c)!} \qquad \text{(V-11)}$$

Because N_c and M are both large numbers, we can approximate the

mean $\sum_{k=1}^{M/2} k\rho_k$ with the value of k that maximizes ρ_k. By using Stirling's approximation for the factorial function and differentiating one gets

$$\bar{\eta} = \frac{15M + \frac{3N_c}{2} - \left[\left(\frac{3N_c}{2}\right)^2 + 45MN_c - 15M^2\right]^{\frac{1}{2}}}{30} \qquad \text{(V-12)}$$

In a system containing M bridges and N_c clusters, the expected number of connections is therefore $M - \bar{\eta}$ and the probability that any two neighboring clusters are connected is

$$p = \frac{M - \bar{\eta}}{(3N_c/2)} \qquad \text{(V-13)}$$

When a bridge breaks, the probability that a connection is destroyed is

$$\mu = \frac{\text{number of connections with only one bridge}}{\text{total number of bridges}} = \frac{M - 2\bar{\eta}}{M} \qquad \text{(V-14)}$$

We now calculate the probabilities P_1 and P_2, respectively, that P_i = Pr {a fragment containing i clusters is released when a connection is destroyed}. For a fragment containing exactly one cluster to be released, there are N_c possible configurations because each cluster is an allowable configuration. Consider one cluster. It can become a volatile fragment by itself only if it has exactly one connection. The probability for this to be true is $3p(1 - p)^2$. We disallow the event that any cluster could be free by itself, or that it is linked to only

one other cluster (assumption 10b (iii)). This event has an *a priori* probability of $(1 - p)^3 + 3p(1 - p)^4$, so that

$$\Pr\{\text{a cluster is a precursor} \mid \text{no singlet or doublet is completely free}\} = \frac{3p(1 - p)^2}{1 - (1 - p)^3 - 3p(1 - p)^4} \qquad \text{(V-15)}$$

In a system of N_c clusters and M bridges, there are expectably $\frac{3N_c p(1 - p)^2}{1 - (1 - p)^3 - 3p(1 - p)^4}$ such precursor clusters. Each such precursor cluster has one connection that on breaking will release it. The total number of connections is $M - \bar{n}$. Hence, the probability $P_1 = \Pr\{\text{a fragment containing exactly one cluster is released when a connection is destroyed}\}$ is

$$P_1 = \frac{N_c}{M - \bar{n}} \frac{3p(1 - p)^2}{1 - (1 - p)^3 - 3p(1 - p)^4} = \frac{2(1 - p)^2}{1 - (1 - p)^3 - 3p(1 - p)^4} \qquad \text{(V-16)}$$

In a similar way, we can calculate P_2. There are $\frac{3N_c}{2}$ ways of selecting from N_c clusters neighboring doublets containing two clusters. The ways of obtaining a two-cluster fragment and the configurations that are prohibited by assumption 10b (iii) are presented in Figure V-2.

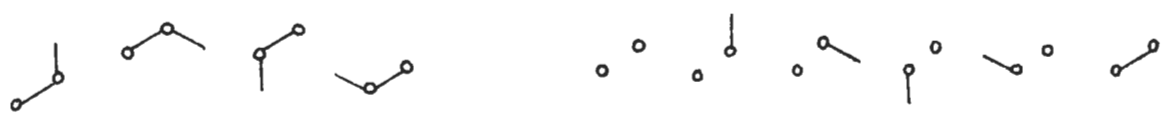

two-cluster fragment precursors disallowed configurations

Figure V-2. The ways to obtain a two-cluster fragment precursor from any given doublet.

The probability of having a two-fragment precursor is $4p^2(1 - p)^3$. The probability of the disallowed events is $(1 - p)^5 + 5p(1 - p)^4$. Hence,

$$\Pr\{\text{a doublet is a two-fragment precursor} \mid \text{no singlet or doublet is completely free}\} \quad \frac{4p^2(1 - p)^3}{1 - [(1 - p)^5 + 5p(1 - p)^4]} \tag{V-17}$$

For each allowable precursor, there is one connection that can break to release the two-cluster fragment. There are $\frac{3N_c}{2}$ different doublets. Similar to the derivation of P_1

$$P_2 = \frac{\left(\frac{3N_c}{2}\right)}{M - \bar{n}} \frac{4p^2(1 - p)^3}{1 - [(1 - p)^5 + 5p(1 - p)^4]}$$

$$= \frac{4p(1 - p)^3}{1 - [(1 - p)^5 + 5p(1 - p)^4]} \tag{V-18}$$

We finally relate the probabilities P_1 and P_2 to the rate of transport of clusters from region I per unit volume of region I. The rate of breaking of bridges per unit volume of region I, which we denote by r_b, is given by

$$r_b = f_1(k_1b_1 + k_2b_2 + k_3b_3) + k_{42}b_3. \tag{V-19}$$

where the four terms represent the only reactions by which bridges are broken. The factor Ω_1 is therefore given by:

$$\Omega_1 = \mu r_b(P_1 + P_2) \tag{V-20}$$

where μ, as given in equation (V-14), is the probability that a connection is destroyed when a bridge is broken. The factors μ, P_1 and P_2 are, under the model that we have proposed, functions only of the total concentration of bridges M which can obviously be calculated from the state variables, and the concentration of clusters which is a constant. The object of the model is merely to allow some quantitative assessment of the tightness of the coal's molecular structure when the number of bridges becomes high. The concentration of bridges is believed to exert a substantial effect on the potential amount of tarry material obtainable from a sample of coal. The decrease of μ, P_1 and P_2 as the value of M increases will bear this out in the pyrolysis simulation results.

The calculation of λ_{iI} is a straightforward, though somewhat tedious, materials accounting. Each cluster is assumed to have h_{aru} peripheral sites. A one-cluster fragment leaves with $(h_{aru} - 1)$ free sites because one of them is determined by the precursor reaction. A two-cluster fragment leaves with one connection or $2(2 - \frac{M\mu}{M-\bar{\eta}})$ bridges on the average. Hence, it leaves with $(2h_{aru} - 5 + \frac{2M\mu}{M-\bar{\eta}})$ free peripheral sites on which functional groups other than bridges may be attached. The total number of peripheral sites not occupied by bridges in the bulk phase is $(h_{aru} N_c - 2M)$. Hence, for the functional groups, other than bridges, that are attached to aromatic clusters (including C_1, C_2, $\alpha^{\cdot}$, $\beta_1^{\cdot}$, $\beta_2^{\cdot}$, $c_1^{=}$, $c_2^{=}$) equation (V-10) can be rewritten as

$$\frac{dc_{iI}}{dt} = \sum_j \nu_{ij} r_{jI} - \mu r_b c_i \left[\frac{P_1(h_{aru} - 1)}{h_{aru} N_c - 2M} + \frac{P_2(2h_{aru} - 5 + 2\xi)}{h_{aru} N_c - 2M} \right]$$

$$+ \frac{\Omega_1 c_{iII}}{N_c} \qquad \text{(V-21)}$$

where $\xi = \frac{M\mu}{M-\bar{n}}$

Each volatile fragment that contains two clusters will leave with one connection or 2 - μ bridges. Hence, for the bridges including b_1, b_2, b_3, $b_2^{\cdot}$, $b_3^{\cdot}$, $b_2^{=}$ and $b_3^{=}$, equation (V-10) takes the form:

$$\frac{dc_{iI}}{dt} = \sum_j \nu_{ij} r_{jI} - \mu r_b P_2 (2 - \xi) \frac{c_{iI}}{M} + \frac{\Omega_1 c_{iII}}{N_c} \qquad \text{(V-22)}$$

The working equations for the state variables are documented in Appendix 2 to facilitate the compilation of the necessary software for their solution.

The Effects of Oxygen Functional Groups

For the reactions among oxygen functional groups, we limit our consideration to those of decarboxylation, decarbonylation and dehydration involving phenolic groups. Of these, decarboxylation and decarbonylation are treated independently, as two first-order reactions, from the set of free radical reactions listed in Table IV-1.
One may write, stoichiometrically,

carboxylic acid $\longrightarrow CO_2$

and carbonyl groups $\longrightarrow CO$

However, the condensation of phenolic groups with hydrogen atoms attached to aromatic clusters results in the creation of a bridge affecting the very important M/N_c ratio. We attempt to model the dehydration as a first-order reaction

57. $\Phi OH + \{H\} \rightarrow$ a bridge + H_2O

with rate $r_{57} = g_2 k_{57}[OH]$ (V-23)

The inclusion of this reaction is considered necessary only for coals with high oxygen and phenolic group contents that exhibit a substantial quantity of chemical water on pyrolysis. For these coals, two more state variables would be incorporated to describe reaction 57; the concentration of phenolic groups [OH] and the resulting bridges of dehydration b_0. Similar to the other chemical species, these groups must be separately accounted for in regions I and II. The stoichiometry and rates of reaction 57 may be written

$$\begin{aligned} &\text{stoichiometry:} \quad OH \rightarrow b_0 + H_2O \\ &\text{rate:} \quad k_{57}[OH]g_2 \end{aligned} \tag{V-24}$$

The derivation of additional differential equations for these new species is identical to the previous ones. We have

$$\frac{dn_{H_2O}}{dt} = k_{57}[OH]_I V_I g_{2,I} + k_{57}[OH]_{II} V_{II} g_{2,II} \tag{V-25}$$

where n_{H_2O} is the amount of chemical water produced per unit volume of original bulk phase.

$$\frac{d[OH]_I}{dt} = -k_{57}[OH]_I g_{2,I} - \mu r_b [OH]_I \left[\frac{P_1(h_{aru} - 1)}{h_{aru}N_c - 2M} + \frac{P_2(2h_{aru} - 5 + 2\xi)}{h_{aru}N_c - 2M}\right]$$

$$+ \mu r_b (P_1 + 2P_2) \frac{[OH]_{II}}{N_c} \tag{V-26}$$

$$\frac{db_{0I}}{dt} = k_{57}[OH]_I g_{2,I} - \mu r_b P_2 (2-\xi)\frac{b_{0I}}{M} + \mu r_b (P_1 + 2P_2)\frac{b_{0II}}{N_c} \qquad (V\text{-}27)$$

$$\frac{d[OH]_{II}}{dt} = - k_{57}[OH]_{II} g_{2,II} \qquad (V\text{-}28)$$

$$\frac{db_{0II}}{dt} = k_{57}[OH]_{II} g_{2,II} \qquad (V\text{-}29)$$

where M is the sum of all bridges including b_{0I} in region I.

The Initial Conditions

The solution of the system of ordinary differential equations will require the values of all the state variables at some point in time, which naturally has to be the starting instant of pyrolysis. These initial values correspond to a characterization of the original structure of the particular coal of interest. Most desirably, they should be based on reliable experimental measurements from which useful deductions may be inferred. Here we attempt an analysis of the sources of experimental data that are presently available and discuss the extent to which these data can help define the initial conditions.

We have only considered that part of coal which is composed entirely of carbon, hydrogen and oxygen, and our state variables are descriptive only of an aromatic-aliphatic skeleton bearing hydrocarbon and phenolic functional groups. When we characterize the starting coal material for pyrolysis, we therefore exclude the components that do not participate in the primary reactions, such as nitrogen, sulfur, physical moisture and ash. Even carboxylic acid and carbonyl groups are

discounted from our consideration inasmuch as the production of carbon oxides is accounted for separately.

Most of the analytical methods used to date to study the chemical structure of coal involve IR or NMR spectroscopy either directly on coal or on its mild degradation products. Direct chemical methods, such as selectively reacting a particular functional group with an outside agent and measuring the specific products (Chakrabartty, 1972) are very difficult to apply because the outside agent has to react completely and specifically with the particular functional group. Such agents are in general hard to discover. Infrared spectroscopy can be applied to identify the presence of many functional groups in both solid coal and its degradation products such as tar and extracts, but it suffers from its lack of quantitative nature. The most powerful tool currently available for the quantitative characterization of coal structure is probably NMR spectroscopy.

Instead of measuring the amounts of various functional groups, proton H^1 NMR distinguishes among different types of hydrogen in a sample. One can obtain from it the proportions of aromatic and phenolic hydrogen (H_{ar}), hydrogen bonded to a carbon α to an aromatic cluster (H_α), and hydrogen farther from the ring (H_β). This is by far the most useful quantitative information for determining the initial values of the state variables. Proton NMR can be used on samples soluble in a solvent but not directly on coal. This may not be an exceedingly difficult problem because many soluble coal derivatives such as low-temperature tars and extracts bear very similar structure to the parent

coal as evidenced by infrared analysis (I. G. C. Dryden, 1963). From our own experimental experience, nearly all of the tarry products we obtain from pyrolysis are soluble in tetrahydrofuran (THF). Moreover, from our previous analysis of the mechanism of pyrolytic processes, the side chains on the aromatic clusters have a much slower rate of breaking than the bridges, so that at least for a brief stage after pyrolysis begins, the tar products should retain a substantial amount of primary characters. NMR analysis of this low-temperature tar, therefore, will closely reflect the hydrogen-type distribution that existed in the original coal, and the results are interpreted as representative of the parent coal sample.

C^{13} NMR is also a technique that shows great promise. It has the potential to provide valuable independent information on the chemical nature of various carbon atoms in a sample. Due to many areas of difficulty, this technique is yet at an exploratory stage. Its inherently low sensitivity means that a larger sample size is required. Also, the resolution of the overlapping signals in a C^{13} NMR spectrum of a mixture as complex as coal derivatives can be exceedingly difficult. Currently, it is only possible to measure the relative proportions of aromatic and aliphatic carbons (C_{ar} and C_{al}). Even so, it is the only technique that gives directly the aromaticity f_a, defined as

$$f_a \equiv \frac{C_{ar}}{C_{ar} + C_{al}} \qquad \text{(V-30)}$$

Undoubtedly, more information on the different types of carbon in coal will be available from C^{13} NMR as the current emphasis on coal

research has attracted much investigation in this area.

Our next quantity of interest is derived from elemental analysis. The elemental hydrogen to carbon H/C ratio is a powerful constraint on the possible assignments of our initial conditions. From the amount of carbon oxides that is obtained from pyrolysis, one can discount the amount of carboxylic acid and carbonyl groups from the H/C ratio obtained on a dry and ash-free basis. The adjusted H/C ratio will essentially be applicable to the carbon hydrogen skeleton to which the initial conditions correspond.

The information obtainable from NMR and elemental analysis can be treated as equivalent to four independent known quantities. They are

$$a \equiv \frac{H_\alpha}{H_\beta}$$

$$b \equiv \frac{H_{ar}}{H_{al}} \qquad \text{(V-31)}$$

$$f_a \equiv \frac{C_{ar}}{C_{ar} + C_{al}}$$

and $$z \equiv H/C$$

We consider a unit volume of the subunits in coal containing N_c aromatic clusters. The nature of the carbon and hydrogen atoms in this volume is described by six quantities: C_α, C_β, C_{ar}, H_α, H_β, and H_{ar} representing the number of carbon or hydrogen in each category, where H_{ar} also includes phenolic hydrogen.

In place of H_α, H_β, and H_{ar}, we introduce three parameters x, y, and S which convey essentially the same information, but which give a

more direct indication of the nature of the carbon hydrogen skeleton.

$$x \equiv \frac{H_\alpha}{C_\alpha}$$

$$y \equiv \frac{H_\beta}{C_\beta} \qquad \text{(V-32)}$$

and $$S \equiv H_{ar} + C_\alpha$$

Here x and y indicate the extent of branching at the α and other aliphatic carbons; the smaller their values, the higher will be the amount of secondary and tertiary substitutions. The parameter S denotes the total number of peripheral sites in the volume. If we define

$$h_{aru} \equiv \frac{S}{N_c}$$

$$c_{ar} \equiv \frac{C_{ar}}{N_c} \qquad \text{(V-33)}$$

it will be apparent that both h_{aru} and c_{ar} are specified by the size of the aromatic ring systems in the coal. As yet the average size of these systems cannot be fully established experimentally, although it has been crudely estimated from x-ray crystallography data (Hirsch, 1958) to range from two to four rings in bituminous coals and up to twelve rings for anthracites. We therefore consider the parameters h_{aru} and c_{ar} as adjustable quantities. After specifying h_{aru} and c_{ar}, we can proceed to calculate N_c as follows.

From the definition of the aromaticity f_a, the total number of carbon and hydrogen atoms in the carbon hydrogen skeleton is given by

$$C = \frac{C_{ar}}{f_a} = \frac{c_{ar}N_c}{f_a}$$

$$H = zC = \frac{zc_{ar}N_c}{f_a} \qquad \text{(V-34)}$$

The total weight of carbon and hydrogen represents an effective density ρ_{eff} of the subunits. In equation form this means

$$\frac{12}{f_a} c_{ar}N_c + \frac{z}{f_a} c_{ar}N_c = \rho_{eff} \qquad \text{(V-35)}$$

where ρ_{eff} is the density of the subunits on a dry, ash- and heteroatom-free basis. ρ_{eff} can be obtained from

$$\rho_{eff} = \frac{\rho_{coal} - \rho_{het} - \rho_{CO} - \rho_{COOH}}{1 - \varepsilon_M} \qquad \text{(V-36)}$$

where ρ_{coal} is the dry and mineral matter free density of the coal particles; ρ_{het} is the weight of all elements other than carbon and hydrogen per unit volume of coal particles; ρ_{CO} and ρ_{COOH} are the weights of the carbon atoms that belong to carbonyl and carboxylic acid groups, respectively, per unit volume of coal particles; and ε_M is the fractional porosity of the macropores and transitional pores. From equation (V-35) we have

$$N_c = \frac{f_a\rho_{eff}}{(12 + z)c_{ar}} \qquad \text{(V-37)}$$

With N_c, c_{ar} and h_{aru} now specified, we proceed to determine C_α, C_β, x, and y. The input parameters which we defined in (V-31) represent four independent equations in these unknowns, namely

$$xC_\alpha = ayC_\beta$$

$$b(xC_\alpha + yC_\beta) = S - C_\alpha \qquad \text{(V-38)}$$

$$\left(\frac{1}{f_a} - 1\right) C_{ar} = C_\alpha + C_\beta$$

$$xC_\alpha + yC_\beta + (S - C_\alpha) = z(C_\alpha + C_\beta + C_{ar})$$

whereby we can express C_α, C_β, x, and y explicitly in terms of a, b, z, f_a, S, and C_{ar}:

$$C_\alpha = S - \frac{b}{b + 1} \frac{z}{f_a} C_{ar}$$

$$C_\beta = \left(\frac{1}{f_a} - 1\right) C_{ar} - C_\alpha \qquad \text{(V-39)}$$

$$y = \frac{1}{b(a + 1)} \frac{S - C_\alpha}{C_\beta}$$

and $$x = ay \frac{C_\beta}{C_\alpha}$$

The parameters C_α, C_β, x, y, C_{ar}, S, and N_c, which we now have, cannot completely determine the initial values of all the state variables in our equation system. However, they do provide many useful relationships.

Returning to the model state variables, we note that all the radical species are formed during pyrolysis and can therefore be considered nonexistent in the original coal. In fact, the only functional groups initially present are the bridges, b_1, b_2, and b_3, the

chains c_1 and c_2, and α hydrogen. The subunit (bulk phase) is homogeneous at the start so that the functional group concentrations are the same for both regions I and II. Three relationships can be written for these functional groups,

$$H_\alpha + b_1 + 2b_2 + 2b_3 + c_1 + c_2 = 3C_\alpha$$

$$c_1 + \ell(c_2 + b_3) = C_\beta \qquad \text{(V-40)}$$

$$H_\alpha = xC_\alpha$$

The first equation merely expresses that the sum of all α carbon substituents must be three times the number of α carbon atoms. The second equation introduces an additional parameter ℓ which denotes an average length of the longer chains and bridges. ℓ is the average number of β and β^+ carbons in the longer chains and bridges. The magnitude of ℓ is indicated by the average molecular size of the alkanes and alkenes besides methane that are obtained from pyrolysis. The third equation is no more than the previous definition of x.

The complete determination of the six initial conditions requires three additional independent pieces of information. This is apparently the least degree of uncertainty that we can achieve, since we have yet no method to distinguish among the bridges or to measure their total concentration. After exhausting all information available, we need to make three assumptions. If we arbitrarily specify the concentrations of the bridges b_1, b_2, and b_3 (which, of course, also fixes the initial value of M/N_c), we will have

$$c_1 = \frac{\ell\left[(3 - x)\, C_\alpha - b_1 - 2b_2 - b_3\right] - C_\beta}{\ell - 1} \qquad \text{(V-41)}$$

and $$c_2 = (3 - x)\, C_\alpha - b_1 - 2b_2 - 2b_3 - c_1$$

and the six non-zero initial conditions completely determined. Finally, we have to prescribe as initial conditions the fractional volume of region II. This quantity, like the concentrations of the bridges, is treated as an adjustable parameter whose proper value must be obtained by comparing simulation results with experimental data.

Information Obtainable from the State Variables

Since the state variables represent the concentrations of the functional groups remaining, they inform us directly of the reactivity of the pyrolyzed coal. In order to be useful, however, the model should also provide practically important quantities such as the weight loss and the product distribution.

From the concentrations of various functional groups, we can obtain the weight of different types of carbon and hydrogen that remain in the carbon-hydrogen skeleton. We have

$$W_{C_\alpha} = \sum_{\text{regions I,II}} \frac{(\text{all } \alpha \text{ carbon substituents})}{3} \times V \times 12$$

$$W_{C_\beta} = \sum_{\text{regions I,II}} [c_1 + \beta_i \cdot + c_1 = + (c_2 + \beta_2 \cdot + c_2 = + b_3 + b_3 \cdot + b_3 =)\ell] \times V \times 12$$

$$W_{H_\alpha} = \sum_{\text{regions I,II}} H_\alpha V$$

$$W_{H_\beta} = \sum_{\text{regions I,II}} y \frac{W_{C_\beta}}{12} - (b_3= + c_1= + c_2=)\, V$$

$$W_{C_{ar}} = \sum_{\text{regions I,II}} c_{ar}\, N_c V \times 12 \qquad \text{(V-42)}$$

$$W_{H_{ar}} = \sum_{\text{regions I,II}} (h_{aru}\, N_c - \frac{W_{C_\alpha}}{12} - 2b_o)\, V$$

$$W_O = \sum_{\text{regions I,II}} [OH] \times V \times 16$$

where W indicates the weight of a particular type of atom remaining, and the summation is done over the two regions in the subunits. Here, the parameters ℓ, y, c_{ar}, h_{aru}, V_I, and N_c are constants and the rest state variables. The first four equations are straightforward accounting. The amount of β-hydrogen remaining is taken to be the amount of β-carbon multiplied by its initial share of substituted hydrogen, and subtracting from the result the amount of β-hydrogen lost because of the double bonds formed. The number of aromatic hydrogens left would be the number of peripheral sites minus the number of α-carbons and twice the number of bridges formed by dehydration of phenolic groups.

Because the system of equations is only concerned with the carbon hydrogen skeleton where the only heteroatoms considered are phenolic OH oxygen, the weight, and hence weight loss, that is considered in equation (V-42) pertains only to the formation of tar, hydrocarbon gases and chemical water. The formation of carbon oxides, which is accounted for separately from the carbon hydrogen skeleton, can be combined with equation (V-42) to yield a good representation of the weight loss on a dry and ash-free basis. Equation (V-42) also allows the computation

of the H/C ratio of the residue.

The system of equations monitors the cumulative amounts of hydrogen, methane, higher alkanes, and light olefins that are formed. We have

$$A_{CH_4} = n_{CH_4} \times 16$$

$$A_{H_2} = n_{H_2} \times 2$$

$$A_{RH} = n_{RH} \times (14\ell + 2) \qquad \text{(V-43)}$$

$$A_{R=} = n_{R=} \times (14\ell)$$

$$A_{H_2O} = n_{H_2O} \times 18$$

where the quantities in parentheses are the assigned molecular weights for RH and R=, and A denotes the amounts in grams.

The weight of tar liberated is the weight loss minus the total weight of the gases.

VI DESCRIBING THE PYROLYSIS PROCESSES: MATHEMATICAL MODELING

PART 3: TRANSPORT IN THE MACROPORES

Transport Processes in the Macropores and Transitional Pore

Complex and detailed as the model has been, it deals only with the physicochemical processes in the subunits while the eventual tar and gas products must be transported through the larger pores to the outside of the coal particle. To this transport process we now address our attention.

We begin the analysis by treating a coal particle being pyrolysed like a porous medium in which chemical reaction and material transport of products are taking place simultaneously. The gas phase in this porous medium is considered to consist of three components: tar, gases, and an inert component. For simplicity, we assume spherical geometry and a radius R_p of the particle. The subscript p is there to avoid confusion with the gas constant. We denote the tar, gas, and inert components, respectively, by the subscripts 1, 2, and 3. If r is the distance from the center of the particle, one can write the continuity equation for component i outside the particle ($r \geq R_p$) as

$$n_i = n_{io} \frac{R_p^2}{r^2} \qquad \text{(VI-1)}$$

where n_i is the molar flux of component i in a direction normal to the particle and o is a subscript pertaining to evaluation at the particle boundary. Moreover, assuming Fick's first law for the diffusion of component i outside the particle (again $r \geq R_p$), and ideal gas behavior for the equation of state, we write

$$n_i = y_i (n_1 + n_2 + n_3) - \frac{p}{RT} D_i \frac{dy_i}{dr} \qquad \text{(VI-2)}$$

where y_i is the mole fraction of component i. D_i is the diffusivity of component i in the mixture, and p, R, and T are the pressure, gas constant, and temperature, respectively. Since there is no resistance to bulk flow, there is no pressure gradient outside the particle so that the total pressure p can be denoted by a constant p_o. Equation (VI-2) can be solved for y_i using the boundary conditions

$$y_1(\infty) = y_2(\infty) = 0 \qquad \text{(VI-2a)}$$

and $$y_3(\infty) = 1$$

For i = 1 and 2 and $n_{To} = n_{1o} + n_{2o} + n_{3o}$ we have

$$y_i = \frac{n_{io}}{n_{To}} \left(1 - e^{\frac{-n_{To} R_p^2 RT}{D_i r p_o}}\right) \qquad \text{(VI-3)}$$

and $$y_3 = 1 - y_1 - y_2$$

However, the fluxes at the boundary must be related to the rate of generation inside the particle by

$$\int_S n_i dS = \int_V \gamma_i dV \qquad \text{(VI-4)}$$

where γ_i is the net rate of generation of component i per unit volume in the particle, and S and V are the particle surface and volume, respectively. If we assume that γ_i is everywhere the same inside, then

$$n_{io} = \frac{\gamma_i R_p}{3} \tag{VI-5}$$

In particular, $\gamma_3 = 0$ because there is no generation of the inert component. This means $n_3 = 0$ everywhere, and equation (VI-3) gives the mole fraction at the boundary.

$$y_i(R_p) = \frac{\gamma_i}{\gamma_1 + \gamma_2} \left(1 - e^{\frac{-(\gamma_1 + \gamma_2)R_p^2 RT}{3D_i p_o}}\right) \tag{VI-6}$$

The equation of continuity must also hold inside the particle so that for $0 \leq r \leq R_p$

$$\frac{1}{r^2} \frac{d}{dr}(r^2 n_i) = \gamma_i \tag{VI-7}$$

with boundary conditions $n_i(0) < \infty$

Consequently, $n_i = \frac{\gamma_i r}{3}$ (VI-8)

To describe the reaction and transport in the particle, we want to solve an equation similar to (VI-2) for the composition and pressure inside the particle. Depending on the rate of product generation, material transport may be predominantly driven by a pressure gradient so that the pressure is generally not constant in the porous medium. To describe the pressure, we need a constitutive flow equation and an equation of state. Without much detailed information on the physical properties of the fluid and the porous medium, we assume the simplest flow equation, i.e., Darcy's law,

$$v = \frac{-\kappa}{\eta} \frac{dp}{dr} \tag{VI-9}$$

$$y_i(R_p) = \frac{\gamma_i}{\gamma_1 + \gamma_2} \left(1 - e^{\frac{-(\gamma_1 + \gamma_2)R_p^2 RT}{3p_o D_i}}\right) \qquad \text{(VI-13a)}$$

as given in equation (VI-7), where $D_{i,e}$ is the effective diffusivity of i within the particle.

From equations (VI-8) to (VI-10)

$$n_i = -\frac{\gamma_i}{\gamma_1 + \gamma_2} \frac{p}{RT} \frac{\kappa}{\eta} \frac{dp}{dr} \qquad \text{(VI-14)}$$

so that

$$\left(y_i - \frac{\gamma_i}{\gamma_1 + \gamma_2}\right)\frac{\kappa}{\eta} \frac{dp}{dr} = -D_{i,e} \frac{dy_i}{dr} \qquad \text{(VI-15)}$$

Integrating and substituting for $y_i(R_p)$

$$y_i = \frac{\gamma_i}{\gamma_1 + \gamma_2} \left[1 - \exp\left(-\frac{(\gamma_1 + \gamma_2)R_p^2 RT}{3p_o D_i}\right) \exp\left(-\frac{\kappa}{\eta D_{i,e}} (p - p_o)\right)\right] \qquad \text{(VI-16)}$$

Equations (VI-12) and (VI-16) essentially relate the concentration profiles of the tar and gases within the particle which result from the interaction of chemical reaction, hydrodynamic flow and diffusive transport. More importantly, they describe the roles of the particle size (R_p) and external pressure p_o, two process variables of major interest, on this interaction. The net rate of generation γ_1 of tar per unit volume of coal particle is related, but not equal, to the rate of release of aromatic fragments from the subunits. As we recall, the aromatic fragments that go into the larger pores originate from the breaking of precursor bridges, which means that they escape to the gas phase with some radical sites. Depending on the concentration of these

sites and the residence time in the particle, these aromatic fragments may to some extent redeposit on the subunit without eventually coming out as tar products. Hence, for the aromatic fragments one can write

$$\gamma_1 = \gamma_f - \gamma_b \tag{VI-17}$$

where γ_f and γ_b are the forward and backward transport to the gas phase per unit particle volume. Specifically,

$$\gamma_f = \mu r_b \, (P_1 + P_2) \, (1 - \varepsilon_M) \tag{VI-18}$$

where $\mu r_b(P_1 + P_2)$ represents the molar rate of generation of fragments per unit volume of subunits (cf. equations (V-5) and (V-20)), and ε_M is the porosity associated with the macropores and transitional pores.

Reattachment to the subunits occurs when a fragment recombines, either with a radical site within the bulk phase, or with another fragment radical forming a large molecule too heavy to remain in the gas phase. The former is taken as a first-order, and the latter as a second-order, process in terms of the partial pressure of the aromatic fragments in the coal particle. In other words

$$\gamma_b = \omega_1 y_1 p + \omega_2 (y_1 p)^2 \tag{VI-19}$$

where ω_1 and ω_2 are the appropriate rate constants. Since γ_b is defined in terms of a unit particle volume, a factor of $(1 - \varepsilon_M)$ is inherently contained in the rate constants ω_1 and ω_2. We assume no further reactions for the gases so that γ_2 is given essentially by the rate of generation of gas within the subunits:

$$\gamma_2 = (1 - \varepsilon_M) \sum_{i,j} \nu_{ij} r_j \qquad \text{(VI-20)}$$

where the summation extends over all gas species i, and all reactions j that pertain to their generation.

Strictly speaking, γ_b represents a backward reaction term which should also be incorporated into the differential equations system for the bulk phase. However, judging from the complexity of the resulting system and the already many assumptions of ideal behavior, we shall ignore this backward contribution of materials to the subunits. This approximation can be justified a posteriori after we calculate γ_b and verify that it is small compared to γ_f.

To estimate γ_b, we need to determine six parameters: κ/η, D_1, $D_{1,e}$, D_2, ω_1, and ω_2. We now examine the simplest case corresponding to pyrolysis in vacuum, $p_o = 0$. From equation (VI-16)

$$y_1 = \frac{\gamma_1}{\gamma_1 + \gamma_2} \qquad \text{(VI-21)}$$

and equation (VI-19) can be written as

$$\gamma_b = \omega_1 \frac{\gamma_1}{\gamma_1 + \gamma_2} \left[\frac{(\gamma_1 + \gamma_2) R_p^2 RT\eta}{3\kappa} \left(1 - \frac{r^2}{R_p^2}\right) \right]^{1/2} + \omega_2 \frac{\gamma_1^2}{\gamma_1 + \gamma_2} \frac{R_p^2 RT\eta}{3\kappa} \left(1 - \frac{r^2}{R_p^2}\right) \qquad \text{(VI-22)}$$

The backward rate per unit volume of coal particles, which we define as Γ_b, is $\frac{1}{V}\int_V \gamma_b dV$. Therefore,

$$\Gamma_b = \frac{3}{4\pi R_p^3} \int_0^{R_p} \gamma_b (4\pi r^2)\, dr \qquad \text{(VI-23)}$$

Substituting equation (VI-22) for γ_b and using the approximation that $\gamma_1 = \gamma_f - \gamma_b$ does not change appreciably over the particle

$$\Gamma_b(\omega_1, \omega_2, \frac{k}{\eta}, R_p) = \frac{3\pi}{16}\, \omega_1 \frac{\gamma_1}{\gamma_1 + \gamma_2} \left[\frac{(\gamma_1 + \gamma_2) R_p^2\, RT\eta}{3\kappa}\right]^{\frac{1}{2}} + \frac{2}{15}\, \omega_2 \frac{\gamma_1^2}{\gamma_1 + \gamma_2} \frac{R_p^2\, RT\eta}{\kappa} \qquad \text{(VI-24)}$$

Equation (VI-24) states that at constant temperature and under vacuum, the backward rate Γ_b has a particularly simple dependence on the particle size, one having the form

$$\Gamma_b = AR_p + BR_p^2 \qquad \text{(VI-25)}$$

The magnitudes of $\omega_1\left(\frac{\eta}{\kappa}\right)^{\frac{1}{2}}$ and $\omega_2 \frac{\eta}{\kappa}$ for a certain temperature can be fitted from vacuum pyrolysis data using various particle sizes. γ_2 can be taken as the measured integral molar rate of generation of the gases, while γ_1, can be estimated from the amount of tar obtained and its measured molecular weight distribution. The difference in γ_1, $(\Delta\gamma_1)$ between different particle sizes then corresponds directly to $-\Delta\Gamma_b$, which can be used to fit $\omega_1 \left(\frac{\eta}{\kappa}\right)^{\frac{1}{2}}$ and $\omega_2 \frac{\eta}{\kappa}$ by equation (VI-24).

For more complicated cases where pyrolysis is done under an external pressure of an inert gas, equations (VI-12),(VI-16),(VI-19), and (VI-23) become the working equations.

Equation (VI-12) gives the pressure distribution p(r) within the particle; equation (VI-16) expresses the mole fraction y_1 in terms of p; while equation (VI-19) relates the local backward rate γ_b to the partial pressure ($y_1 p$). In principle, one can always integrate equation (VI-23) over the particle volume and get the volumetric backward contribution Γ_b in terms of p_o, γ_1, γ_2, R_p, T, $\frac{\kappa}{\eta}$, D_1, $D_{1,e}$, ω_1, and ω_2. One then fits the values of κ/η, D_1, $D_{1,e}$, ω_1, and ω_2 from experimental Γ_b data at various conditions and one will have explicitly the dependence of Γ_b on the external pressure, the particle size, and the temperature. Here, we examine more closely the roles of the permeability, the diffusivity, and the external pressure in some specific cases, aiming to obtain some simplified expressions as we did in the case of vacuum pyrolysis. This analysis should guide the design of future experiments to study macropore transport as well as aid the interpretation of the data obtained.

For a cylindrical pore of radius a, the average linear velocity is given by the Poiseuille formula

$$v_{pore} = \frac{a^2}{8\eta} \frac{\Delta p}{L} \qquad \text{(VI-26)}$$

where η is the viscosity of the fluid flowing and $\Delta P/L$ is the pressure gradient. If we assume that the macropore system is penetrated by cylindrical pores of a uniform size, we can identify equation (VI-26) with equation (VI-10) and estimate the permeability κ in terms of the uniform radius a and the porosity ε_M. Suppose also that the length L of these uniform pores is equal to the particle radius R_p. Then the number of pores in a particle can be expressed as

$$\frac{\varepsilon_M\left(\frac{4\pi R_p^3}{3}\right)}{\pi a^2 R_p} = \frac{\varepsilon_a(4\pi R_p^2)}{\pi a^2} \qquad \text{(VI-27)}$$

where ε_a is the fraction of external surface area that belongs to the macropores. Hence,

$$\varepsilon_a = \varepsilon_M/3 \qquad \text{(VI-28)}$$

Identifying $\Delta p/L$ with dp/dr, we have

$$v = -\frac{\kappa}{\eta}\frac{dp}{dr} = \varepsilon_a v_{pore} = \varepsilon_a \frac{a^2}{8\eta}\left(\frac{\Delta p}{L}\right) \qquad \text{(VI-29)}$$

so that

$$\kappa = \varepsilon_a \frac{a^2}{8} = \varepsilon_M \frac{a^2}{24} \qquad \text{(VI-30)}$$

For estimation purposes, we assign minimum values of 0.05 for ε_M and 300 $\mathring{A}$ for a, so that

$$\frac{\kappa}{\eta} \geq \frac{1.875 \times 10^{-6}}{\eta} \text{ atm}^{-1} \text{ cm}^2 \text{ sec}^{-1} \qquad \text{(VI-31)}$$

where η must be expressed in centipoise. This value has a magnitude similar to that reported by Feng and Stewart (Feng, 1973) for the permeability of a Harshaw porous solid ($\kappa/\eta = 0.8 \times 10^{-6}/\eta$). For this minimum value of κ/η, we can examine equation (VI-12) for the internal pressure buildup during pyrolysis, the key parameter now being

$\frac{(\gamma_1 + \gamma_2)R_p^2 RT\eta}{3\kappa}$. We have

$$p^2 = p_o^2 + \frac{(\gamma_1 + \gamma_2)R_p^2 RT\eta}{3\kappa}\left(1 - \frac{r^2}{R_p^2}\right)$$

We consider now a case of low temperature and low pressure pyrolysis (500^o C, and near atmospheric pressure).

Experimental observation indicates that at 500^o C the kinetics of weight loss are about 25% in half a minute. Taking the density of coal to be 1.2 gm/cm^3, the average molecular weight of the volatile products to be 50, and a particle radius of 100 microns

$$\frac{(\gamma_1 + \gamma_2)R_p^2 RT\eta}{3\kappa} \leq \frac{0.25 \times 1.2 \times 10^{-4} \times 82.06 \times 773 \times \eta}{3 \times 1.876 \times 10^{-6}}$$

$$= 226 \times \eta \text{ atm}^2 \qquad \text{(VI-32)}$$

where η is in centipoise. The viscosity of most gases is of the order 10^{-2} centipoise, so that under these conditions the internal pressure developed $(p - p_o)$ would be at most between one and several atmospheres.

We have seen that for vacuum pyrolysis the mole fraction y_1 is $\frac{\gamma_1}{\gamma_1 + \gamma_2}$. Under an external pressure p_o, y_1 is given by equation (VI-16)

$$y_1 = \frac{\gamma_1}{\gamma_1 + \gamma_2}\left[1 - \exp\left(\frac{-(\gamma_1 + \gamma_2)R_p^2 RT}{3p_o D_1}\right)\exp\left(\frac{-\kappa}{\eta D_{1,e}}(p - p_o)\right)\right]$$

which leads us first to examine the arguments of the two exponentials. The spatial dependence of y_1 is explicit in the second exponential, where we may put

$$p - p_o = \frac{1}{p + p_o}\,\frac{(\gamma_1 + \gamma_2)R_p^2 RT\eta}{3\kappa}\left(1 - \frac{r^2}{R_p^2}\right) \qquad \text{(VI-33)}$$

For 500° C and atmospheric pressure, p is about the same order of magnitude as p_o so we will, as a first approximation, replace $p + p_o$ by $2\,p_o$. Consequently,

$$y_1 = \frac{\gamma_1}{\gamma_1 + \gamma_2}\left[1 - \exp\left(\frac{-(\gamma_1 + \gamma_2)\,R_p^2 RT}{3p_o D_1}\right) \exp\left(\frac{-(\gamma_1 + \gamma_2)R_p^2 RT}{6p_o D_{i,e}}\left(1 - \frac{r^2}{R_p^2}\right)\right)\right] \qquad \text{(VI-34)}$$

Substituting previous values for γ_1, γ_2, R_p, T, and p_o

$$y_1 = \frac{\gamma_1}{\gamma_1 + \gamma_2}\left\{1 - \exp\left[-1.27 \times 10^{-3}\left(\frac{1}{3D_1} + \frac{1}{6D_{1,e}}\left(1 - \frac{r^2}{R_p^2}\right)\right)\right]\right\} \qquad \text{(VI-35)}$$

For most gases at 500° C the diffusivity D_1 would have value between 0.1 and unity (cm^2/sec). The effective diffusivity may be roughly taken as

$$D_{1e} = \frac{\varepsilon_M}{\delta} D_1 \qquad \text{(VI-36)}$$

where ε_M is the porosity and δ is a tortuosity factor of order 1, so that the argument in the exponential term in equation (VI-16) will be small under these conditions. Approximating $1 - e^{-x}$ by x, we have, from equation (VI-34)

$$y_1 = \frac{\gamma_1 R_p^2 RT}{3p_o}\left(\frac{1}{D_1} + \frac{1}{2D_{1,e}}\left(1 - \frac{r^2}{R_p^2}\right)\right) \qquad \text{(VI-37)}$$

Furthermore, from equation (VI-36), $D_{1,e}$ is expected to be a few percent of D_1 so that $1/D_1$ may be ignored when compared to $1/2D_{1,e}$ and

$$y_1 = \frac{\gamma_1 R_p^2 RT}{6p_o D_{1,e}} \left(1 - \frac{r^2}{R_p^2}\right) \tag{VI-38}$$

We define

$$C_1 = \frac{(\gamma_1 + \gamma_2) R_p^2 RT\eta}{3\kappa}$$

$$m^2 = \left(\frac{p_o^2}{C_1} + 1\right) \tag{VI-39}$$

$$C_2 = \frac{\gamma_1 R_p^2 RT}{6p_o D_{1,e}}$$

so that

$$y_1 = C_2\left(1 - \frac{r^2}{R_p^2}\right) \tag{VI-40}$$

and $$p^2 = C_1\left(m^2 - \frac{r^2}{R_p^2}\right)$$

Substituting equation (VI-37) into equation (VI-19) and integrating equation (VI-23), we may obtain a complicated but analytical expression for Γ_b

$$\Gamma_b = 3C_2\omega_1\left[\frac{m^2}{8}\left(p_o + C_1^{\frac{1}{2}} m^2 \sin^{-1}\frac{1}{|m|}\right) - \frac{1}{4}\frac{p_o^3}{C_1}\right]$$

$$- 3C_2\omega_1 C_1^{\frac{1}{2}}\left[\frac{m^6}{16}\sin^{-1}\frac{1}{|m|} + \frac{m^4}{16}\frac{p_o}{C_1^{\frac{1}{2}}} - \frac{m^2}{8}\left(\frac{p_o^2}{C_1}\right)^{3/2} - \frac{1}{6}\left(\frac{p_o^2}{C_1}\right)^{3/2}\right]$$

$$+ 3\omega_2 C_1 C_2^2\left(\frac{8m^2}{105} + \frac{97}{315}\right) \tag{VI-41}$$

γ_1, γ_2, R_p, and p_o are experimentally known quantities. From the

definition (VI-39), C_1 and m can be thought of as functions only of κ/η, while C_2 depends only on the diffusivity $D_{1,e}$

$$C_1 = C_1\ (\kappa/\eta)$$
$$C_2 = C_2\ (D_{1,e}) \qquad \text{(VI-42)}$$
$$m = m\ (\kappa/\eta)$$

Γ_b is a kinetic expression which consists of a first-order term involving ω_1 and a second-order term involving ω_2.

$$\Gamma_b = 3\omega_1 C_2(D_{1,e})\ f(\tfrac{\kappa}{\eta}) + 3\omega_2 C_2^{\,2}\ (D_{1,e})\ g(\tfrac{\kappa}{\eta}) \qquad \text{(VI-43)}$$

where

$$f(\tfrac{\kappa}{\eta}) = \left[\frac{m^2}{8}\left(p_o + C_1^{\frac{1}{2}}\, m^2 \sin^{-1}\frac{1}{|m|}\right) - \frac{1}{4}\frac{p_o^{\,3}}{C_1}\right] \qquad \text{(VI-44)}$$
$$- C_1^{\frac{1}{2}}\left[\frac{m^2}{16}\sin^{-1}\frac{1}{|m|} + \frac{m^4}{16}\,\frac{p_o}{C_1^{\frac{1}{2}}} - \frac{m^2}{8}\left(\frac{p_o^{\,2}}{C_1}\right)^{3/2} - \frac{1}{6}\left(\frac{p_o^{\,2}}{C_1}\right)^{3/2}\right]$$

and $$g(\tfrac{\kappa}{\eta}) = C_1\left(\frac{8m^2}{105} + \frac{97}{315}\right)$$

The relatively simple form of equation (VI-43) suggests that the values of $D_{1,e}$ and $\frac{\kappa}{\eta}$ may be fitted from pyrolysis weight loss data at 500^{o} C and various pressures and particle sizes. From equation (VI-24) and vacuum pyrolysis data, one can estimate the values of $\omega_1(\frac{\eta}{\kappa})^{\frac{1}{2}}$ and $\omega_2\,\frac{\eta}{\kappa}$. If we define

$$\theta_1 \equiv \omega_1(\tfrac{\eta}{\kappa})^{\frac{1}{2}}$$
$$\theta_2 \equiv \omega_2\,\tfrac{\eta}{\kappa} \qquad \text{(VI-45)}$$

$$F(\frac{\kappa}{\eta}) \equiv (\frac{\kappa}{\eta})^{\frac{1}{2}} f(\frac{\kappa}{\eta})$$

$$G(\frac{\kappa}{\eta}) \equiv (\frac{\kappa}{\eta})\, G(\frac{\kappa}{\eta})$$

then

$$\Gamma_b = \theta_1(\frac{\gamma_1 R_p^2 RT}{2p_o})\frac{1}{D_{1,e}} F(\frac{\kappa}{\eta}) + \frac{\theta_2}{12}(\frac{\gamma_1 R_p^2 RT}{p_o})^2 \frac{1}{D_{1,e}} G(\frac{\kappa}{\eta}) \qquad \text{(VI-46)}$$

With θ_1 and θ_2 already obtained from vacuum pyrolysis data, κ/η and $D_{1,e}$ can be fitted from experimental Γ_b values by varying p_o and R_p. The questionable assumption here is that $p = p_o$ can be taken as $2p_o$ ($\Delta p/p$ is small). This can be justified a posteriori by substituting the fitted value of κ/η into the pressure equation (VI-12) and calculating $p - p_o$. If necessary, one can iterate on Δp and κ/η to obtain the adjusted equation for Γ_b that corresponds to equation (VI-46). The adjusted equation will have the form

$$\Gamma_b = \theta_1(\frac{\gamma_1 R_p^2 RT}{cp_o})\frac{1}{D_{1,e}} F(\frac{\kappa}{\eta}) + \frac{\theta_2}{3}(\frac{\gamma_1 R_p^2 RT}{cp_o})^2 \frac{1}{D_{1,e}} G(\frac{\kappa}{\eta}) \qquad \text{(VI-47)}$$

where c is a constant in the approximation

$$p + p_o = cp_o \qquad \text{(VI-48)}$$

Chapters IV, V, and VI have been devoted to developing the theory and the equations for the model and describing the procedures with which we can assign the best available values to the necessary parameters. In the next chapter, we shall apply these equations and procedures systematically to simulate the pyrolysis of some coals, drawing information from all sources that are presently available, and identifying along the way

some relevant areas in which future experimentation would be of the most benefit.

VII. NUMERICAL SIMULATION OF THE PYROLYSIS PROCESSES

Scope

Coal is broadly classified, in descending order of rank, into anthracites, bituminous and subbituminous coals and lignites. In general, the higher its rank, the lower is its hydrogen to carbon ratio. Of these classes, bituminous and subbituminous coals are by far the most employed in commercial conversion processes because of their high reactivity and their ability to yield products of high hydrocarbon content. In this section we attempt to apply our mathematical model to the simulation of one bituminous and one subbituminous coal. The two types of coal are selected from those that have been studied experimentally in the author's own laboratory. The information that is used to estimate initial conditions and to adjust rate parameters includes:

1. elemental composition of the coals provided by their respective sources,
2. weight loss kinetics and gas analysis data obtained in pyrolysis experiments, and
3. proton NMR and gel permeation chromatography (GPC) data on pyrolysis tar products and solvent extracts.

The purpose of the simulation is threefold: first, to study the changes of each functional group during pyrolysis as an aid to understanding the physicochemical mechanism of pyrolysis; secondly, to examine the effects of temperature and coal type on the pyrolysis weight loss and product distribution; and thirdly, to identify the crucial parameters in the model through sensitivity testing so as to pinpoint critical areas where future experimentation can be most profitably

directed.

The procedures adopted in this simulation work are indicated in the schematic diagram of figure (VII-1). Using structural information from the elemental composition and the density of the coal, and from NMR analysis of its extracts and low temperature tars, we make necessary additional assumptions to determine initial values of all the state variables that are compatible with the input data. These initial conditions, together with the first estimated values of the rate parameters, complete the system of ordinary differential equations, which can now be solved numerically. The simulation is compared with experimental weight loss kinetics and product distribution. Some of the original assumptions and adjustable parameters are changed accordingly to bring the model simulation to agreement with observed phenomena. The final set of initial conditions and adjustable parameters constitutes an acceptable base case that describes the pyrolysis behavior of the coal in question. This base case is studied thoroughly in relation with the behavior of each functional group and with the physicochemical mechanism and how it is affected by the temperature. Finally, sensitivity testing is performed to identify the more critical parameters of the model.

Numerical Techniques

The initial value problem has forty-four variables (forty-nine when phenolic groups are included) and contains rate constants that are many orders of magnitude apart. It belongs to the class of stiff systems for which conventional numerical methods are unstable unless the time-step is kept exceedingly small. Its numerical solution is therefore effected by

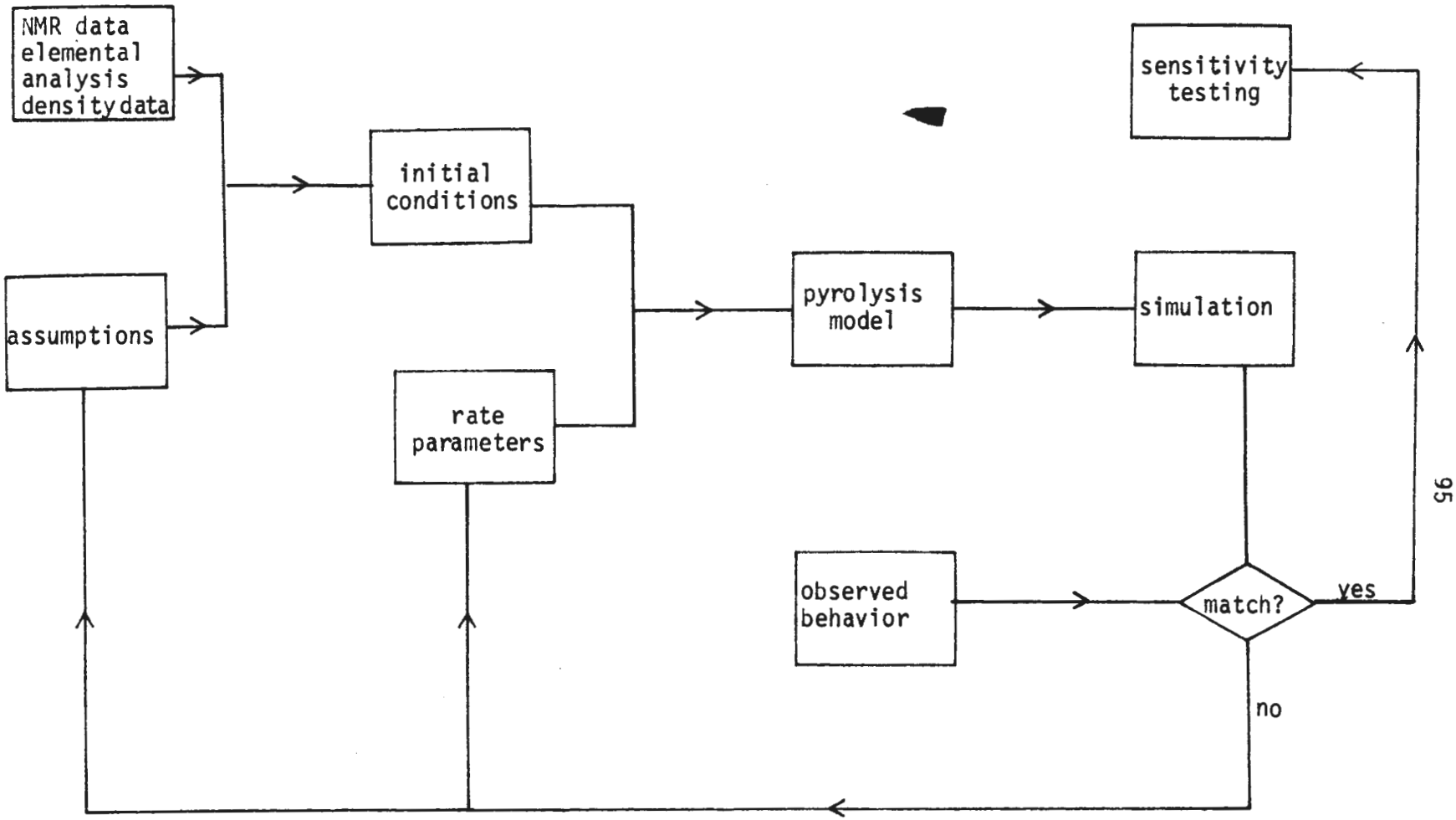

FIGURE (VII-1) Schematic diagram of the simulation procedures

an algorithm developed by Gear (Gear, 1971) which applies specifically to stiff equations. Gear's method requires the input of a Jacobian matrix $\{\frac{\partial \dot{y}_i}{\partial y_j}\}$ where the y's are the variables to be integrated. This matrix is obtained analytically by partial differentiation of each variable, a task which consumes most of the labor involved in the programming.

The equations are integrated with an error tolerance of 0.1% in double precision on an IBM 370/158 computer. Tighter error control did not appear to change the results. Integration is terminated when the rate of weight loss is less than 0.1% of the initial rate. The average computing time required for each integration is approximately 30 seconds.

Case 1: Hamilton High Volatile C Bituminous Coal

Available Data

Experimental data have been collected for a Hamilton high volatile C bituminous coal provided by the Occidental Research Corporation. The coal entails the following proximate and ultimate analyses.

Proximate (wt. %)		Ultimate (wt.% as received)	
volatile matter	35.08%	carbon	69.55%
moisture	4.49%	hydrogen	5.31%
ash	8.06%	nitrogen	1.47%
fixed carbon	52.37%	sulfur	2.66%

Pyrolysis experiments at various conditions of temperature, pressure and particle size were carried out and their corresponding weight loss measured. Proton NMR and GPC analyses were performed on the tar products obtained under vacuum at 500°C. The gaseous products including carbon

dioxide and hydrocarbons up to C_2 were collected and their amounts determined by gas chromatography. Inasmuch as the experimental part of this project involves the combined efforts of many investigators besides the author, its detailed procedures and methodology will not be discussed here but will be reported in a separate future publication.

Proton NMR spectroscopy on the tar products shows the following hydrogen distribution in a low temperature tar sample obtained under vacuum at 500°C after half a minute.

$$H_\alpha = 37\%$$
$$H_\beta = 30\%$$
$$H_{ar} = 33\%$$

The density of a dry sample of coal particles is measured by hexane displacement and the value found to be 1.20 gm/cm^3.

From the vacuum pyrolysis of 60-80 mesh coal samples with a duration of 30 seconds, the amounts of gaseous products obtained are (in mg/gm sample)

	CO_2	11.15	mg/gm sample
	CH_4	4.47	
	C_2H_4	1.56	
and	C_2H_6	3.75	

The total weight loss of the coal is 27.5%.

Initial Conditions

The proximateanalysis indicates that physical moisture accounts for 4.49 wt. % of the coal so that the hydrogen content in the carbon hydrogen skeleton is $(5.31 - 4.49 \times \frac{2}{18})$ or 4.81%.

To get the carbon content in the C-H skeleton, we exclude from the elemental analysis those carbon atoms belonging to carboxylic acid and carbonyl groups. The amount of carbon dioxide that is liberated on pyrolysis by this coal amounts to only 1%, which indicates only 0.27% by weight of carbon. The quantity of CO has not been determined accurately because of interference of air and methane in the gas chromatography analysis. An amount of 1% by weight of the coal is assumed so that 0.43% of the carbon will belong to carbonyl groups. The carbon content is therefore taken to be 68.84% and the atomic H/C ratio is 0.838. The macropores and transitional pores not penetrated by the hexane in the density measurement should be accounted for when we calculate the density of the carbon hydrogen skeleton per unit volume of bulk phase. This value is not available for this coal, but a value of between 2 to 10% for the macroporosity of coal in general is known (Gan, 1972). A value of 5% is taken for the macroporosity ε_M so that the effective density is

ρ_{eff} = density in hexane x weight fraction of the carbon hydrogen skeleton ÷ fraction of volume in the bulk phase

$$= \frac{1.20 \times (0.6884 + 0.0481)}{(1 - 0.05)} = 0.9303 \text{ gm/cm}^3$$

$$= 930.3 \text{ gm/}\ell \qquad \text{(VII-1)}$$

C^{13}NMR data are not available to the author at the time of writing. The following scheme is devised to determine appropriate initial conditions. The working equations are (V-37), (V-39) and (V-41)

$$\left.\begin{aligned} \rho_{eff} &= 930.3 \text{ gm}/\ell \\ a &= \frac{H_\alpha}{H_\beta} = 1.233 \\ b &= \frac{H_{ar}}{H_{al}} = 0.493 \\ z &= \frac{H}{C} = 0.838 \end{aligned}\right\} \quad \text{(VII-2)}$$

The schematic procedures of choosing a set of initial conditions are given in figure (VII-2) and described as follows.

We let the aromaticity vary between 0.4 and 0.8 at 0.005 intervals and compute the values of N_c, C_α, C_β, x and y corresponding to each value of f_a. To be consistent in this first step, we note that $0 \leqslant x \leqslant 3$ and $0 \leqslant y \leqslant 3$ by the very nature of the definitions of x and y. The values of f_a that will not meet these criteria are rejected. Instead of independently varying b_1, b_2 and b_3, we let their ratios $b_1:b_2:b_3$ be 1:2:1 and let the bridge-cluster ratio

$$\frac{M}{N_c} = \frac{b_1 + b_2 + b_3}{N_c} \qquad \text{(VII-3)}$$

be a free parameter varying from 1.1 to 1.9 at 0.1 interval, so that

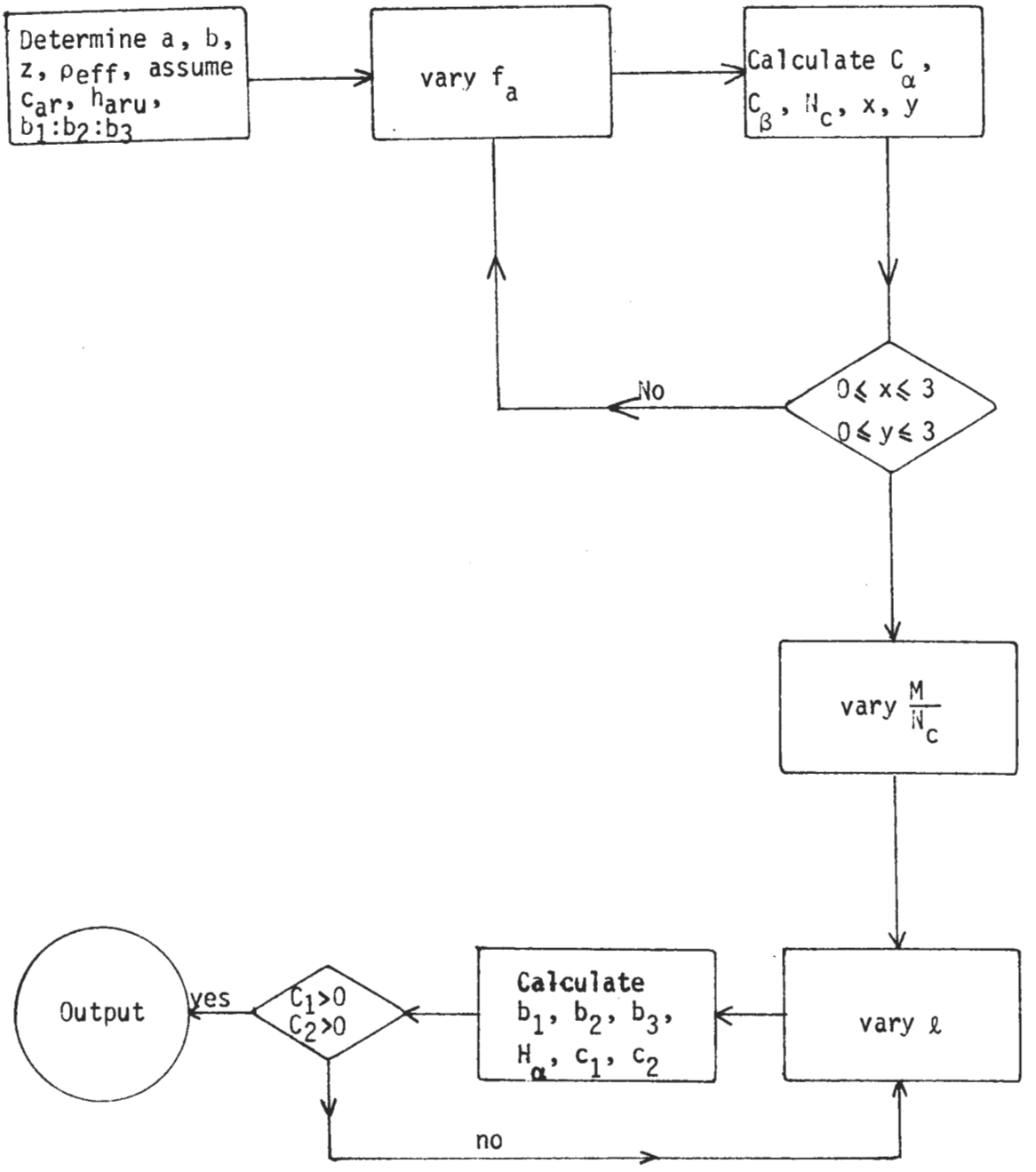

Figure (VII-2) Schematic Procedures of Choosing the Initial Conditions

$$\left.\begin{aligned} b_1 &= \left(\frac{M}{N_c}\right)\frac{N_c}{4} \\ b_2 &= \left(\frac{M}{N_c}\right)\frac{N_c}{2} \\ b_3 &= \left(\frac{M}{N_c}\right)\frac{N_c}{4} \end{aligned}\right\} \quad \text{(VII-4)}$$

Finally, we let the chain length ℓ vary from 2.1 to 3.0 at 0.1 interval and calculate c_1 and c_2 according to (IV-60) for each value of f_a, $\frac{M}{N_c}$, and ℓ. A computer program is written that outputs only those sets of values for which c_1 and c_2 are both positive. This computer experiment generates a multitude of initial conditions that are compatible with the information that we have and the assumptions that we make. These sets of allowable initial conditions all have aromaticity f_a between 0.605 and 0.64. The following set is chosen for the simulation.

$f_a = 0.635$, $\ell = 2.5$, $\frac{M}{N_c} = 1.5$, ring size = 3

$$\left.\begin{aligned} b_1 &= 1.2325 \text{ moles}/\ell \\ b_2 &= 2.4651 \text{ moles}/\ell \\ b_3 &= 1.2325 \text{ moles}/\ell \\ c_1 &= 5.2339 \text{ moles}/\ell \\ c_2 &= 2.1273 \text{ moles}/\ell \\ H_\alpha &= 22.459 \text{ moles}/\ell \\ x &= 1.7524 \\ y &= 1.3360 \end{aligned}\right\} \quad \text{(VII-5)}$$

$$\left.\begin{aligned} N_c &= 3.2868 \text{ moles}/\ell \\ V_I &= 0.15 \\ V_{II} &= 0.85 \end{aligned}\right\} \quad \text{(VII-5)}$$

The relatively low value of ℓ is selected because we have observed small proportions of propane and butane as compared to ethane. The higher value of c_1 than c_2 is chosen because methane is found to be the predominent product of pyrolysis.

Rate Parameters

The system of equations that describe the carbon hydrogen skeleton contain 56 rate constants for which Arrhenius factors and activation energies have been compiled and listed in Appendix 1. We start the simulation with these values but we have to adjust some of them to obtain a base case that demonstrates kinetic behavior similar to what is experimentally observed. Some adjustments of this nature are anticipated because the numbers listed in Appendix 1 are theoretical values for substituted benzenes which should reflect, but not necessarily be equal to, the actual rate constants suggested by the observed bahavior of coal. Hence to obtain the base case compatible with the observed kinetics of tar and gas evolution, we have to lower the activation energies of all dissociation reactions by about 8 Kcal/mole as shown in Table (V-1).

Table (VII-1) Adjustments of Reaction Rates to Fit Observed Kinetics

Reaction	Estimated rate		Adjusted rate	
Bond Dissociation	$\log_{10}A$	E (Kcal/mole)	$\log_{10}A$	E (Kcal/mole)
1. $b_1 \rightarrow \alpha\cdot + \Phi\cdot$	14.4	78.5	14.4	69
2. $b_2 \rightarrow \alpha\cdot + \alpha\cdot$	14.4	56.8	14.4	49
3. $b_3 \rightarrow \alpha\cdot + \beta_2\cdot$	14.4	68.6	14.4	61
4. $c_1 \rightarrow \alpha\cdot + CH_3\cdot$	15.3	73	14.9	62
5. $c_2 \rightarrow \alpha\cdot + R\cdot$	14.9	68.6	14.9	62
β-scission				
43. $\beta_2\cdot \rightarrow \alpha\cdot + R=$	12.8	28	12.8	33

The differences between the adjusted rate parameters and those for monosubstituted benzenes can be accounted for by two main reasons: the effects of many neighboring activating groups in coal and the differences in ring size of the aromatic units.

The rate constant for the β-scission reaction (#43) is also adjusted to match the amount of light olefins that is generated. The adjusted activation energy is 5 Kcal/mole over the estimated value.

To account for the cage and the gel effects, we have introduced three adjustable rate parameters. The Arrhenius factors for the dissociation of those bridges which do not generate any volatile fragments are reduced by a constant δ_{cage}. For hydrogen abstraction and recombination involving aromatic clusters, we have

for hydrogen abstraction $$k = k_o \exp\left(-\frac{s_1 M/N_c}{RT}\right)$$

for recombination $$k = k_o \exp\left(-\frac{s_2 M/N_c}{RT}\right) \qquad \text{(VII-6)}$$

where k and k_o are the rate constants with and without the gel effect, and s_1 and s_2 are adjustable parameters. In view of the lack of information, we have assumed $s_1 = s_2$ for the simulation, although our computer program for the model can accommodate different input values of s_1 and s_2. For the base case, the values of s_1 and δ_{cage} are 5 Kcal/mole and 0.1 respectively.

Incorporation of Carbon Oxides

The presence of carboxylic acid and carbonyl groups accounts for a total of 2% of the original weight of the coal. In this simulation the depletion of these groups is represented as first order reactions. Thus

$$W_{COOH} = W_{o,COOH}\, e^{-k_{COOH} t} \qquad \text{(VII-7)}$$

and $$W_{CO} = W_{o,CO}\, e^{-k_{CO} t}$$

where W is the weight of the functional group remaining, W_o is the original weight and k is the first order rate constant.

Since the liberation of carbon dioxide is very fast at pyrolysis temperature, a large value of 1 sec^{-1} is assumed for k_{COOH}. A correspondingly smaller value of 0.1 sec^{-1} is assigned for k_{CO}. The loss of carbon oxides is incorporated in the overall weight loss kinetics.

Simulation Results and Discussion

Following the pathway indicated in figure (VII-1), we obtain a base set of initial conditions and rate parameters as discussed earlier, and the system of equations is integrated for four temperatures (450°C, 500°C, 550°C, and 600°C) up to a minute or until the rate of weight loss has decreased to less than 0.1% of its initial value. The simulation results of this base case are presented from figure (VII-4) to figure (VII-23) where available experimental data points are represented by X marks.

The practically important variables that are included in this model are the weight loss, the relative amounts of the tar and gas products, and the amounts of the different gases obtained. As is generally observed, the weight loss (figure (VII-4)) undergoes an initial fast phase and then appears to taper off to a steady level. The relative (cumulative) weight ratio of the tar and gases (figure (VII-5)) is much higher at the start and again tapers off in time to a steady value. In calculating this ratio, the gases include the species CH_4, RH, R= and H_2. The cumulative amounts of various gases, and the olefin/paraffin ratio $A_{R=}/(A_{CH_4} + A_{RH})$ are shown in figures (VII-6) to (VII-10).

This particular behavior of product evolution can best be explained by considering the changes of the relevant model state variables in the context of the pyrolysis mechanism. These variables can roughly be divided into two categories and five classes:

Category A active species

1. breakable bridges, (b_1, b_2, b_3)
2. free radicals, ($\alpha\cdot$, $b_2\cdot$, $b_3\cdot$, $\beta_1\cdot$, $\beta_2\cdot$)
3. breakable chains, (c_1, c_2)

Category B inactive species

4. inactive bridges (b_2= and b_3=)
5. inactive chains (c_1= and c_2=)

The breakable bridges are intimately related with the kinetics of tar generation inasmuch as volatile aromatic fragments can only be created through the breakage of bridges. The breakable chains are much related with the gases because they produce small alkyl radicals that most likely will abstract hydrogen to become alkanes. The inactive species tend to deactivate the coal with two basic effects:

(1) the double bond deactivates its neighboring group (e.g., the dissociation $\Phi\overset{CH_3}{\overset{|}{C}}=CH_2 \rightarrow \Phi\dot{C}=CH_2 + CH_3\cdot$ does not occur), and

(2) the inactive bridges raise the M/N_c ratio which reduces the probability of volatile fragments.

The free radicals which interact with each other through hydrogen abstraction can be thought of as the center of communication among these classes of species. Figure (VII-3) is an attempt to bring out the role of the free radicals. Here the circles represent eventual pyrolysis products and the rectangles the five classes of species. The transformation from one class to another is indicated by an arrow accompanied by the corresponding reactions. Those reactions with only

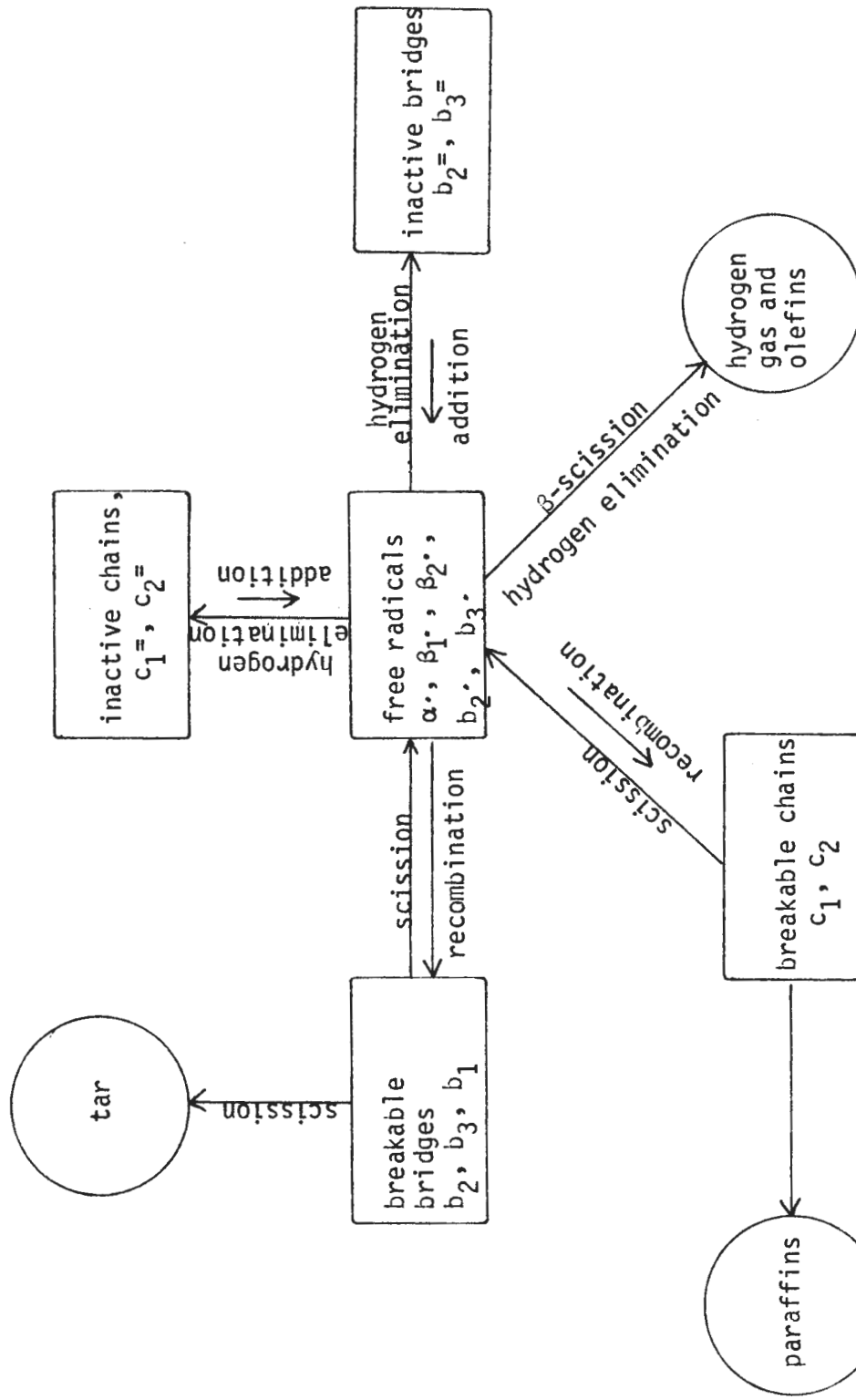

Figure (VII-3) A Simplified Schematic Representation of the Role of the Free Radicals

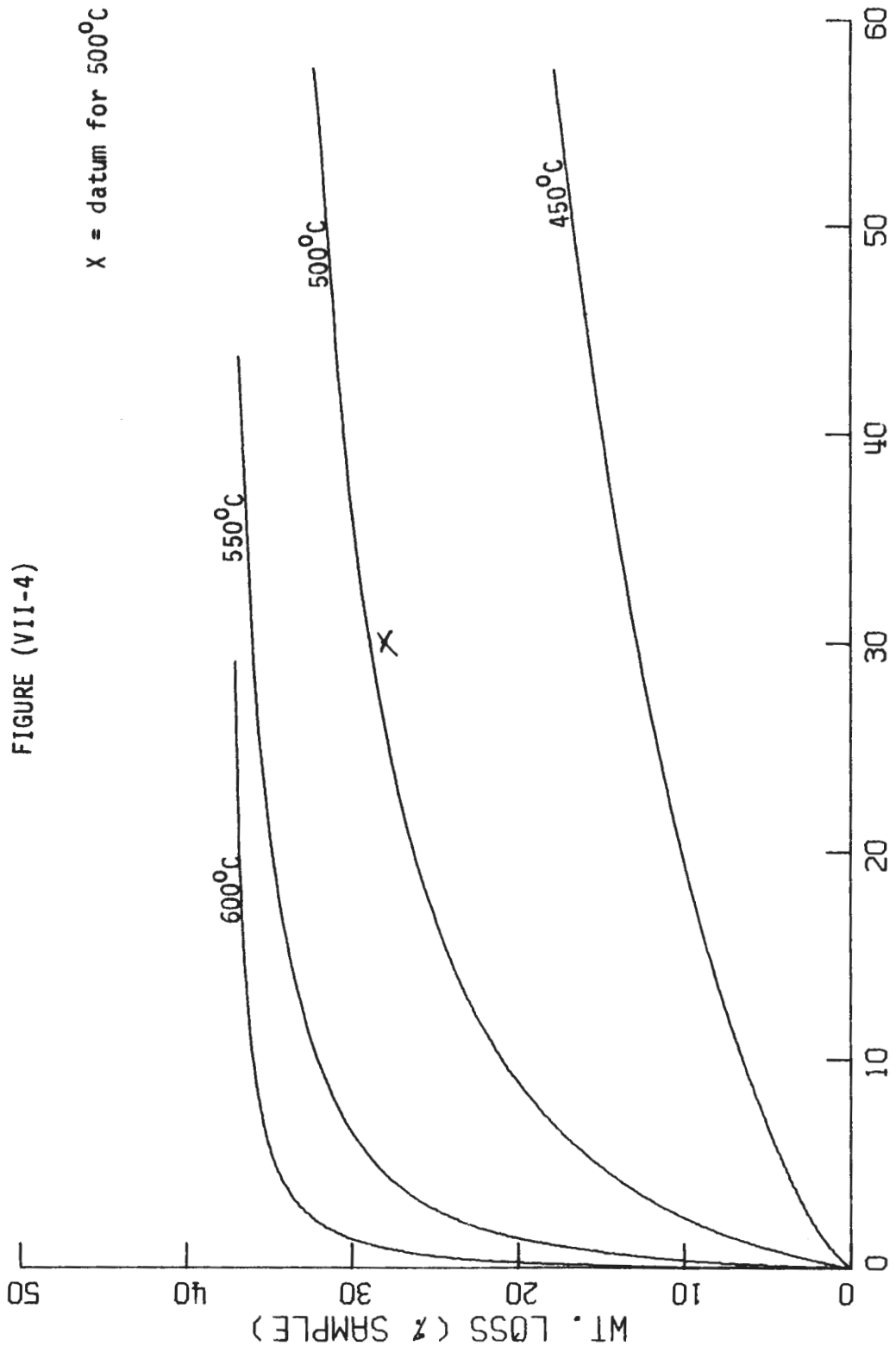
X = datum for 500°C
600°C
550°C
500°C
450°C
X
WT. LOSS (% SAMPLE)
0
10
20
30
40
50
TIME (SEC)
0
10
20
30
40
50
60

FIGURE (VII-4)

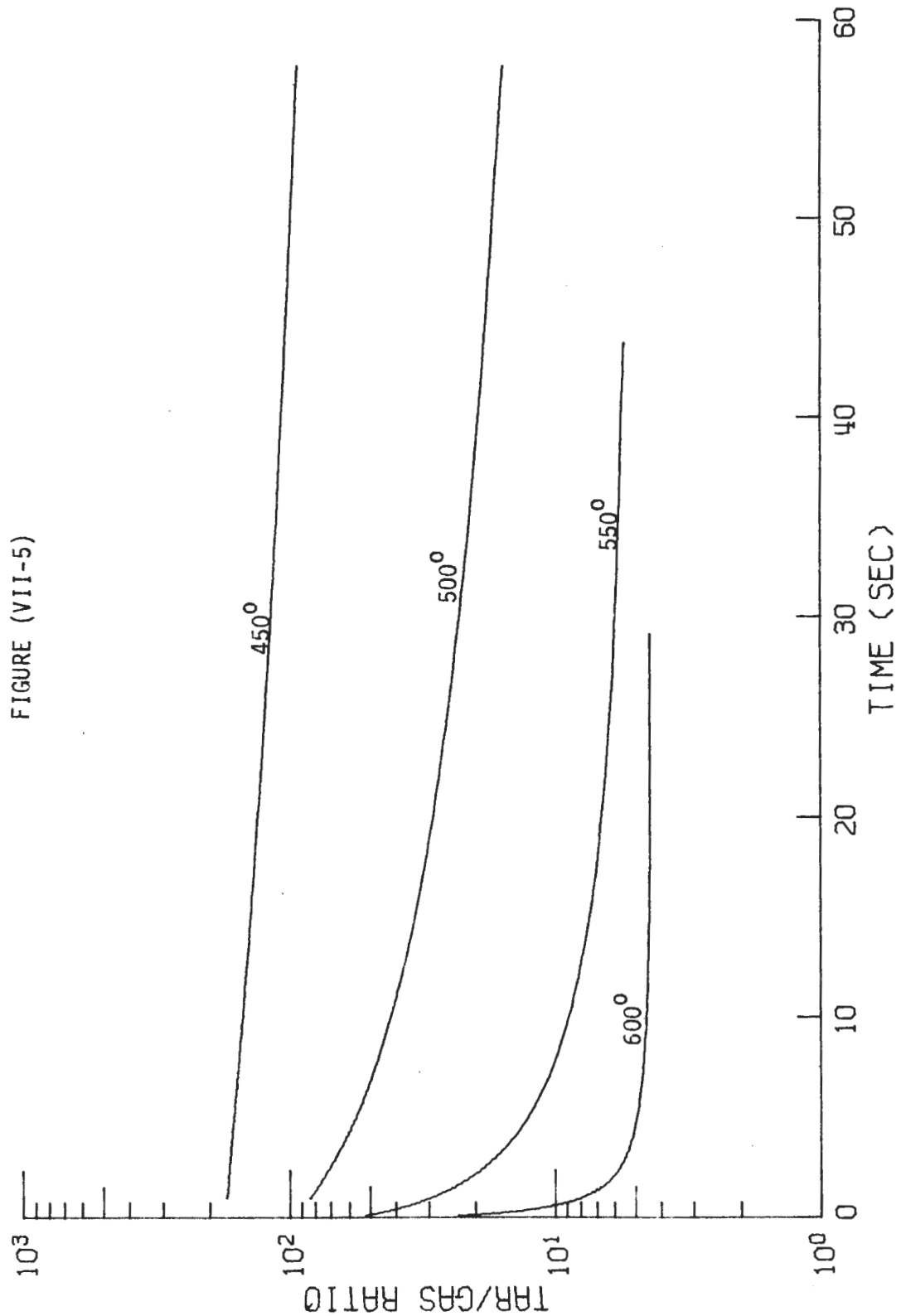
TAR/GAS RATIO
10^3
10^2
10^1
10^0
0
10
20
30
40
50
60
TIME (SEC)
450°
500°
550°
600°

FIGURE (VII-5)

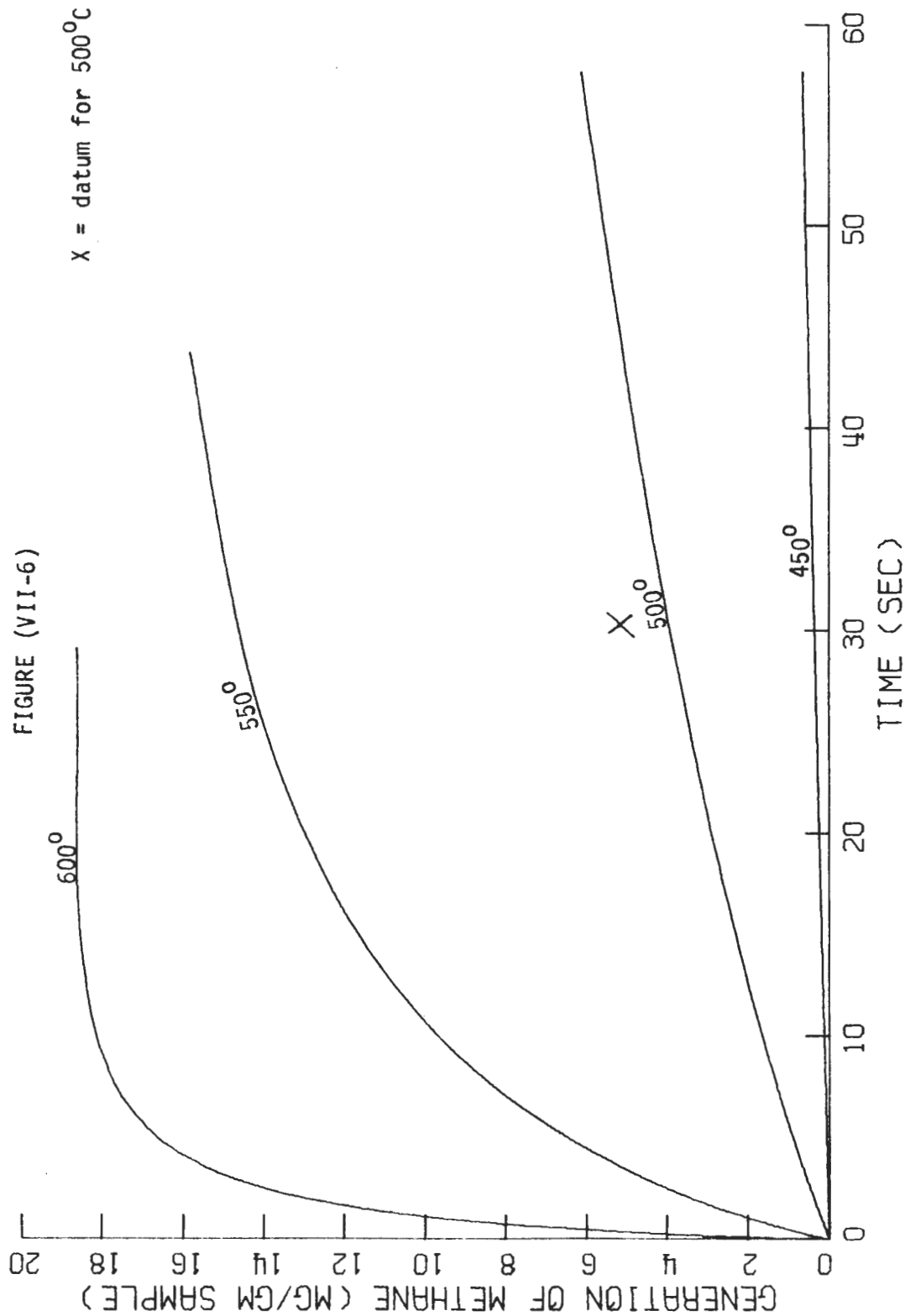
FIGURE (VII-6)
X = datum for 500°C
600°
550°
500°
450°
X
GENERATION OF METHANE (MG/GM SAMPLE)
0
2
4
6
8
10
12
14
16
18
20
TIME (SEC)
0
10
20
30
40
50
60

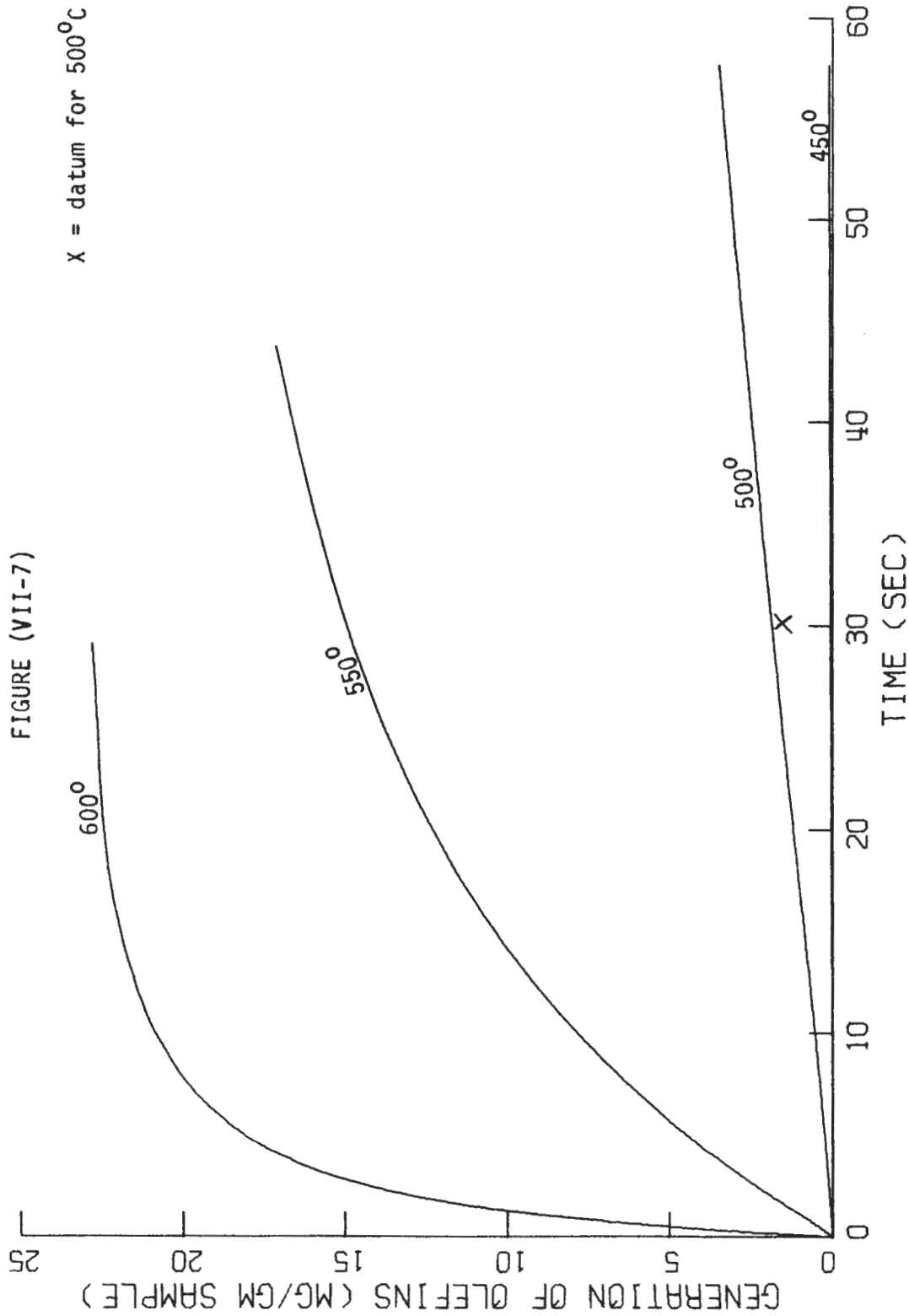
FIGURE (VII-7)
X = datum for 500°C
600°
550°
500°
450°
X
GENERATION OF OLEFINS (MG/GM SAMPLE)
TIME (SEC)
0
5
10
15
20
25
0
10
20
30
40
50
60

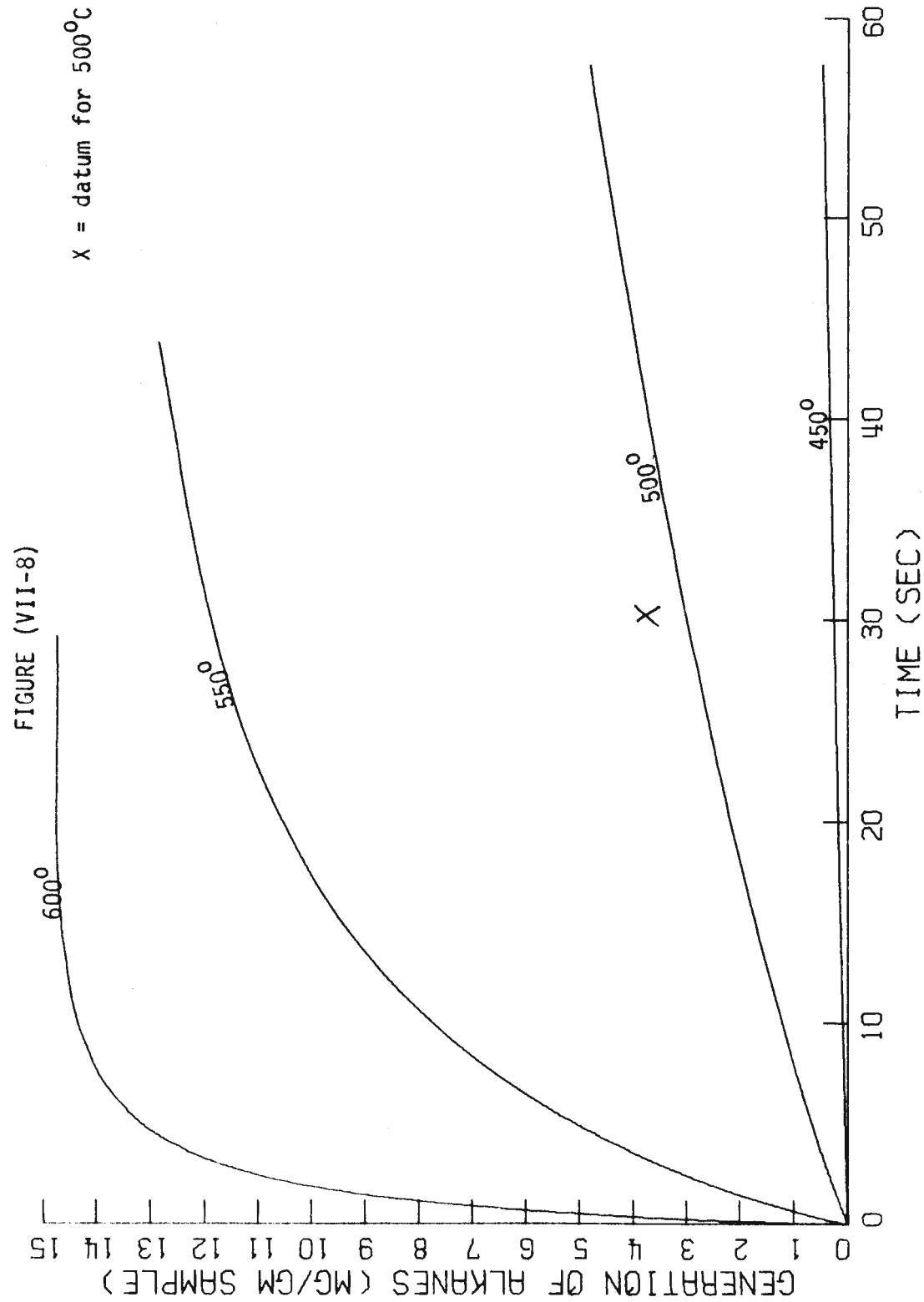
FIGURE (VII-8)
X = datum for 500°C
600°
550°
500°
450°
X
GENERATION OF ALKANES (MG/GM SAMPLE)
0 1 2 3 4 5 6 7 8 9 10 11 12 13 14 15
TIME (SEC)
0 10 20 30 40 50 60

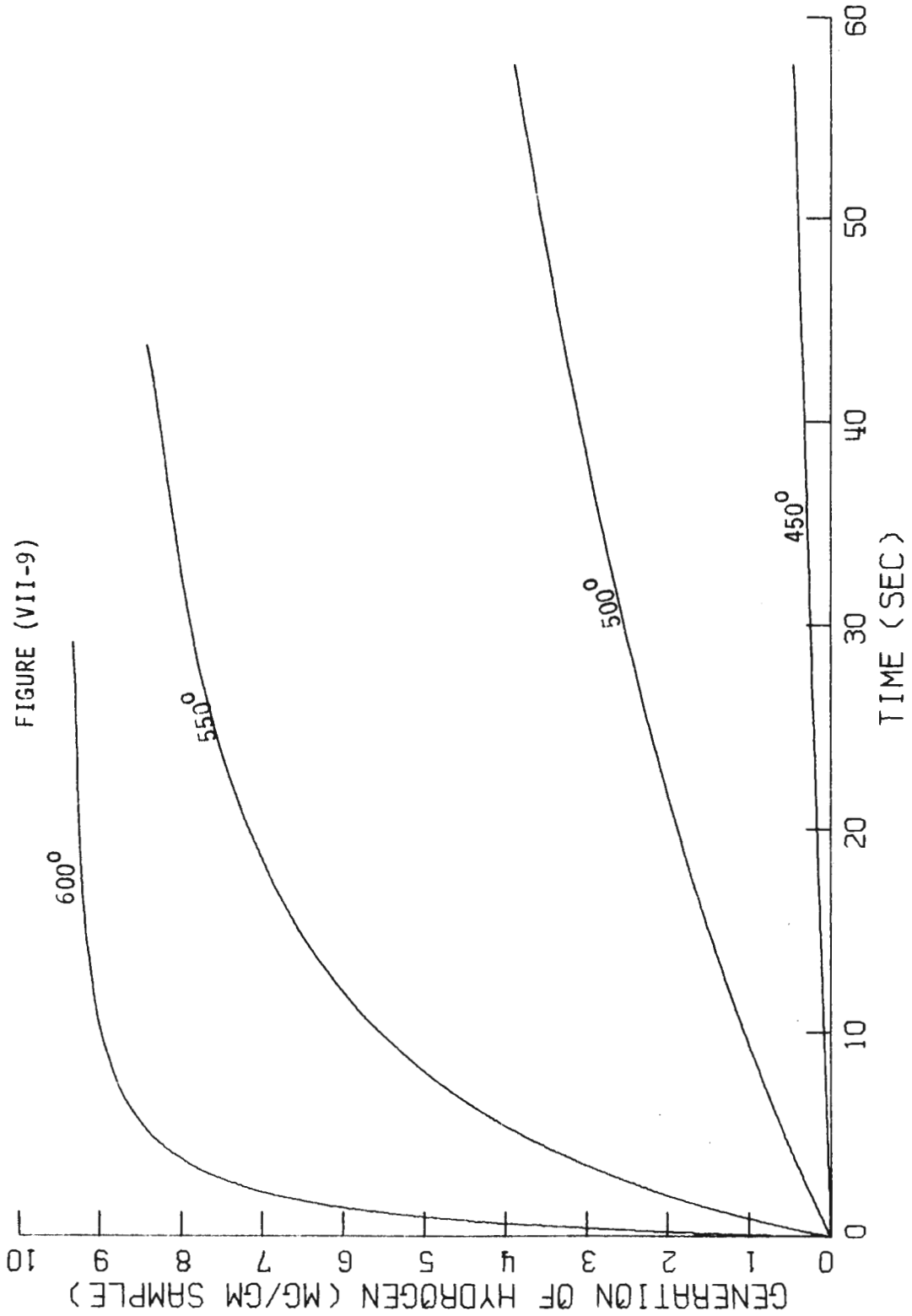
GENERATION OF HYDROGEN (MG/GM SAMPLE)
0
1
2
3
4
5
6
7
8
9
10
TIME (SEC)
0
10
20
30
40
50
60
600°
550°
500°
450°

FIGURE (VII-9)

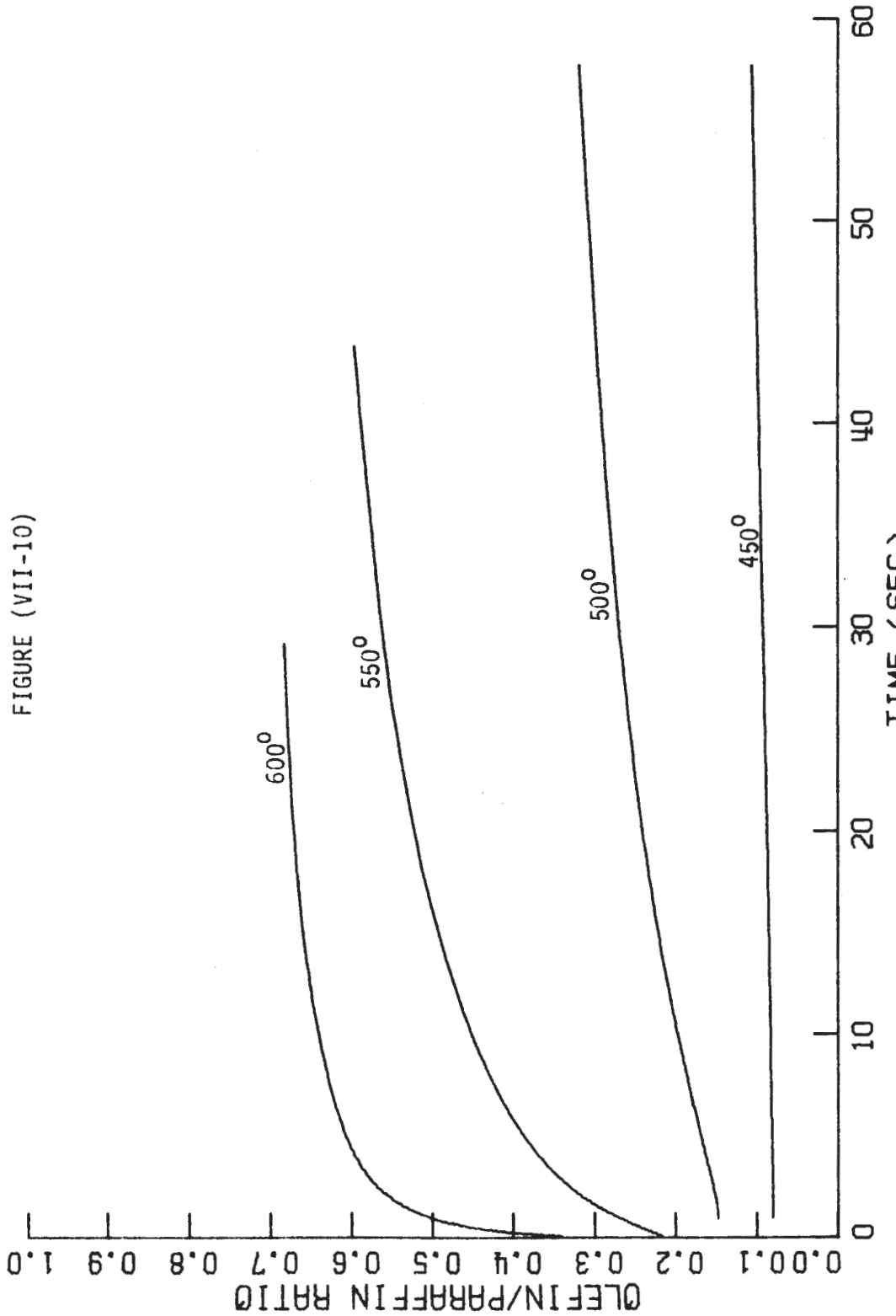

FIGURE (VII-10)

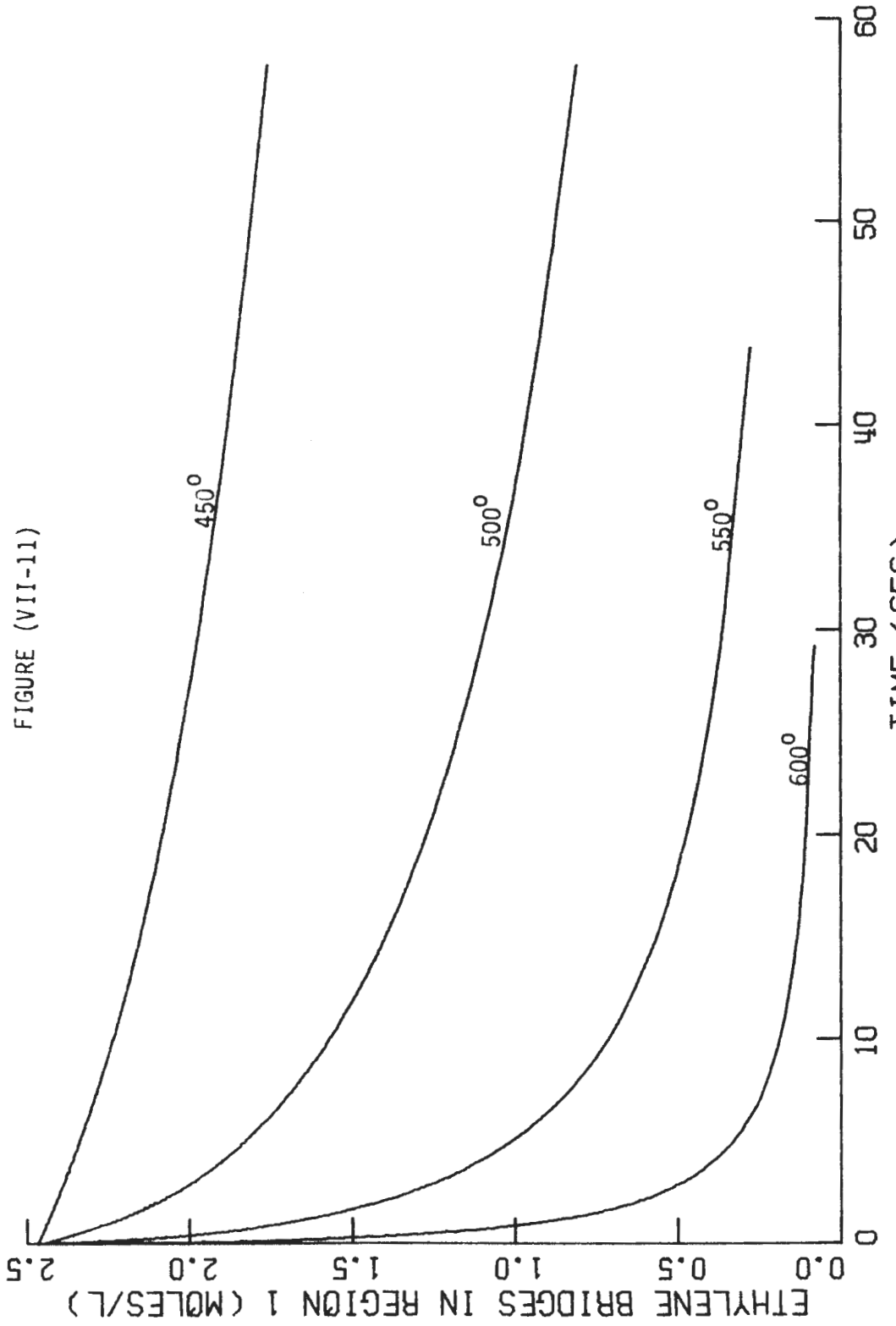

FIGURE (VII-11)

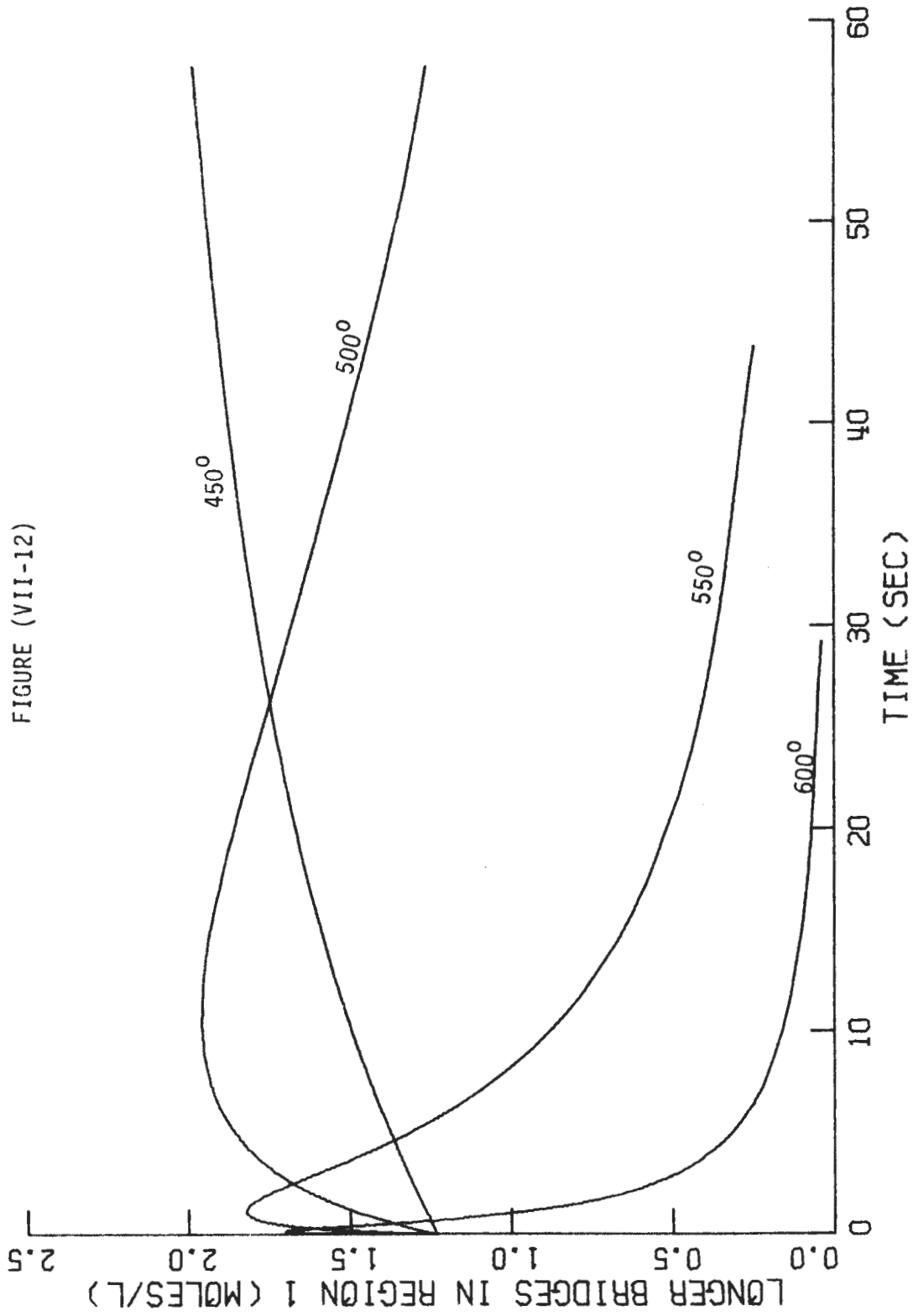

FIGURE (VII-12)

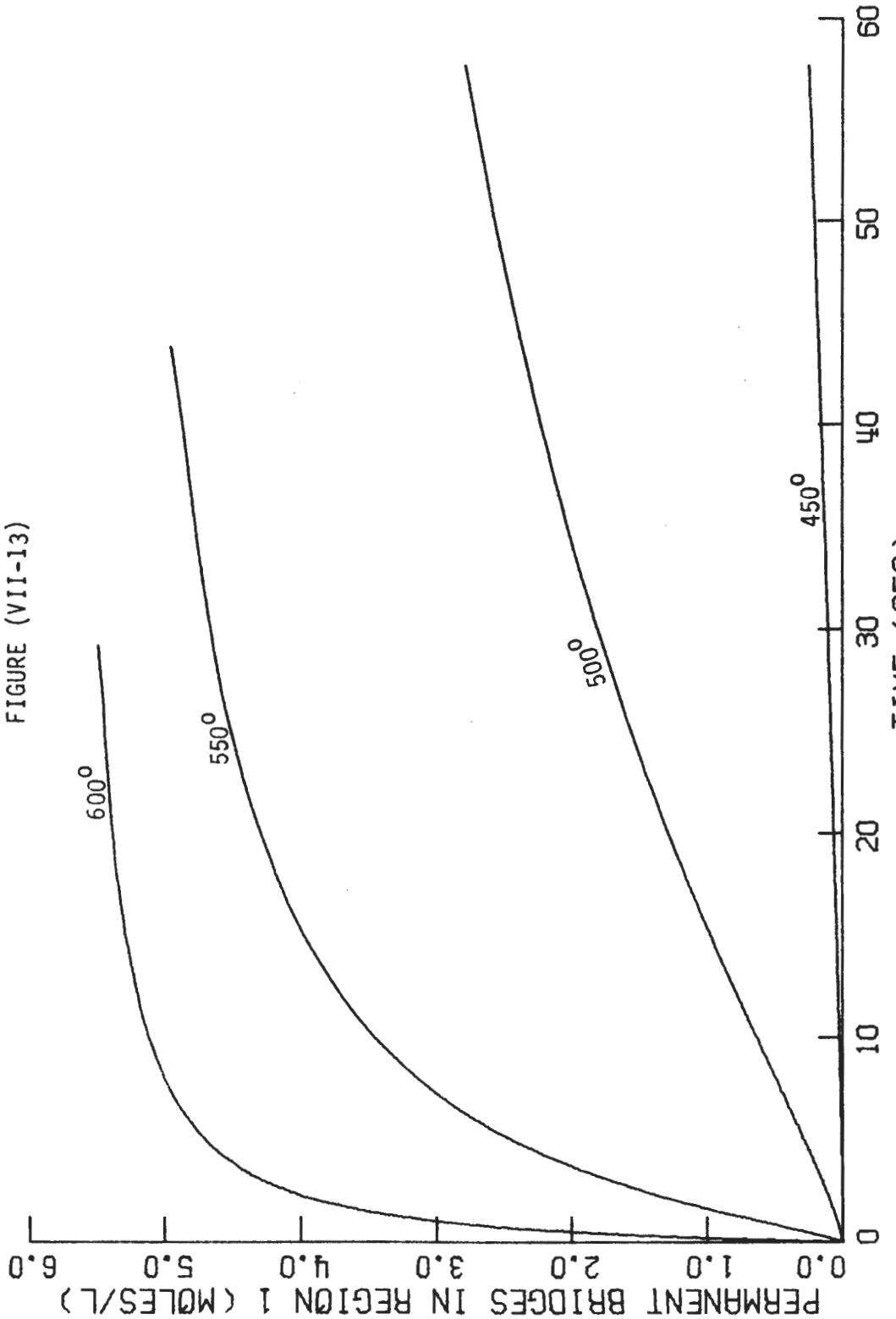

FIGURE (VII-13)

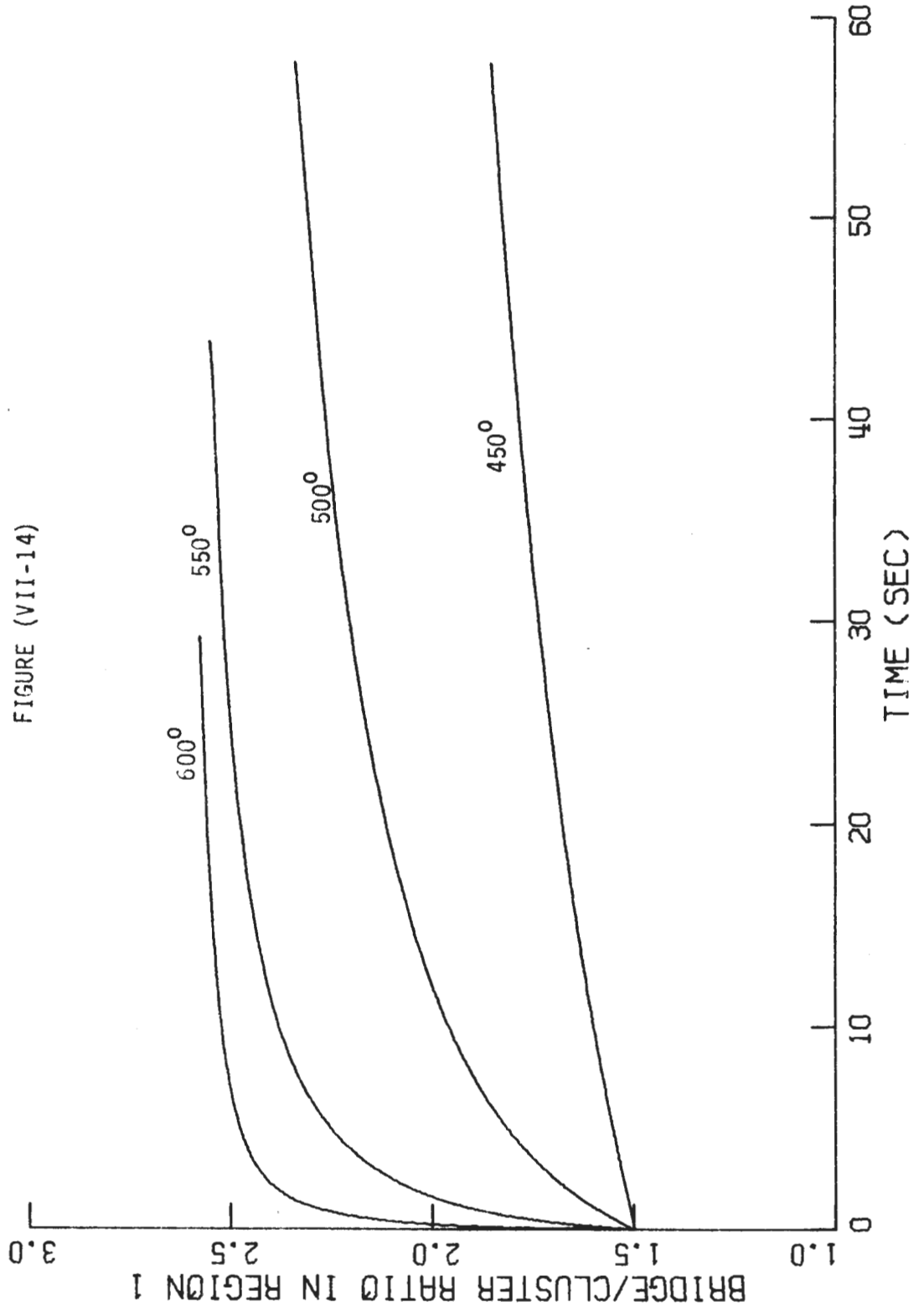

FIGURE (VII-14)

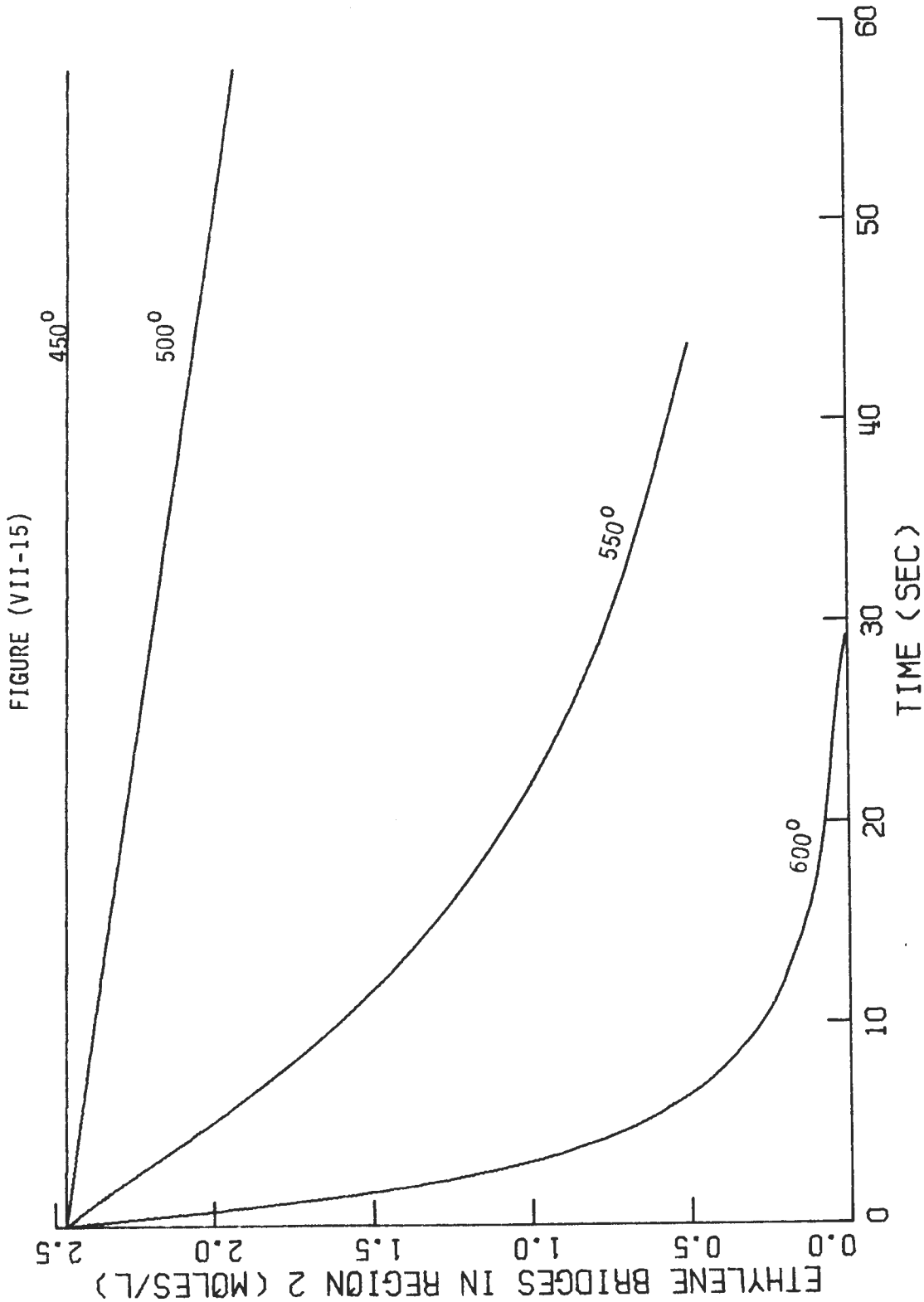

FIGURE (VII-15)

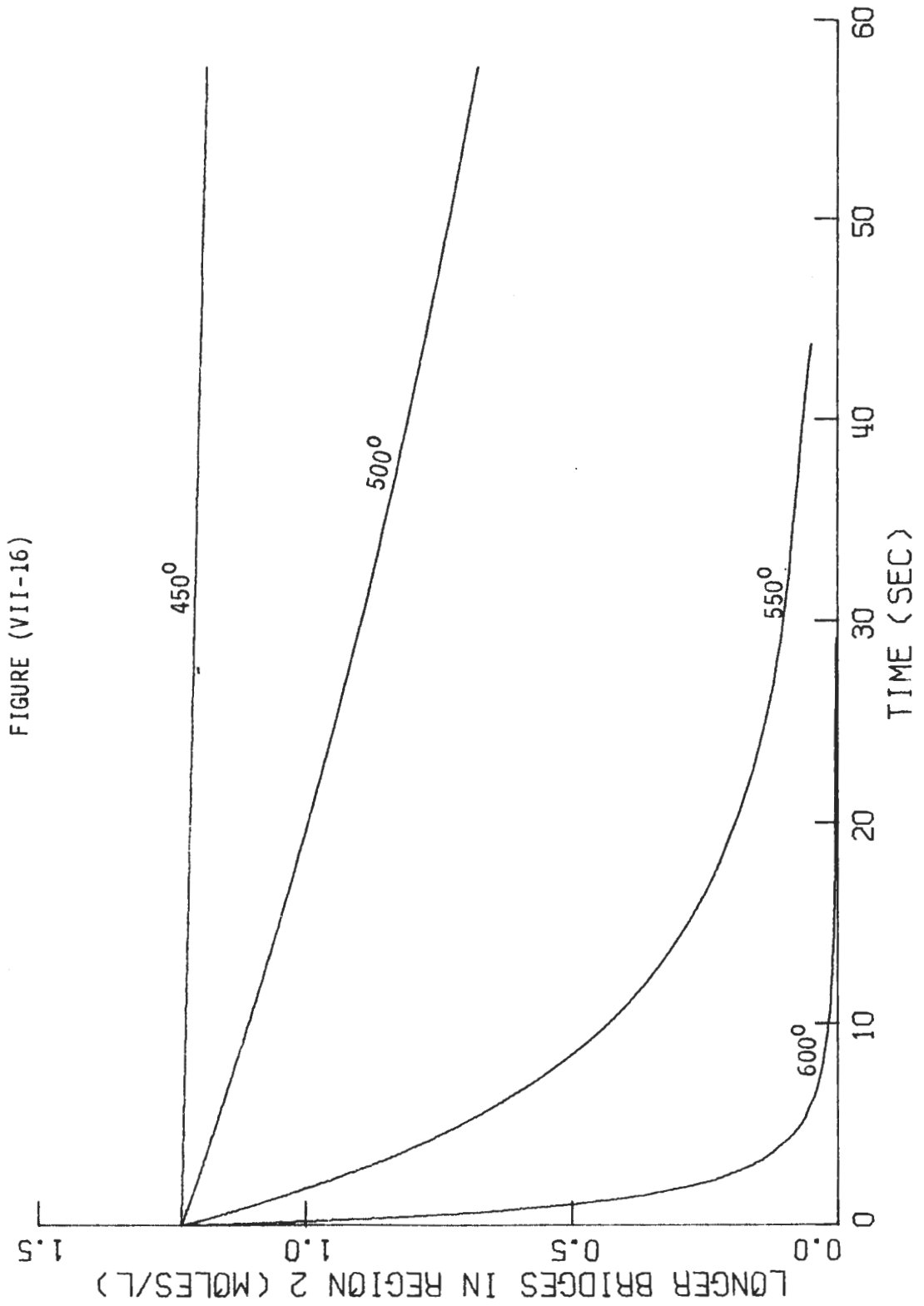

FIGURE (VII-16)

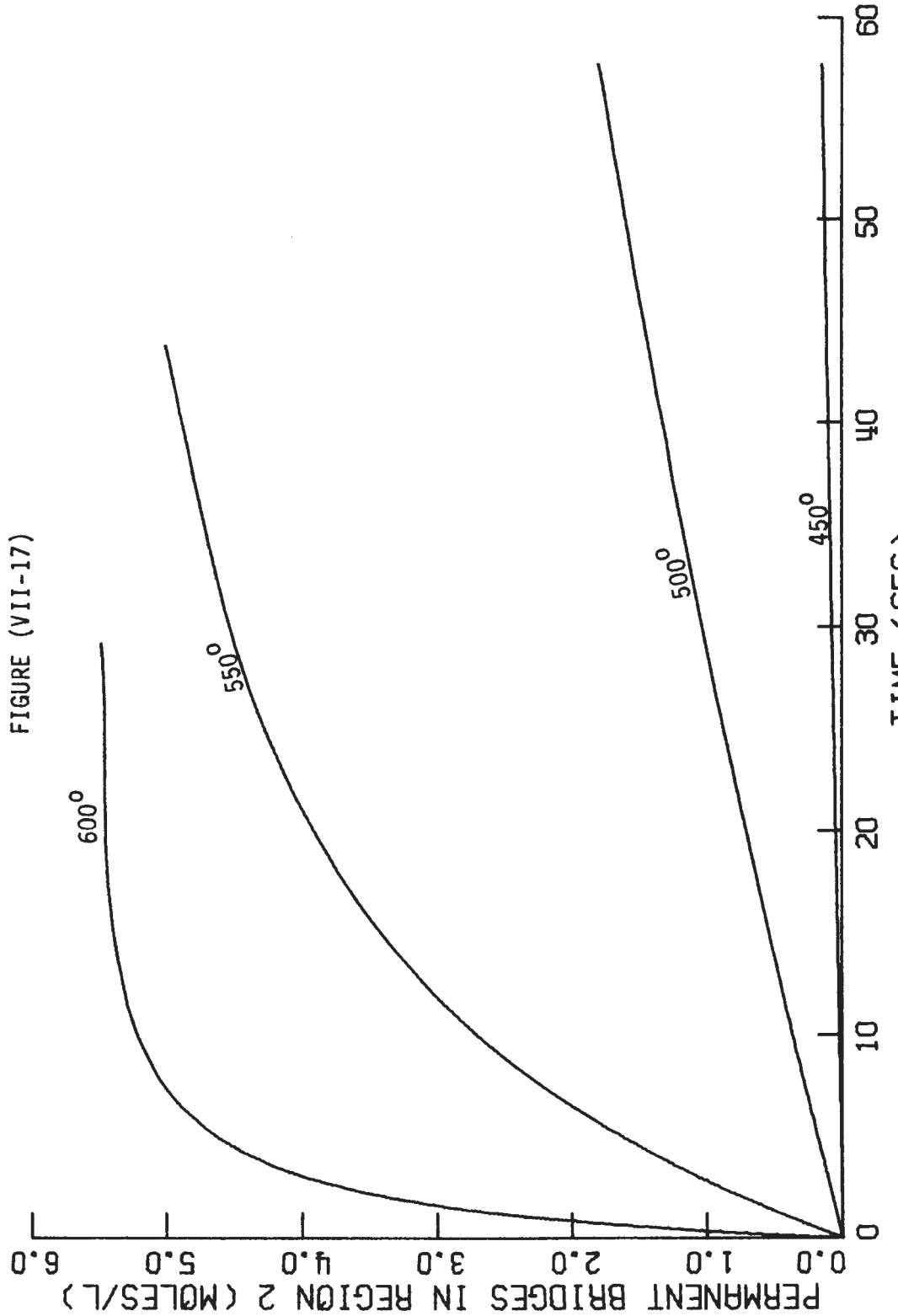

FIGURE (VII-17)

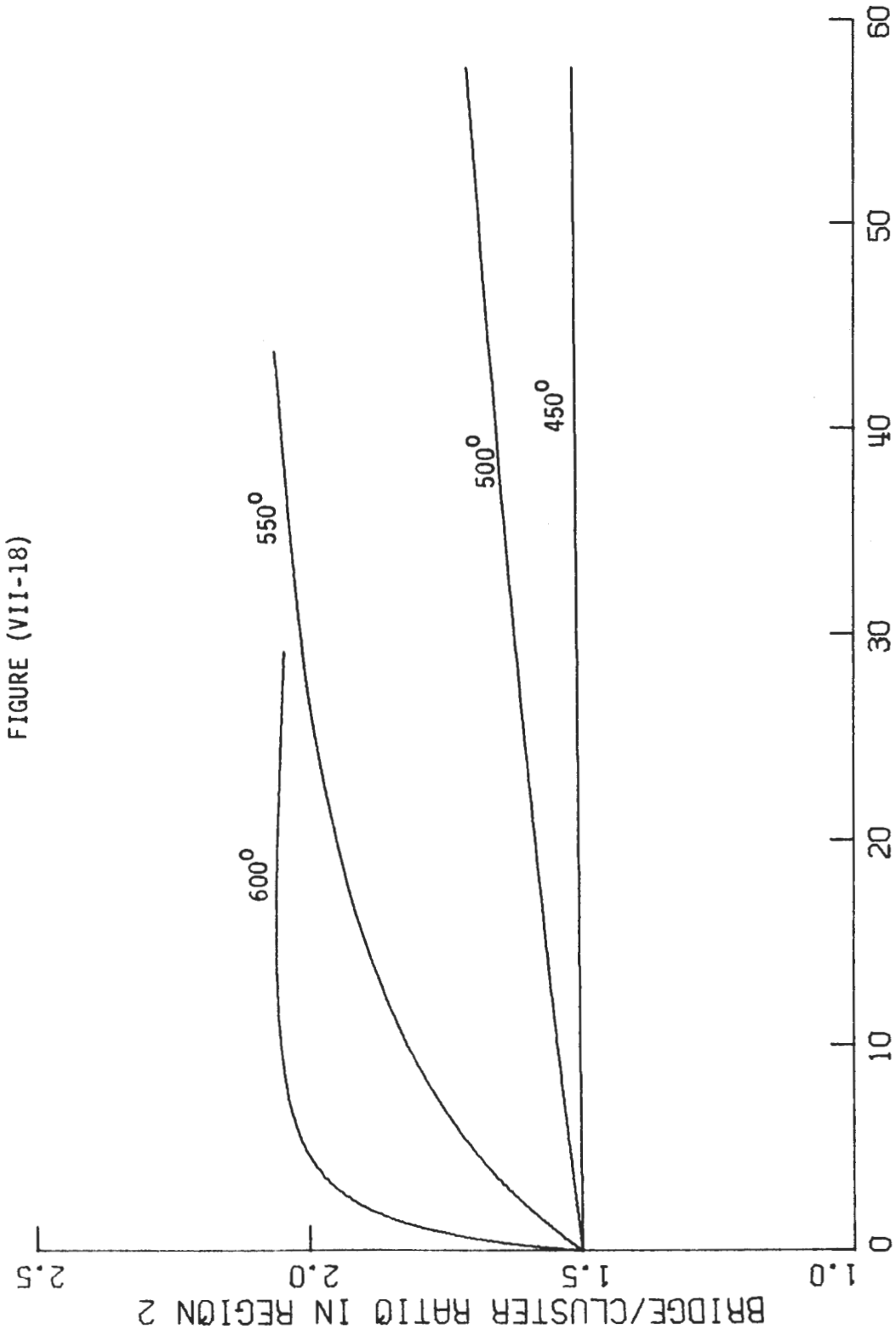

FIGURE (VII-18)

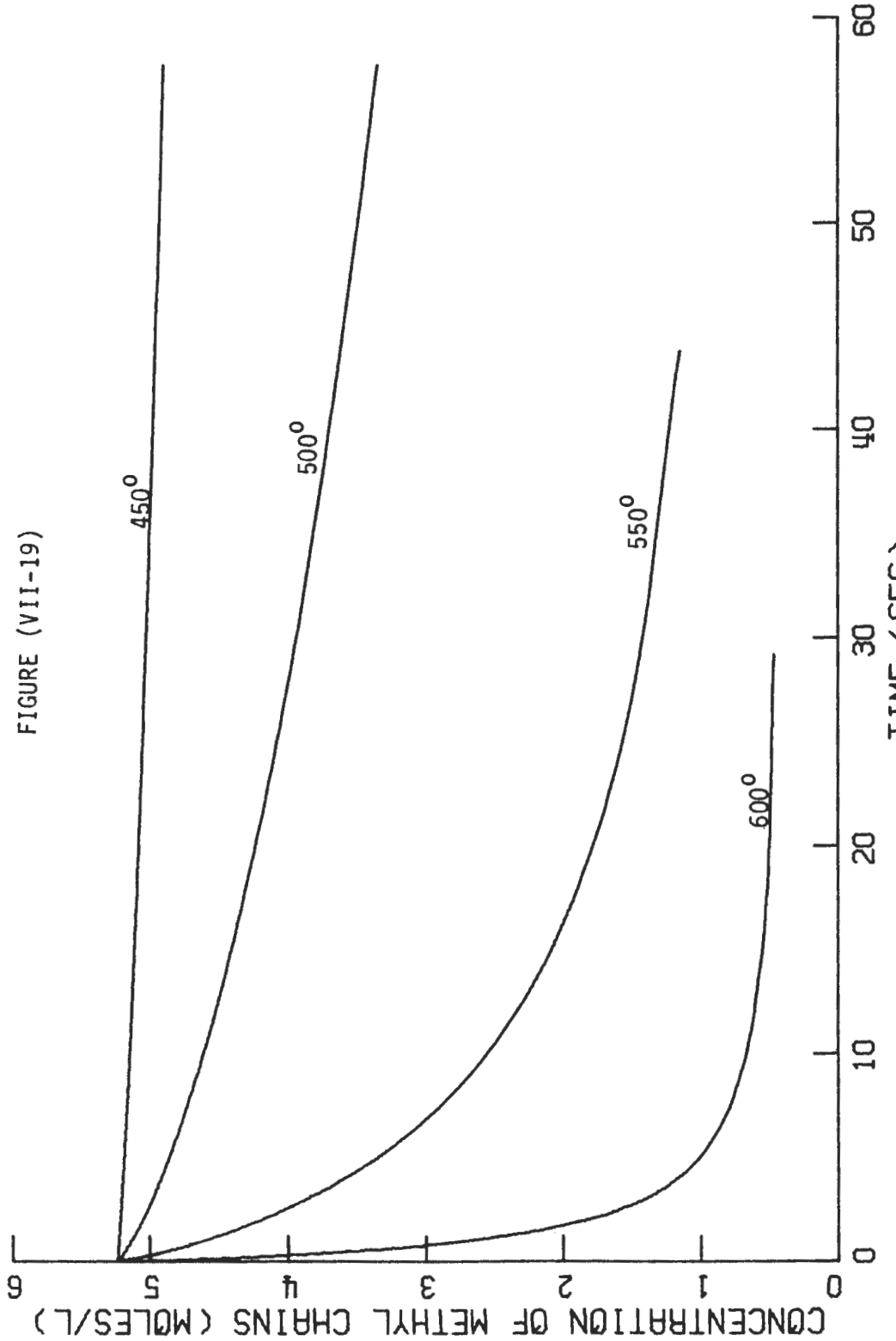

FIGURE (VII-19)

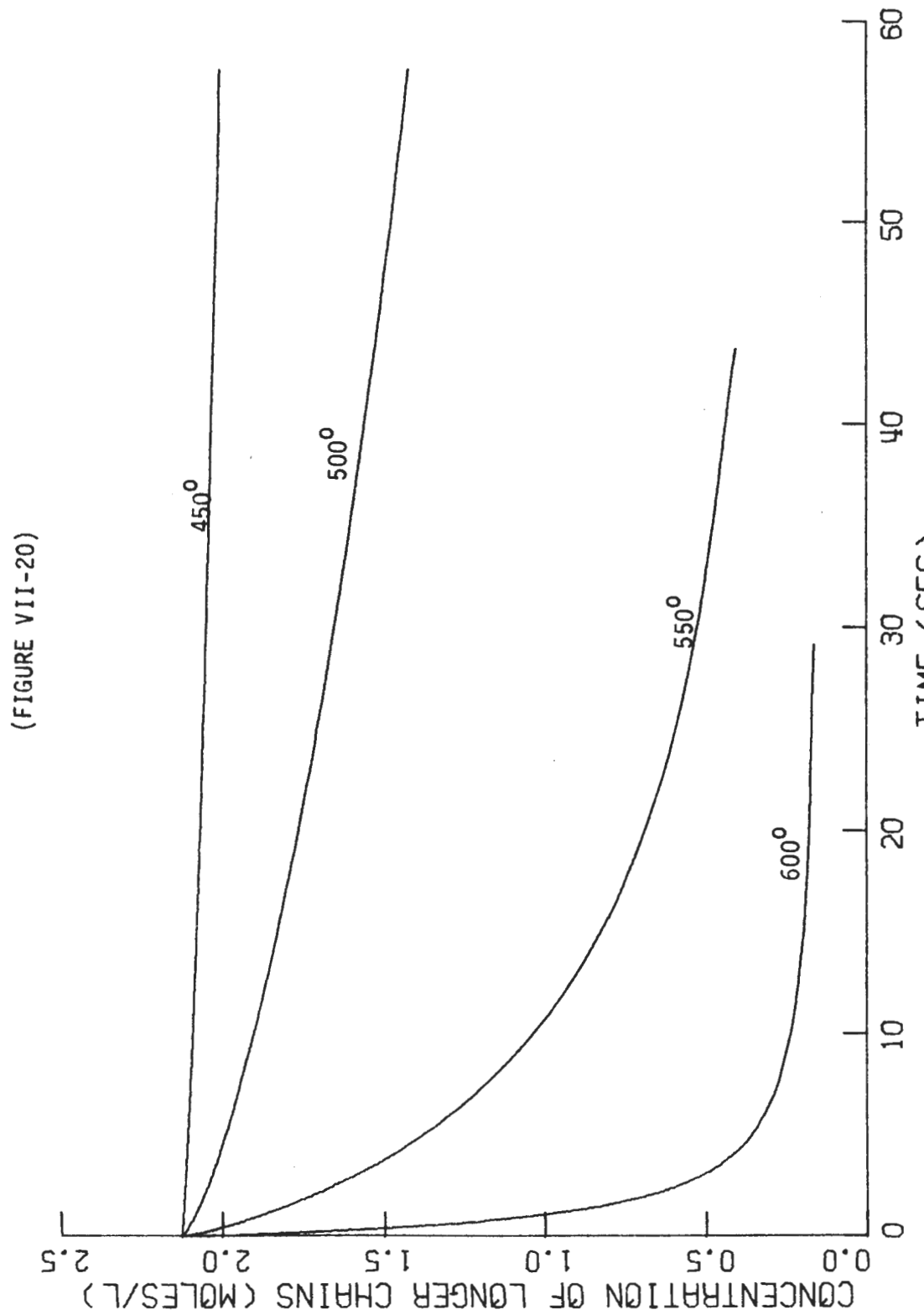

(FIGURE VII-20)

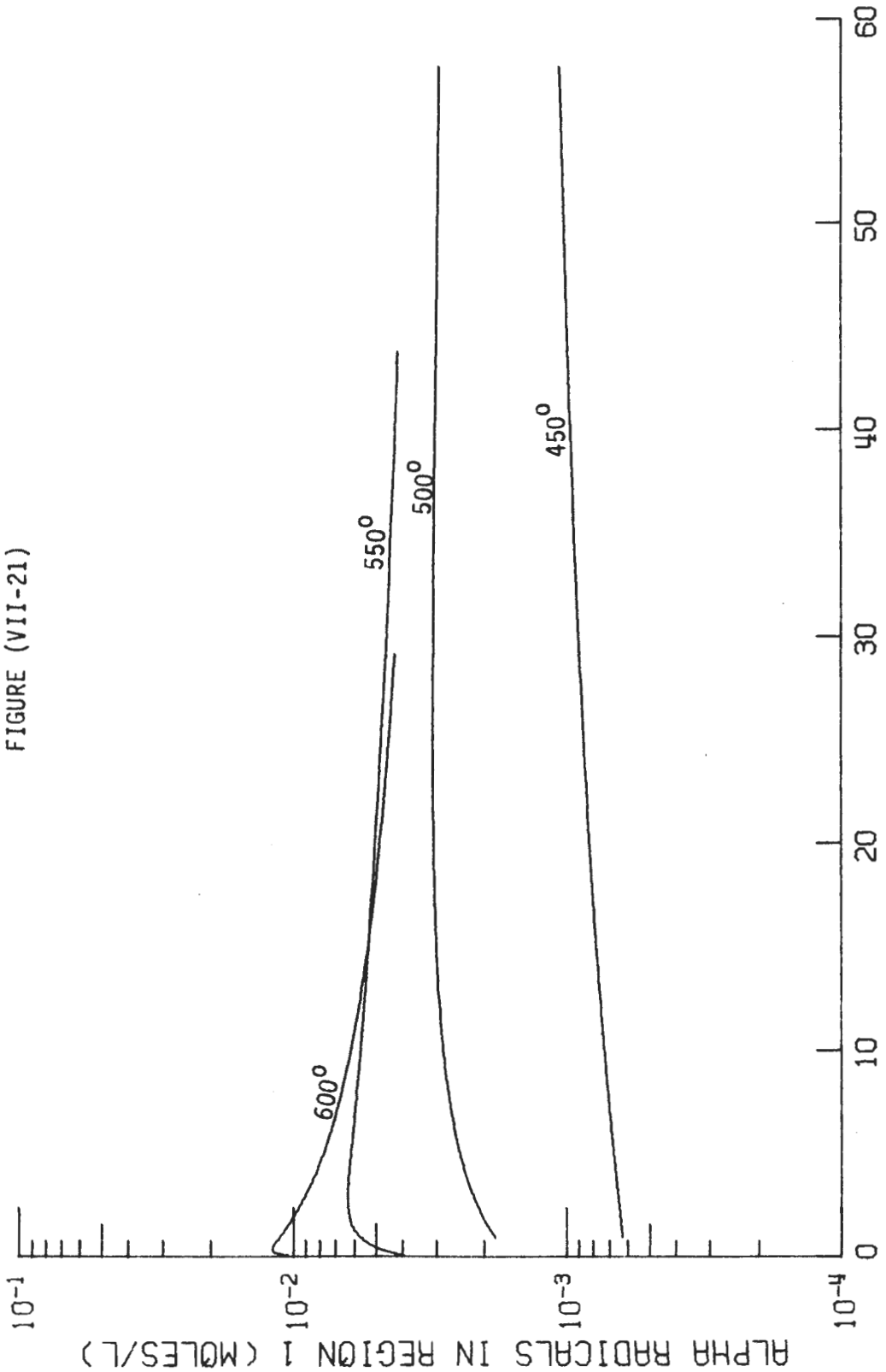

FIGURE (VII-21)

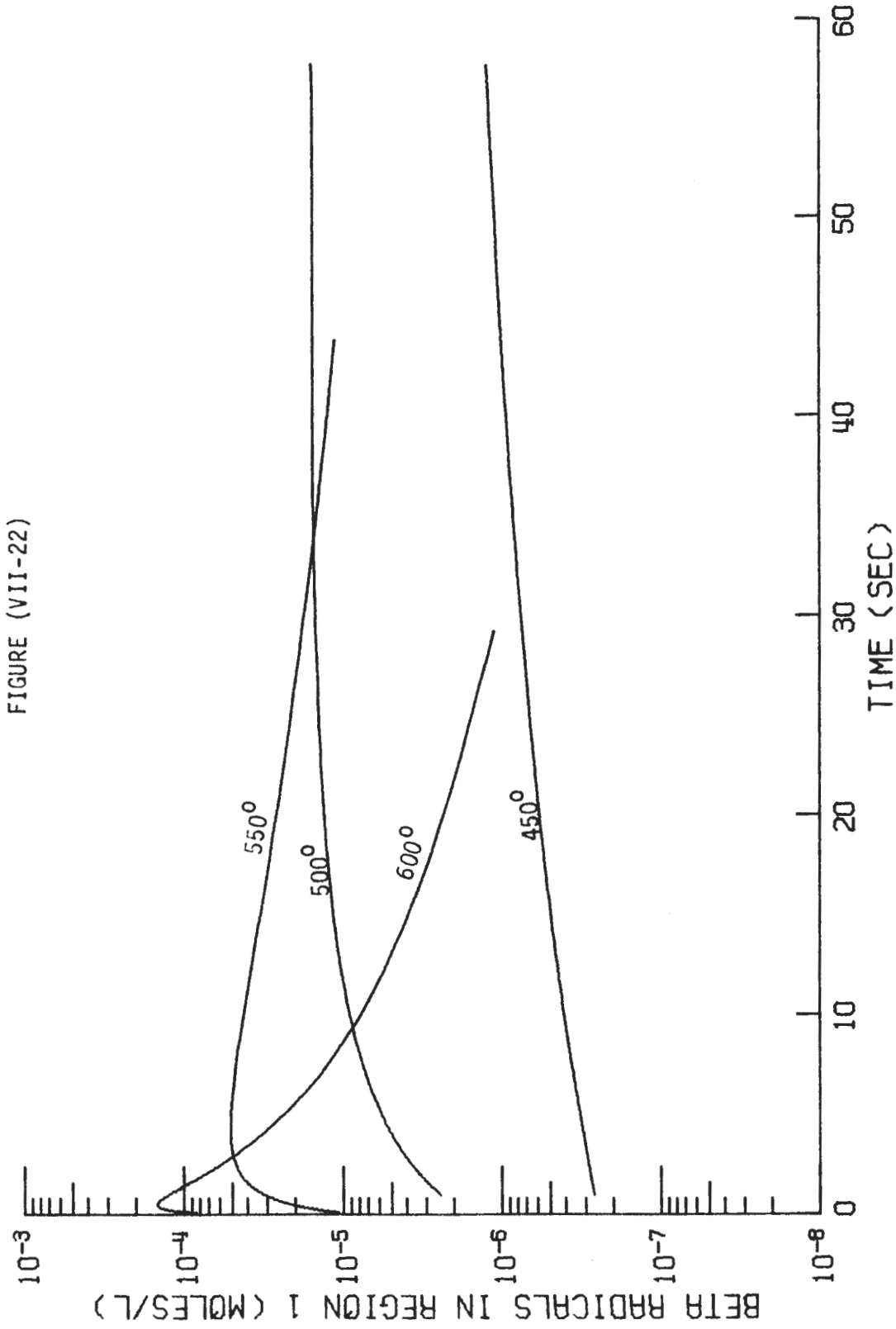

FIGURE (VII-22)

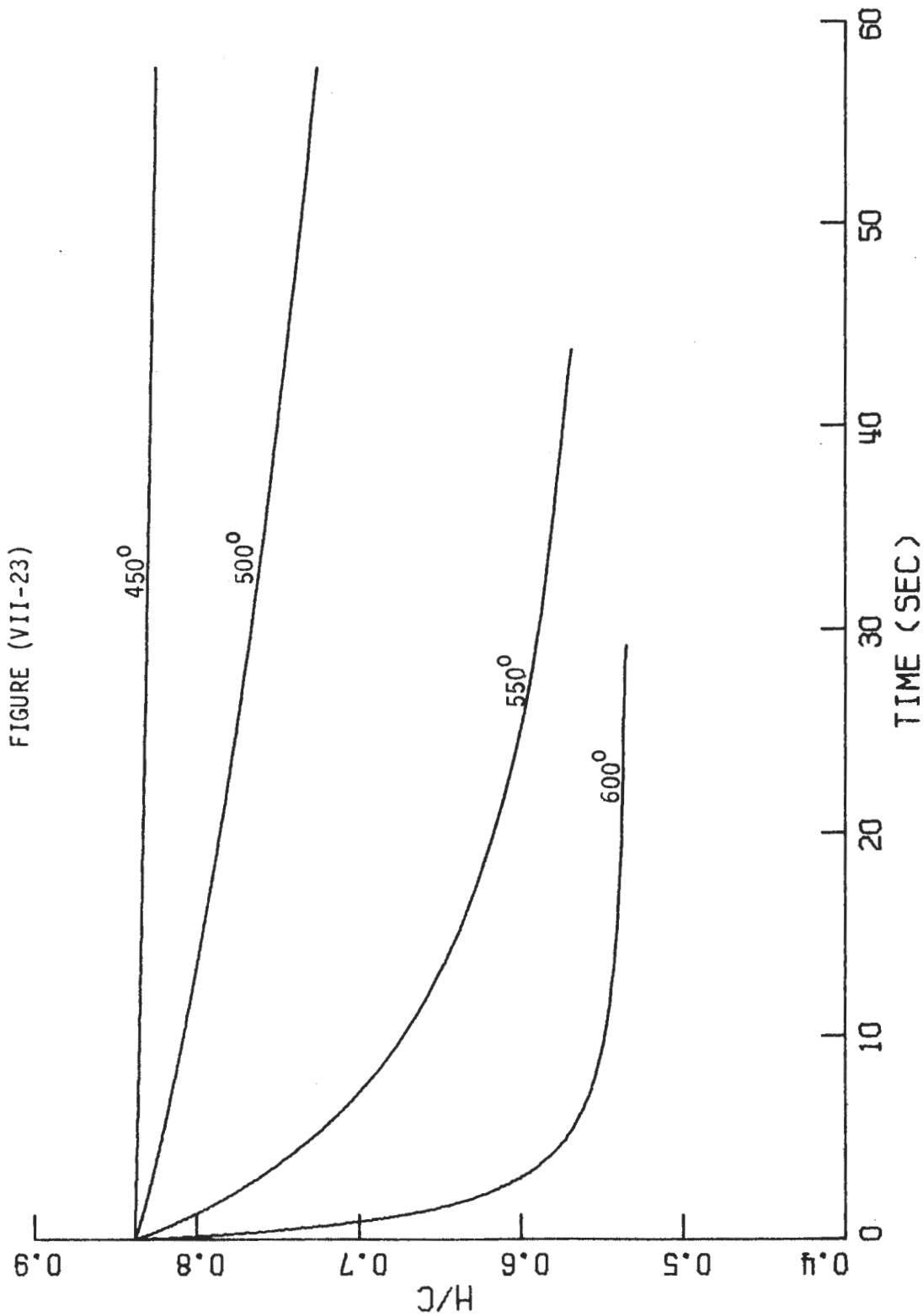

FIGURE (VII-23)

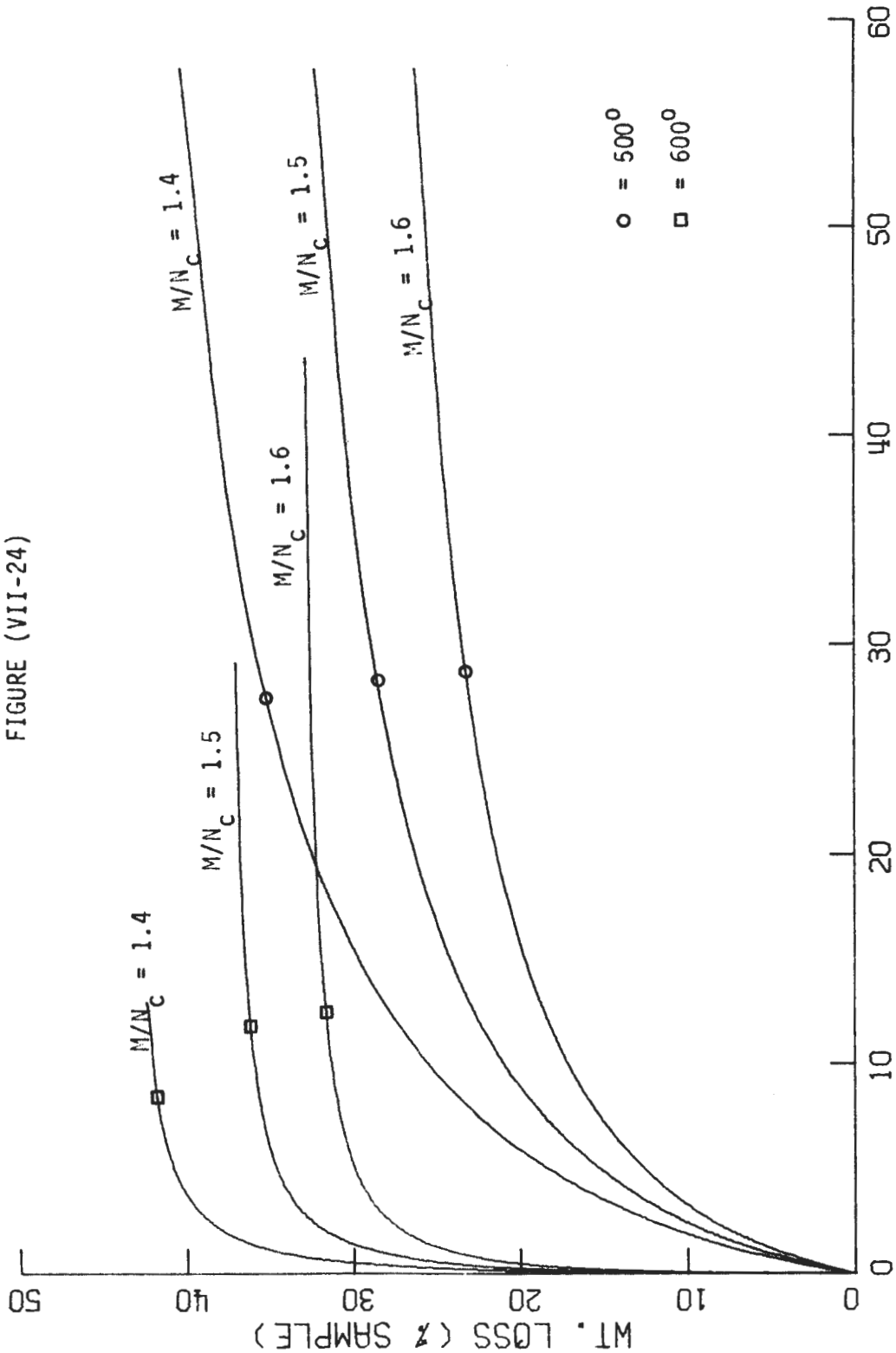

FIGURE (VII-24)

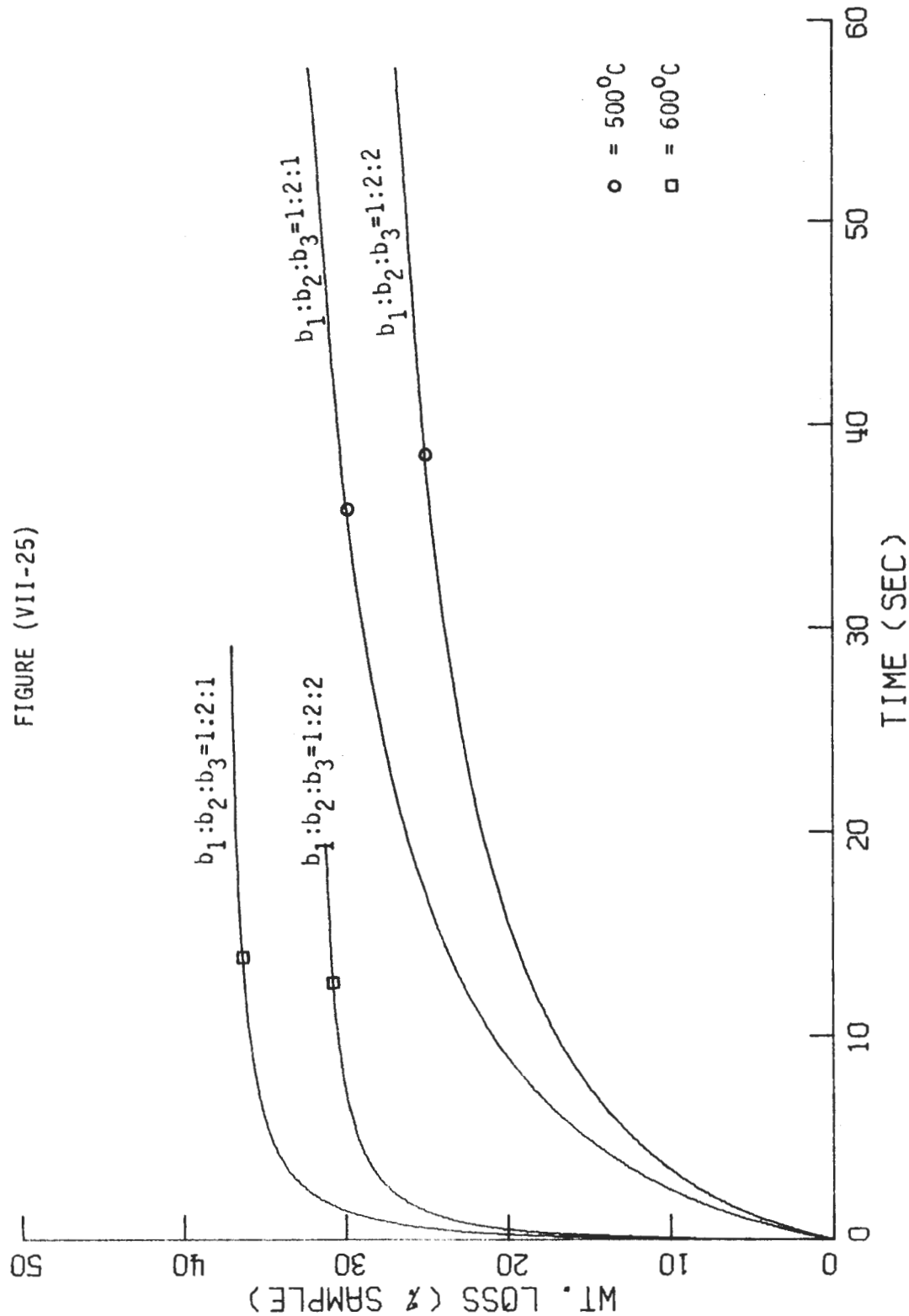

FIGURE (VII-25)

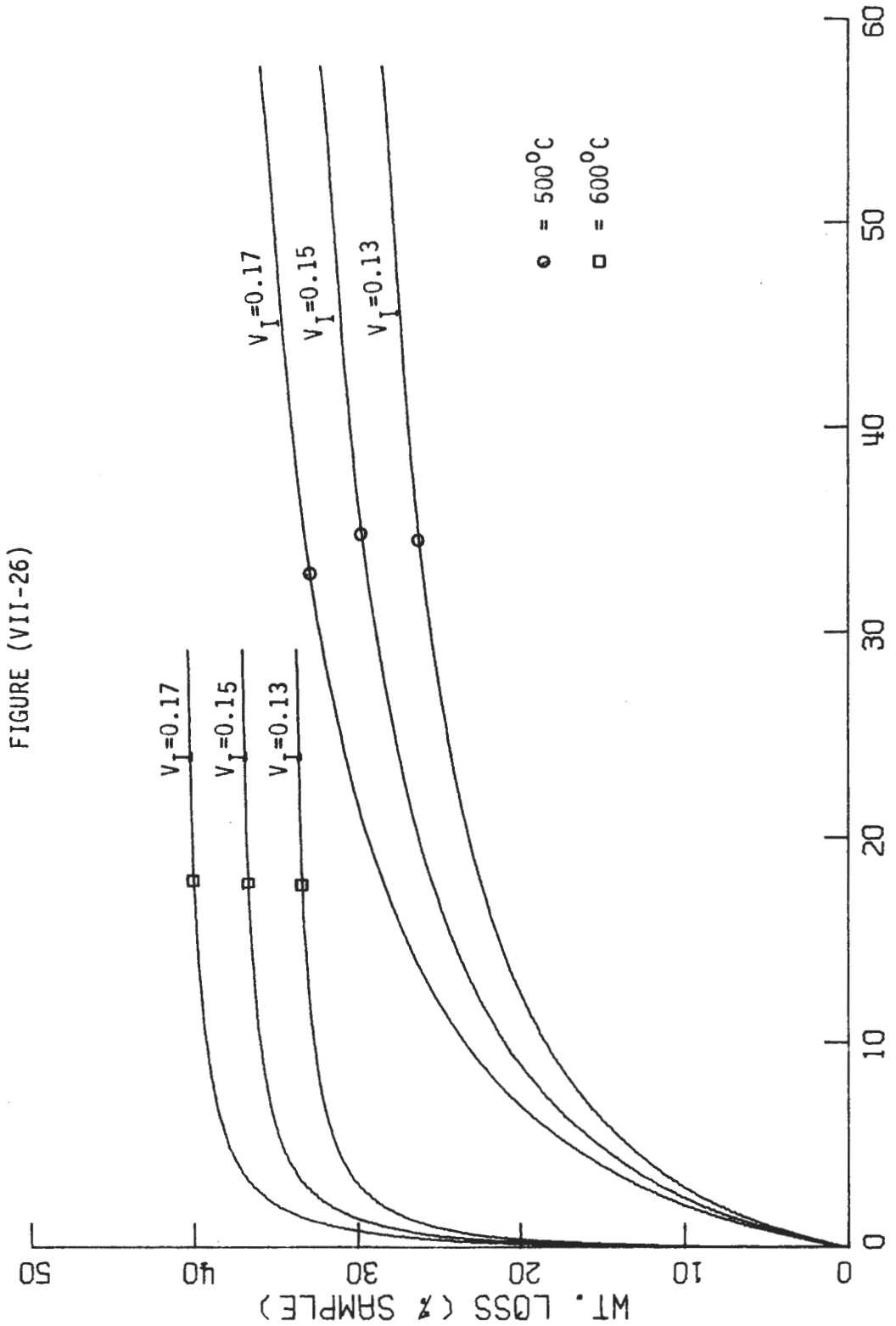

FIGURE (VII-26)

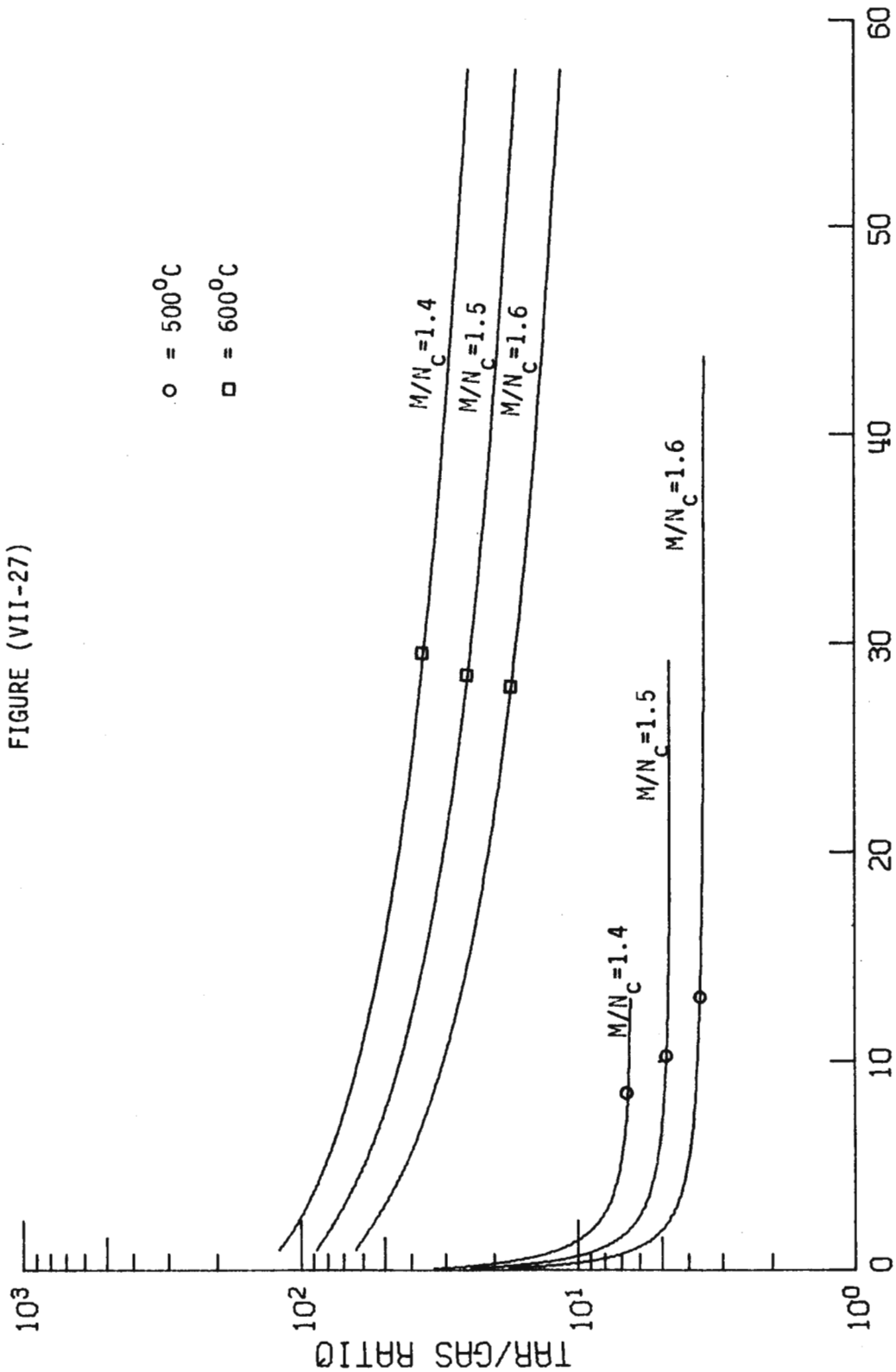
FIGURE (VII-27)
o = 500°C
□ = 600°C
M/N_c=1.4
M/N_c=1.5
M/N_c=1.6
M/N_c=1.4
M/N_c=1.5
M/N_c=1.6
TAR/GAS RATIO
TIME (SEC)
10^3
10^2
10^1
10^0
0
10
20
30
40
50
60

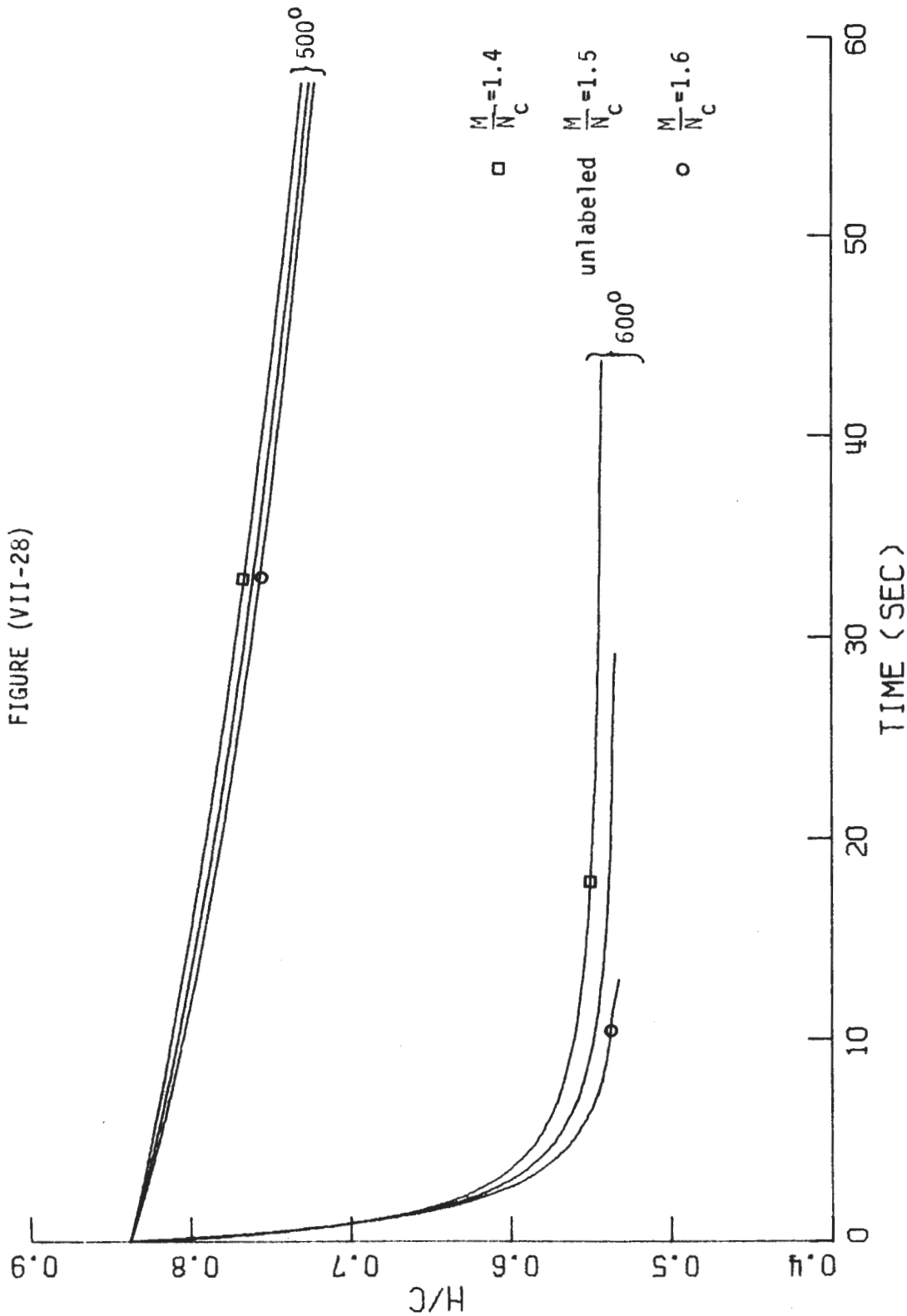

FIGURE (VII-28)

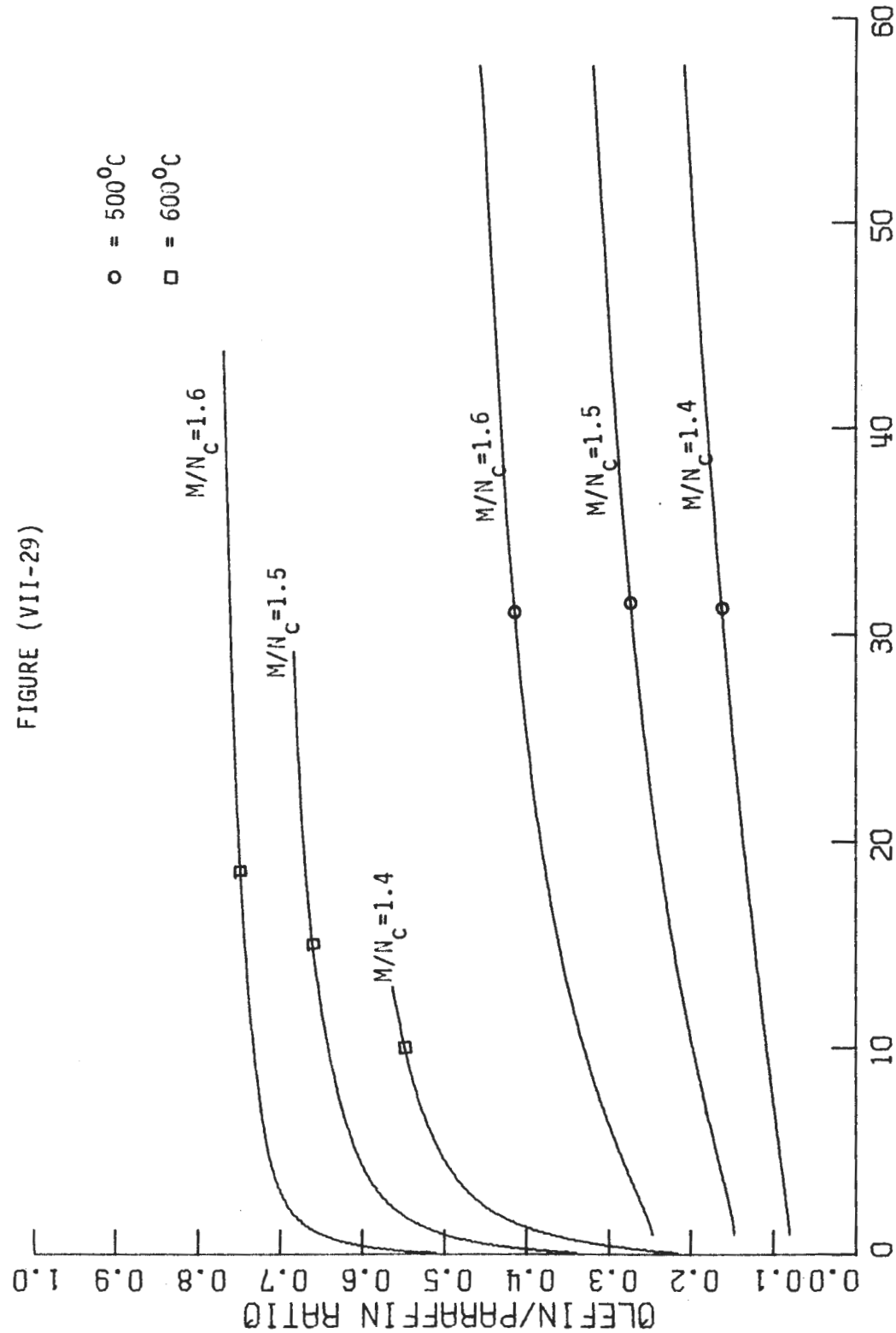

FIGURE (VII-29)

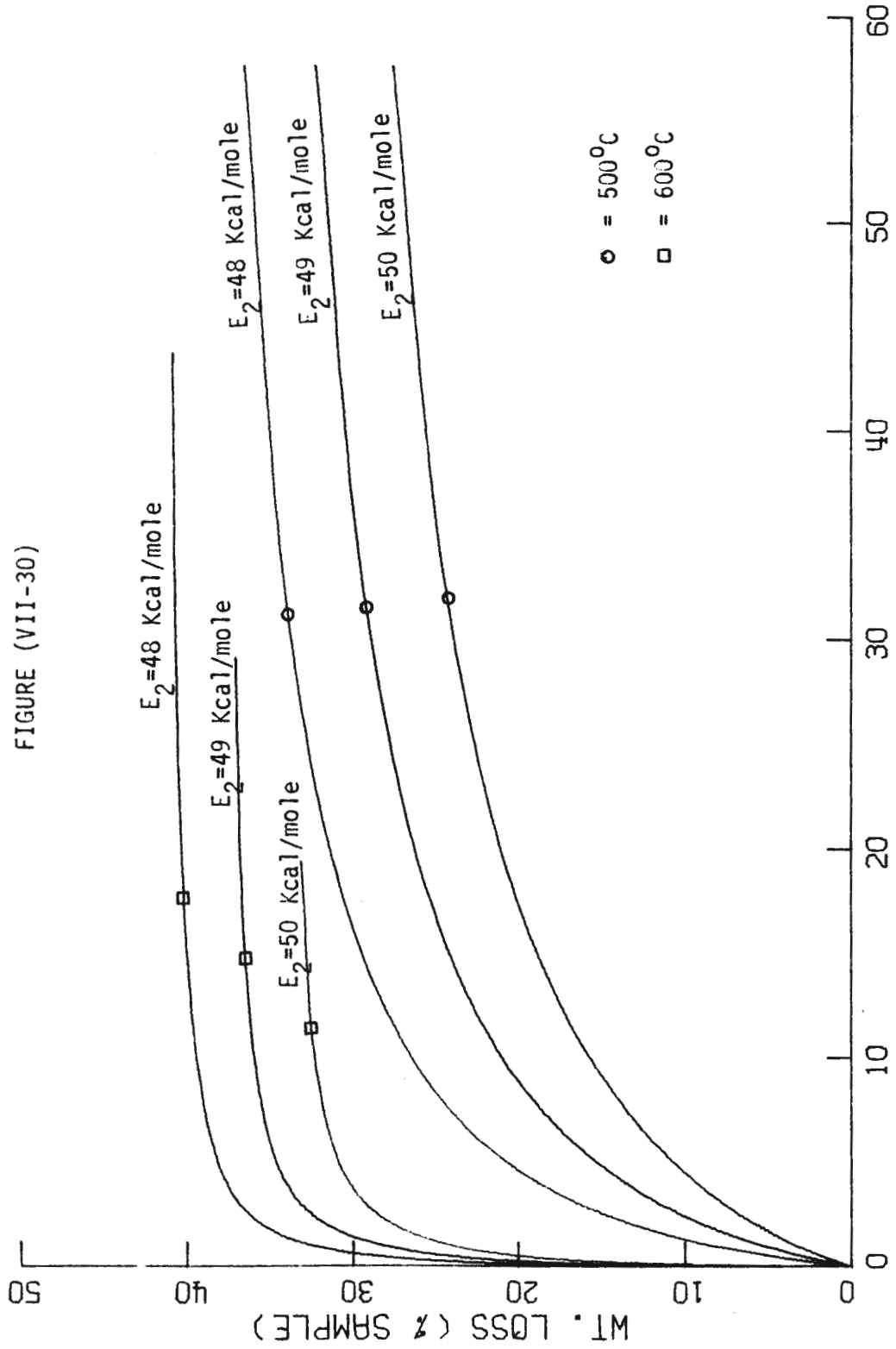

FIGURE (VII-30)

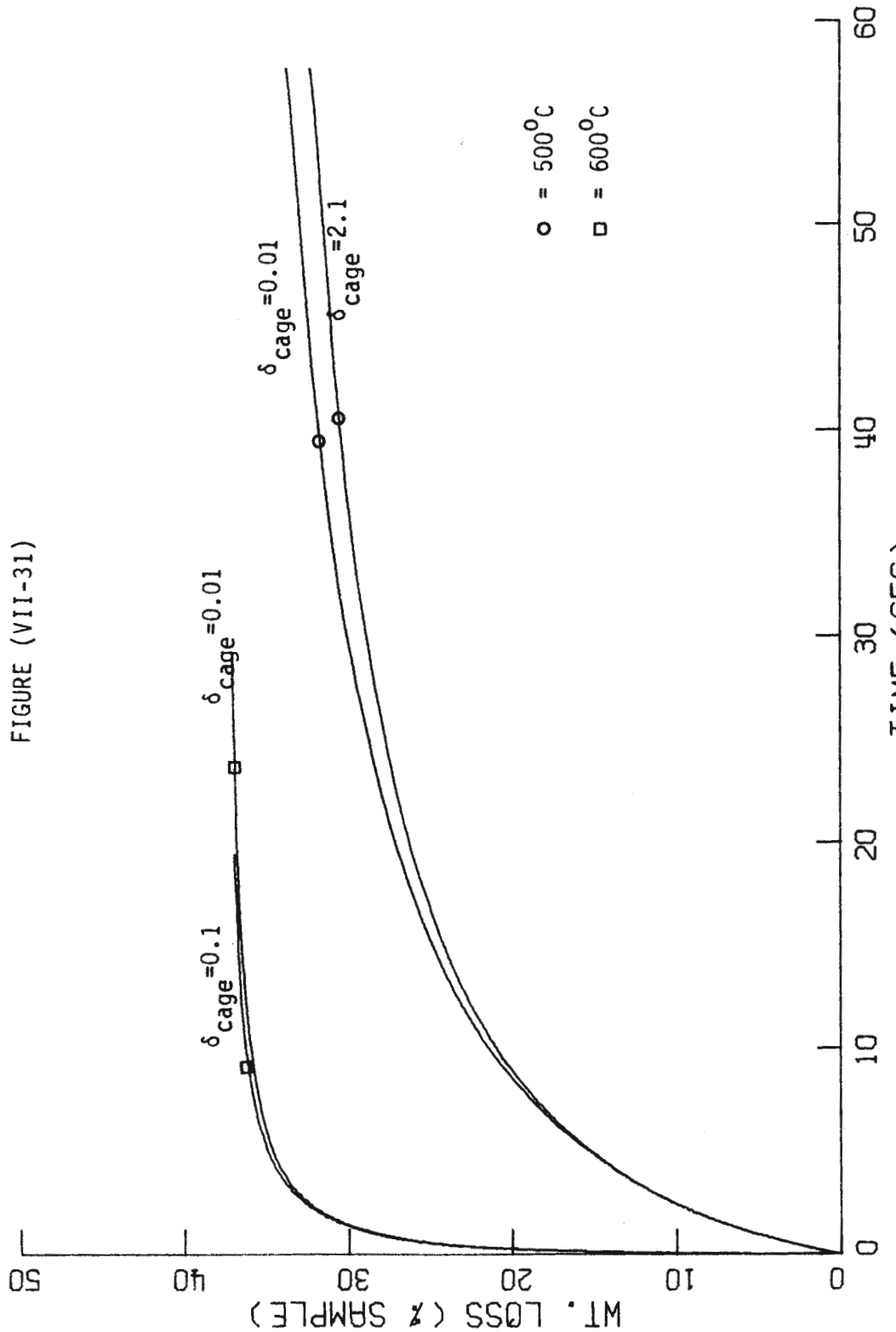

FIGURE (VII-31)

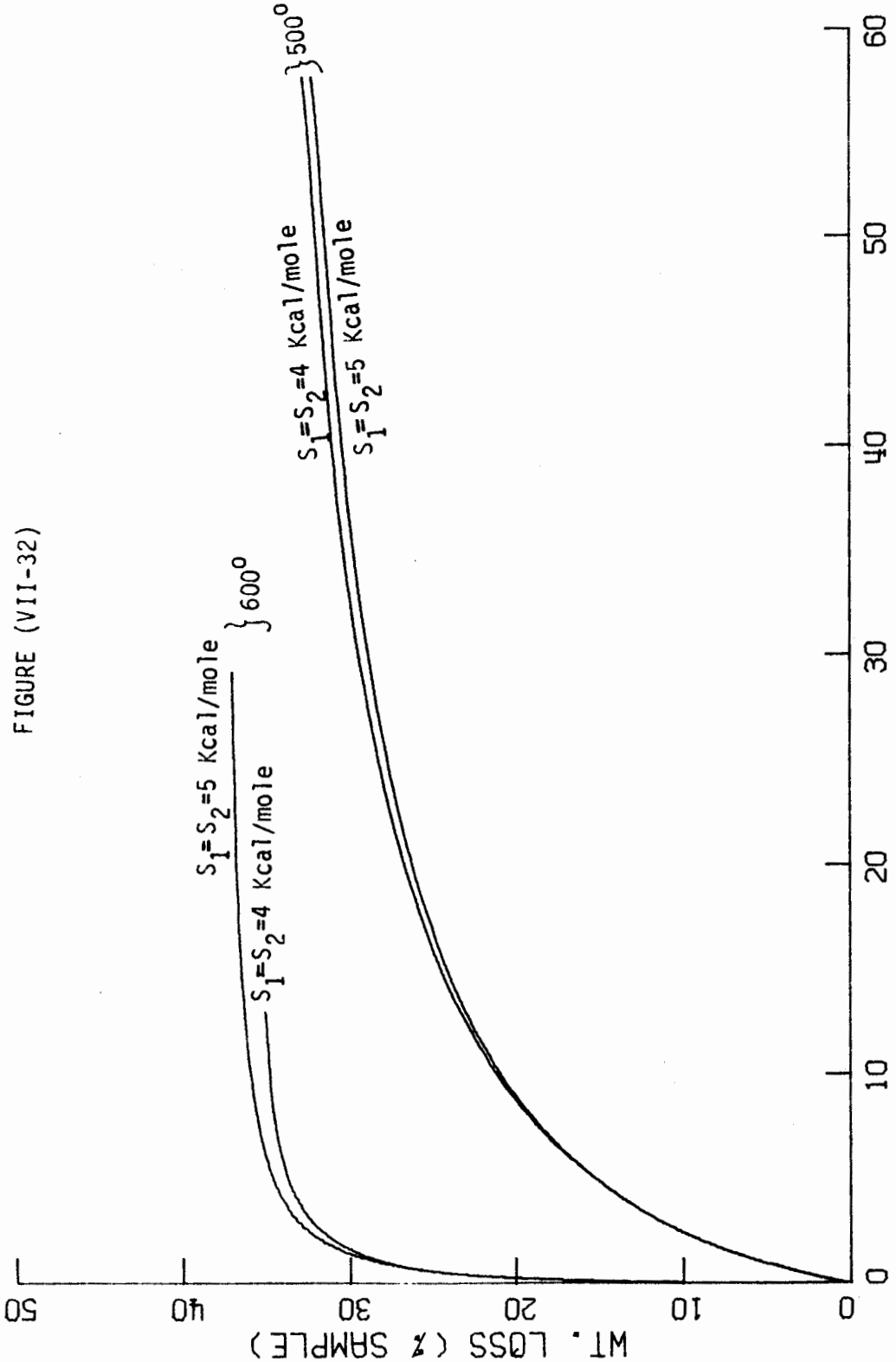

FIGURE (VII-32)

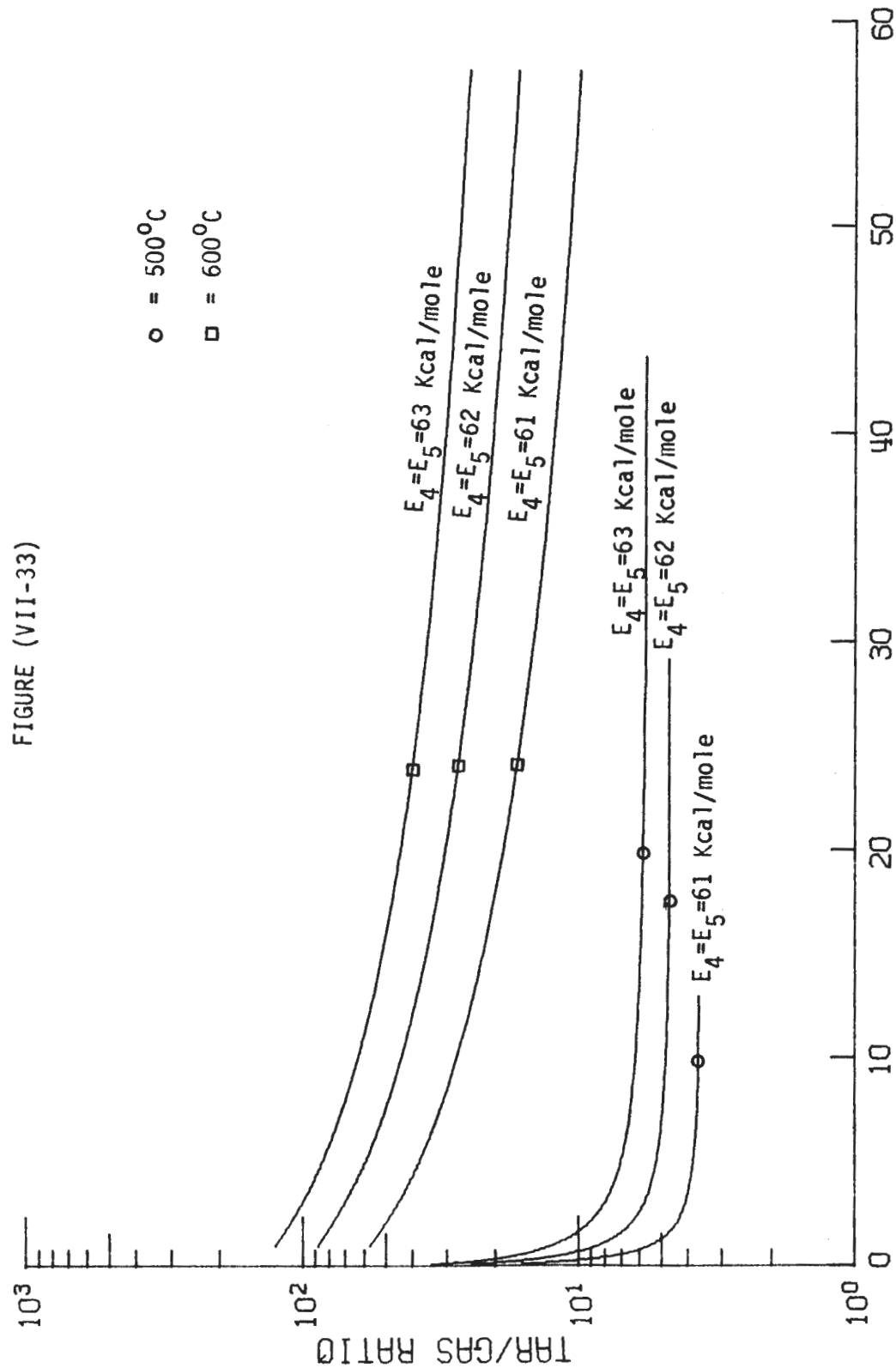
FIGURE (VII-33)
o = 500°C
□ = 600°C
$E_4=E_5=63$ Kcal/mole
$E_4=E_5=62$ Kcal/mole
$E_4=E_5=61$ Kcal/mole
$E_4=E_5=63$ Kcal/mole
$E_4=E_5=62$ Kcal/mole
$E_4=E_5=61$ Kcal/mole
TAR/GAS RATIO
10^3
10^2
10^1
10^0
0
10
20
30
40
50
60
TIME (SEC)

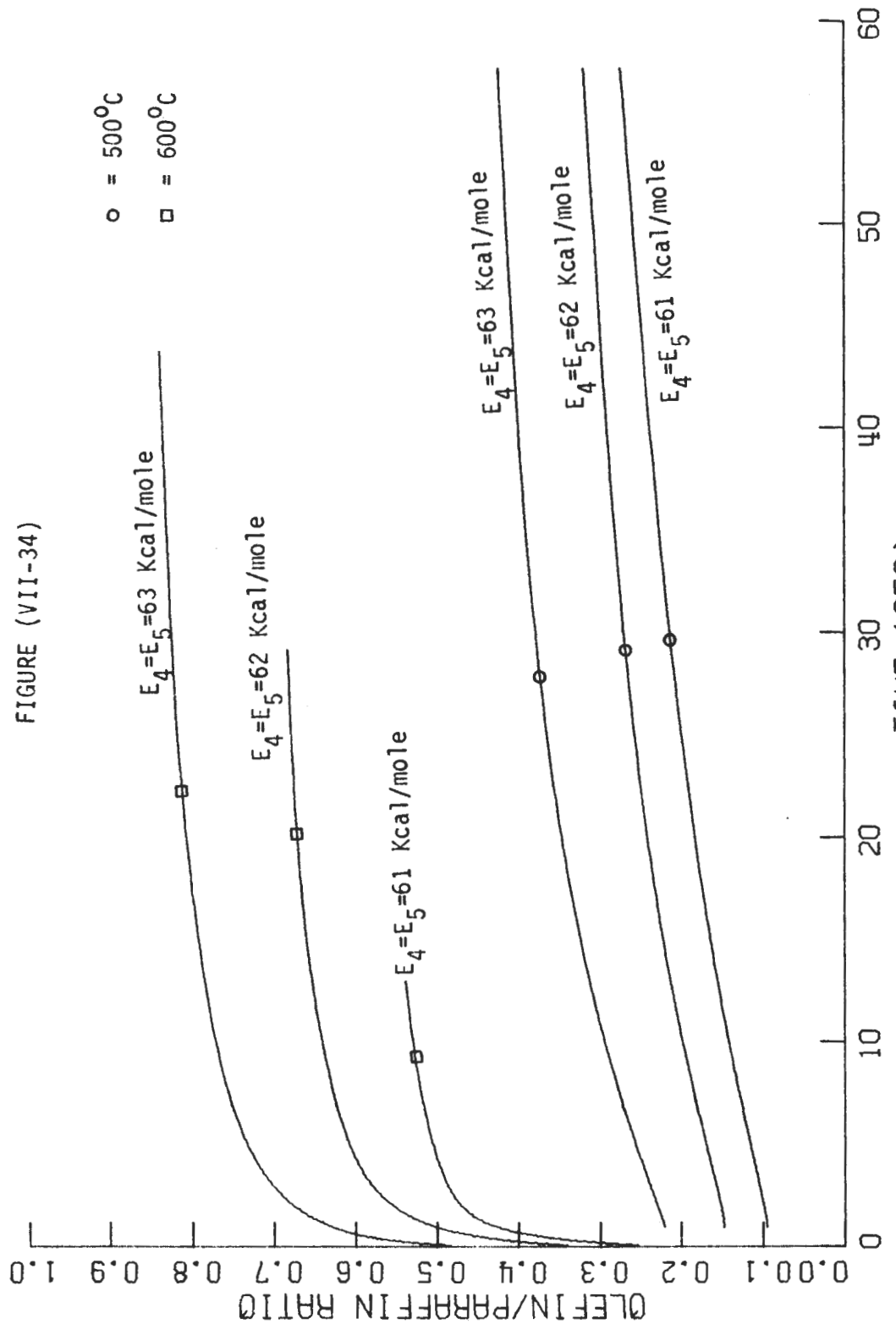
FIGURE (VII-34)
o = 500°C
□ = 600°C
$E_4=E_5=63$ Kcal/mole
$E_4=E_5=62$ Kcal/mole
$E_4=E_5=61$ Kcal/mole
$E_4=E_5=63$ Kcal/mole
$E_4=E_5=62$ Kcal/mole
$E_4=E_5=61$ Kcal/mole
OLEFIN/PARAFFIN RATIO
0.00.1 0.2 0.3 0.4 0.5 0.6 0.7 0.8 0.9 1.0
0 10 20 30 40 50 60
TIME (SEC)

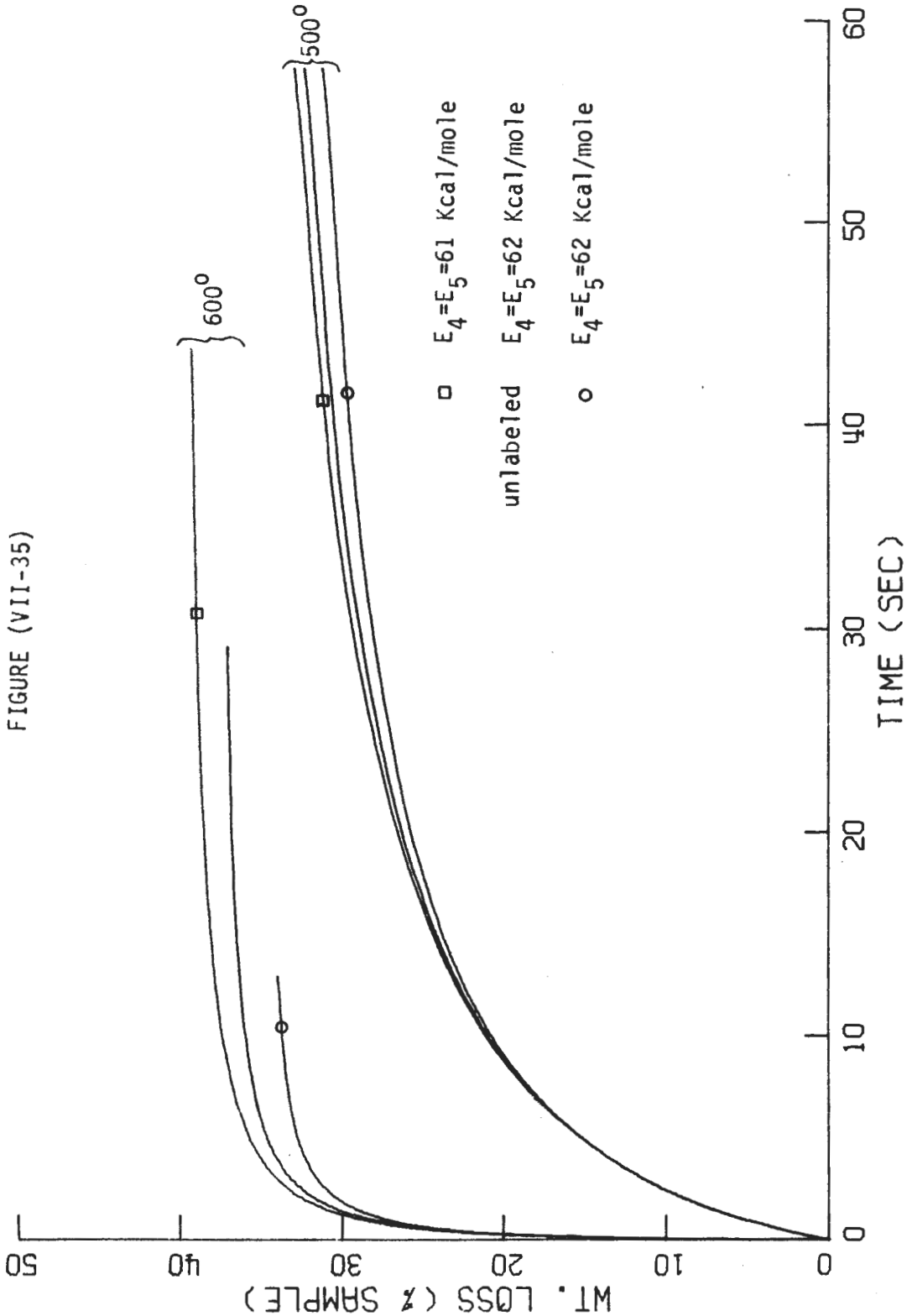

FIGURE (VII-35)

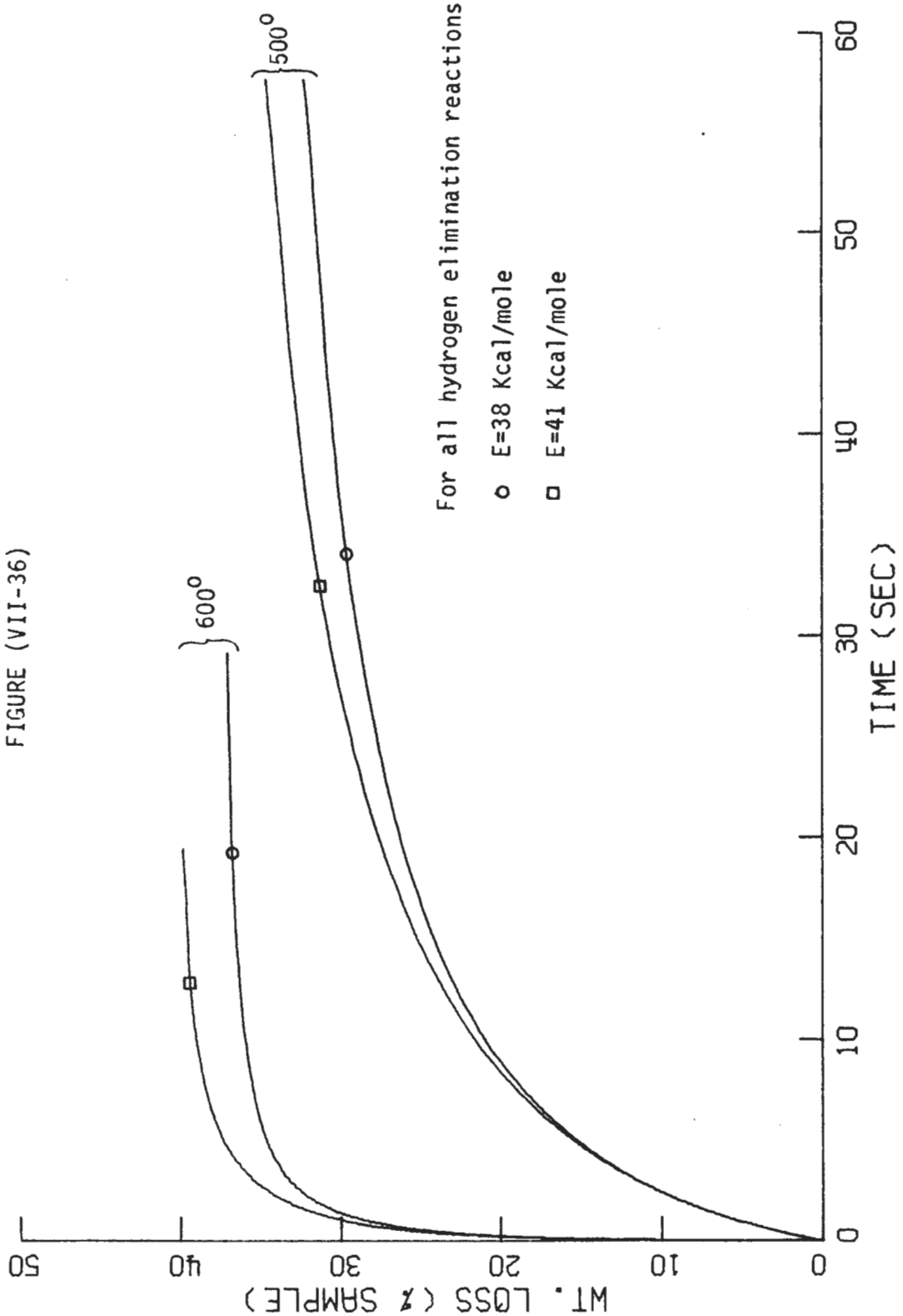
FIGURE (VII-36)
For all hydrogen elimination reactions
o E=38 Kcal/mole
□ E=41 Kcal/mole
600°
500°
WT. LOSS (% SAMPLE)
TIME (SEC)
0
10
20
30
40
50
60

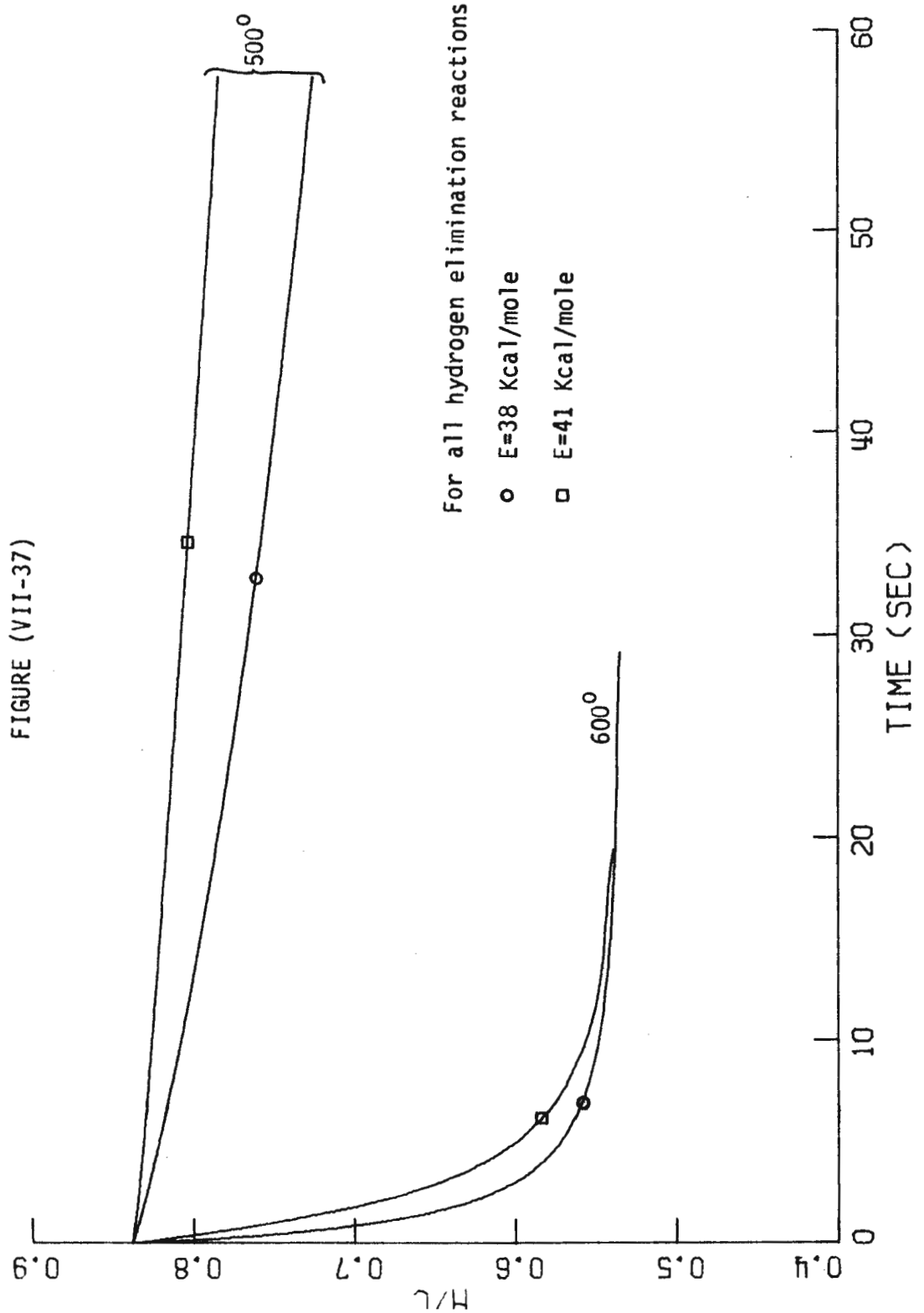
FIGURE (VII-37)
For all hydrogen elimination reactions
o E=38 Kcal/mole
□ E=41 Kcal/mole
500°
600°
H/L
0.4
0.5
0.6
0.7
0.8
0.9
0
10
20
30
40
50
60
TIME (SEC)

a small contribution are represented by shorter arrows.

Adding to the complexity of these chemical transformations, the transport processes separate the subunits into two regions. We now examine the various functional groups in region I that are directly related to the formation of tar.

The ethylene bridges b_2 (figure (VII-11)) decrease monotonically in time due to a very fast rate of dissociation and to its vulnerability to become a stilbene type of inactive bridges. The longer bridges b_3 (figure (VII-12)), however, have a much higher activation energy of dissociation so that initially, the transport from region II to region I outweighs the loss terms, and its concentration shows a maximum for the higher temperatures. On the other hand, we observe a corresponding increase in the inactive bridges (b_2= + b_3=) and the M/N_c ratio (figure (VII-13))and (VII-14)). Since the concentration of aromatic clusters N_c is constant, the M/N_c ratio also indicates the total number of bridges in the region. There are two reasons for the monotonic increase of the M/N_c ratio. When the volatile fragments escape from region I, the concentration of clusters there is replenished by material transport from region II, but the new clusters carry with themselves a characteristically higher number of bridges than the leaving fragments. Physically, when the volatile fragments escape, the heavier network of clusters they leave behind will link with materials in the interior of the subunits, thus forming a more compact structure exemplified in the higher M/N_c ratio. The second reason is that α-radicals that are formed by the breaking of chains can recombine to increase the overall

number of bridges. The depletion of the active b_2 and b_3 bridges and the increase of the M/N_c ratio in region I together constitute the strong deactivating effect on the weight loss kinetics.

Figures (VII-15) to (VII-18) show the concentrations of these bridges in the interior region (region II). They demonstrate the same trends of kinetics as in region I, except that the longer bridges b_{3II}, instead of showing a maximum, steadily decrease in number having no transport replenishment.

The concentrations of the chains c_1 and c_2 are directly related to the formation of methane and the higher alkanes. The quantities on the ordinates of figures (VII-19) and (VII-20) are total concentrations defined as

$$c_1 = \frac{c_{1,I}V_I + c_{1,II}V_{II}}{V_1 + V_{II}}$$

$$c_2 = \frac{c_{2,I}V_I + c_{2,II}V_{II}}{V_1 + V_{II}} \qquad \text{(VII-7)}$$

In figures (VII-21) and (VII-22) we plot the concentrations of the α and β radicals in region I. The α radicals, due to their stability, can be seen to outnumber the β radicals by a few orders of magnitude. The changes in concentrations of these radicals are quite responsive to the corresponding changes of the ethylene and longer bridges (cf figures (VII-11) and (VII-12)). In figure (VII-23) we show the changes in the H/C ratio predicted by the model.

Some general observed phenomena of coal pyrolysis can now be

summarized and discussed in regards to the model simulation. Of particular practical and theoretical interest is the ultimate amount of tar and gases that can be obtained for a certain temperature. Many authors have observed apparently asymptotic yields of volatile materials on pyrolysis at different temperatures, i.e., the "effective" volatile content of coal, which we denote by V*, is a function of the highest temperature attained. (Anthony, 1975.) This phenomenon is not predicted by previous models and the dependence of V* on pyrolysis temperature has never been theoretically predicted. Although the present model has no a priori provision for an asymptotic weight loss, we observe from the simulation results (figure (VII-4)) that the system of competing reactions contains an inherent deactivation mechanism sufficient to cause the weight loss to steady off to some ultimate value. For the input values of the rate parameters, this ultimate weight loss increases with temperature in agreement with experimental findings. Moreover, the ultimate weight loss above 550^{o}C slightly exceeds the amount of "volatile matter" reported in the proximate analysis of the coal (35.08%). Investigators have found that under fast heating conditions the amount of volatiles generated is generally more than that obtained under standard assay conditions which involve much slower heating. The numerical simulation for isothermal conditions represents an idealized situation where the coal is heated infinitely fast to and kept at a desired temperature. Hence, this excess is in line with general observed behavior.

Many other general trends of pyrolysis behavior are in agreement

with the model simulation. Because of the larger depletion of breakable bridges (figures (VII-11) and (VII-12)) and chains (figures (VII-19) and (VII-20)), and the higher accumulation of double bonds (figure (VII-13)), it can be inferred that higher temperature chars are correspondingly less reactive, a phenomenon that has been known for a long time.

In addition to the total quantity of volatile products, the relative amounts of tar and gases (figure (VII-5)) are also of prime importance from the practical standpoint of coal utilization. This model predicts correctly that the tar-to-gas ratio is larger at the initial stage of pyrolysis, and that this ratio decreases with increasing temperature. Mechanistically this is due to the breakage of chains having a much higher activation energy than the bridges.

As the atomic H/C ratio shows (figure (VII-23)), the remaining char is more carbonaceous in nature indicating a general carbonization process. Of course, this can be expected because the volatile materials are more aliphatic in nature.

In the course of this model simulation, initial conditions and rate parameters have been adjusted only to match available experimental data points for 500^{o}C. The agreement of the simulation results with the observed thermal behavior of coal in general is supportive of the physicochemical mechanism proposed. Further progress from this point appears to call for the elucidation of some of the uncertainties that are associated with our adjustable parameters. To this end we perform sensitivity testing of individual parameters to examine how critically

each uncertainty can affect our simulation results. The design and planning of future experiments should then be emphasized on the study of the most crucial parameters.

Sensitivity Testing

As indicated in figures (VII-1) and (VII-2), the simulation adjustments include structural assumptions that pertain to the initial conditions, and the variation of some rate parameters, notably the rates of bond dissociation. Our sensitivity testing procedures involve perturbing one adjustable parameter at a time and studying the corresponding deviation on the simulation results. Four practically important output quantities are under consideration: the weight loss, the relative amounts of tar and gases generated, the ratio of the paraffins and the olefins, and the atomic H/C ratio. Comparison of these results is performed for two temperatures: $500^{o}C$ and $600^{o}C$.

The Structural Parameters

Table (VII-2) lists the structural parameters studied and the different cases that are tried. The effect of each parameter is entered in table (VII-3). Because of the many parameters that are tested, actual computation results are presented only for the more sensitive parameters.

Table (VII-2) List of Structural Parameters Tested

Parameters	Base Values	Perturbed Values
M/N_c	1.5	1.4, 1.6
V_I	0.15	0.13, 0.17
$b_1:b_2:b_3$	1:2:1	1:2:2
f_a	0.635	0.630, 0.640
ℓ	2.5	3.0
ring size (C_{ar})	14 (3 rings)	10 (2 rings)
ring size (h_{aru})	10 (3 rings)	8 (2 rings)

Table (VII-3) Sensitivity of Simulation Results on Structural Parameters

Parameters \ Effect	Weight loss	tar/gas	H/C	Olefin/Paraffin
M/N_c	large	moderate	small	large
V_I	large	small	small	small
$b_1:b_2:b_3$	large	moderate	small	large
f_a	small	small	small	small
ℓ	small	small	small	moderate
ring size	small	small	small	small

In interpreting sensitivity of the parameters, we must examine the amount of their perturbation as well as the deviation in the simulation results, and the description of their effects being large, moderate or

small is, to a certain extent, a matter of engineering judgment. Nevertheless, we have found the effects of certain parameters to be distinctly larger, and those are the ones identified as the most crucial parameters.

The bridge to cluster ratio M/N_c (figure (VII-24)) and the distribution of different bridges $b_1:b_2:b_3$ have the largest effects on the weight loss kinetics (figure (VII-25)). This can be anticipated because the volatile fragments which account for most of the weight loss are generated by the scission of bridges. The size of the surface region in the bulk phase (V_I) also have a strong effect on the weight loss because it determines how much of the volatile fragments can escape directly to the macropores. (figure (VII-26))

The response of the tar/gas and the H/C ratios to the perturbation of the M/N_c ratio is presented in figures (VII-27) and (VII-28) as example cases. The olefin to paraffin ratio is sensitive to almost every parameter tested except V_I. An example is also presented for different M/N_c ratios (figure (VII-29)). The reason is apparent from figure (VII-3), where we observe that the changes in any initial conditions can affect the concentrations of the free radicals and change the amount of olefins generated.

Sensitivity testing of the aromaticity f_a and the ring size calls for some comments. Table (VII-4) shows the effects of small changes in f_a on the initial conditions:

Table (VII-4) Effects of the Aromaticity f_a on the Initial Conditions (M/N_c=1.5, ℓ=2.5, ring size=3, $b_1:b_2:b_3$=1:2:1)

f_a	b_1	b_2	b_3	c_1	c_2	c_1+c_2	H_α	N_c
0.630	1.22	2.44	1.22	3.62	3.03	6.65	22.46	3.26
0.635	1.23	2.46	1.23	5.23	2.13	7.36	22.46	3.29
0.640	1.24	2.48	1.24	6.85	1.22	8.07	22.46	3.31

The relative amounts of the side chains are most affected by the aromaticity while the other quantities including the total concentration of side chains (c_1+c_2) are generally the same. Consequently, perturbation of the aromaticity has little effect on the output variables studied.

When the initial conditions are estimated with the average ring size being 2, the allowable range of f_a falls between 0.555 and 0.590, whereas in the case of three rings it falls between 0.605 and 0.640. The choice of f_a=0.585 yields initial conditions closest to those for the base case, as shown in Table (VII-5).

Table (VII-5) Effects of the Ring Size on the Initial Conditions M/N_c=1.5, ℓ=2.5, $b_1:b_2:b_3$=1:2:1

ring size	c_{ar}	h_{aru}	f_a	b_1	b_2	b_3	c_1	c_2	H_α	N_c
2	10	8	0.635	1.59	3.18	1.59	5.17	2.82	22.45	4.24
3	14	10	0.585	1.23	2.46	1.23	5.23	2.13	22.46	3.29

For this set of initial conditions, the simulation results are

very close to those of the base case. The above computation involving the aromaticity and the ring size shows that the ring size cannot be varied independently of the aromaticity and that the direct measurements of the aromaticity by C^{13}NMR may be a useful tool in estimating the average ring size of a sample.

The Rate Parameters

Similar to the structural parameters, the various rate parameters tested are summarized in Table (VII-6) and actual computation results presented for the more sensitive ones. The effect of each parameter is described in Table (VII-7).

Table (VII-6) List of Rate Parameters Tested

Parameters	Reaction category	Base values	Perturbed values
E_2	ethylene bridge dissociation	49 Kcal/mole	48, 50 Kcal/mole
E_4, E_5	dissociation of side chains	62 Kcal/mole	61, 63 Kcal/mole
E_{36} up to E_{41}	hydrogen elimination	38 Kcal/mole	41 Kcal/mole
δ_{cage}	cage effect	0.1	0.01
s_1, s_2	gel effect	5 Kcal/mole	4 Kcal/mole

Table (VII-7) Sensitivity of Simulation Results on the Rate Parameters

Parameters \ effect	weight loss	tar/ gas	H/C	Olefin/ paraffin
E_2	large	moderate	small	large
E_4, E_5	moderate	large	small	large
E_{36} up to E_{41}	moderate	moderate	large	large
δ_{cage}	small	moderate	moderate	large
s_1, s_2	small	small	small	large

Figure (VII-30) shows how the rate of dissociation of the ethylene bridges (reaction #2) affects the overall weight loss. The large sensitivity is consistent with the previous observation that the amounts of the different bridges are the most sensitive of the structural parameters. The cage effect parametrized by δ_{cage}, however, have a less sensitive effect on the weight loss than E_2 (figure (VII-31)), the main reason being that it affects only those bridges that do not yield volatile fragments on breaking. Similar to the cage effect, the weight loss is relatively insensitive to the gel effect parametrized by s_1 and s_2 (figure (VII-32))*. The rate of dissociation of the side chains is more related with the generation of gases. Its largest effect is therefore on the tar/gas and olefin/paraffin ratios (figures (VII-33)

---

* The lower two curves in figure (VII-32) have a point of intersection at t=3.75 sec. The initial rates of weight loss are higher for $s_1=s_2=5$ Kcal/mole for both temperatures.

and (VII-34) and not on the weight loss (figure (VII-35)). The hydrogen elimination reactions are largely related to the formation of double bonds. The effects of their rates on the weight loss and H/C ratio are shown in figures (VII-36) and (VII-37). The weight loss curves for different rates of hydrogen elimination coincide for an initial period of time. Increasing the activation energy for this reaction slows down the formation of unbreakable bridges which explains the higher weight loss after some time. The effect of this reaction on the elemental composition, however, occurs right from the start of pyrolysis due to different rates of loss of hydrogen (figure (VII-37)).

The general results in Tables (VII-3) and (VII-7) show that the amounts of various bridges and their dissociation rates are the most crucial factors that determine the potential amount of volatile material that can be obtained. This presents a challenging problem in fundamental studies because there is yet no satisfactory methods that can measure the distribution of bridges. In parallel, from the standpoint of coal utilization, this suggests that one can very well enhance the reactivity of coal by some pretreatment processes that can reduce its overall number of bridges. Recommendation of some areas in which further investigation may prove most fruitful is discussed in the next chapter.

Case 2: A monarch seam channel subbituminous coal PSOC-241

This coal is provided by the Organic Sediments Laboratory of the Pennsylvania State University. The following data are available:

(1) Proximate Analysis (wt. %) Ultimate Analysis (wt. % dmmf*)

volatile matter	33.72%	C	73.91%
moisture	4.49%	H	5.36%
ash	5.76%	N	1.45%
fixed carbon	42.92%	O (by diff)	19.28%

* dmmf - dry and mineral matter free basis

This coal contains 8.01% mineral matter.

(2) Proton NMR of 500°C tar (30 sec. , vacuum, 60-80 mesh particles)

H_α = 20%

H_β = 60%

H_{ar} = 20%

(3) Density in hexane = 1.26 gm/cm^3

(4) Analysis of product gases (500°C, 30 sec. , vacuum, 60-80 mesh particles)

CO_2	= 49.5 mg/gm sample
CH_4	= 2.40 mg/gm sample
C_2H_4	= 0.88 mg/gm sample
C_2H_6	= 1.24 mg/gm sample
$C_3H_6 + C_3H_8$	= 2.05 mg/gm sample
H_2O	= 7.5 mg/gm sample

(5) Weight loss of 60-80 mesh particles at 500°C for 30 seconds in vacuum = 18.7%

Initial Conditions

To utilize equations (V-37), (V-39) and (V-41) for the initial conditions, the structural parameters H/C and ρ_{eff} of the carbon-hydrogen skeleton must be estimated from elemental analysis and density data. The amount of carbon dioxide generated indicates that carbon atoms in carboxylic acid groups account for 13.5 mg/gm sample. Assuming the carbonyl groups account for 1 wt. % of the sample, we have 4.3 mg carbon in carbonyl groups per gm sample. We base our calculations on 1 gm of dry sample, of which 8.01% is mineral matter. The amounts of hydrogen and carbon in the sample are respectively,

$$H = 5.36 \times (1 - 0.801) = 4.93 \text{ moles/gm sample}$$

$$C = \frac{(73.91 - 1.35 - 0.43) \times (1 - 0.801)}{12} = \frac{66.35}{12} \qquad \text{(VII-8)}$$

$$= 5.53 \text{ moles/gm sample}$$

The effective density can be estimated using equation (VII-1), assuming a porosity ε_M of 0.05 so that

$$\rho_{eff} = \frac{1.26 \times (66.35 + 4.93)}{(1 - 0.05)} \qquad \text{(VII-9)}$$

$$= 0.945 \text{ gm/cm}^3 = 945 \text{ gm/}\ell$$

Since the proportion of oxygen in this coal is very substantial, we are interested in how the phenolic groups may affect its pyrolysis behavior. Inasmuch as very little is known about the phenolic groups and their reactions in coal other than that several mg of water has been observed from the pyrolysis of about 200 mg of dry sample at 500°C, our incorporation of phenolic condensation should be viewed as a numerical

experiment to estimate the importance of the phenolic groups. The initial concentration of phenolic groups is taken to be 3 moles/ℓ for this simulation. Similar to the previous case, the generation of CO and CO_2 is treated as first order reactions having rate constants of 1 and 0.1 sec^{-1} respectively.

Repeating the computation indicated in figure (VII-2) for this coal, and letting the ratio $b_1:b_2:b_3$ be 1:1:2 in view of the relatively small value of $H_\alpha/H_\beta(0.33)$, we find the allowable values of f_a to lie between 0.430 and 0.490. The following set of initial conditions is chosen:

f_a = 0.470, ℓ = 2.5, $\frac{M}{N_c}$ = 1.5, ring size = 3

b_1 = 0.9212 moles/ℓ

b_2 = 0.9212 moles/ℓ

b_3 = 1.8424 moles/ℓ

c_1 = 9.7291 moles/ℓ

c_2 = 5.1860 moles/ℓ

H_α = 13.082 moles/ℓ

x = 1.1394

y = 1.4378

N_c = 2.4565 moles/ℓ

V_I = 0.15

V_{II} = 0.85

[OH] = 3 moles/ℓ

Before presenting the simulation results, it may be fruitful to compare the initial conditions adopted for the two coals studied (Table (VII-8)).

Amidst the many assumptions and uncertainties, the power of the structural parameters (a, b, z and ρ_{eff}) to specify the initial conditions is still apparent.

Table (VII-8) Comparison of Initial Conditions Adopted for the Two Coals Studied

	Hamilton (bituminous)	PSOC-241 (subbituminous)
f_a	0.635	0.470
b_1	1.2325 moles/ℓ	0.9212
b_2	2.4651 moles/ℓ	0.9212
b_3	1.2325 moles/ℓ	1.8424
c_1	5.2339 moles/ℓ	9.7291
c_2	2.1273 moles/ℓ	5.1860
H_α	22.459 moles/ℓ	13.082
x	1.7524	1.1394
y	1.3360	1.4378
N_c	3.2868 moles/ℓ	2.4565

First, the allowable range of values of the aromaticity f_a for the subbituminous coal is considerably lower indicating a more predominantly aliphatic structure. The values of x and y indicate that branching at an α carbon occurs more often in the subbituminous coal. If one defines the degree of substitution χ as

$$\chi = \frac{C_\alpha}{S} \qquad \text{(VII-10)}$$

then χ has values 0.39 and 0.47 for the bituminous and subbituminous coals respectively. These trends are in line with the general belief

that higher rank coals have structures closer to graphite.

Rate Parameters

The relatively small amounts of weight loss and of hydrocarbons generation suggest that the rates of some reactions may be smaller than those for the Hamilton coal studied in Case 1. The following adjustments have been made to match simulation results and measured data.

Table (VII-9) Comparison of Adjusted Rate Parameters for the Two Cases Studied

Reactions	Rates for Hamilton Coal		Adjusted Rates	
Bond Dissociation	$\log_{10}A$	E (Kcal/mole)	$\log_{10}A$	E (Kcal/Mole)
1. $b_1 \rightarrow \alpha\cdot + \Phi\cdot$	14.4	69	14.4	70
2. $b_2 \rightarrow \alpha\cdot + \alpha\cdot$	14.4	49	14.4	50
3. $b_3 \rightarrow \alpha\cdot + \beta_2^{\cdot}$	14.4	61	14.4	63
4. $c_1 \rightarrow \alpha\cdot + CH_3\cdot$	14.9	62	14.9	64
5. $c_2 \rightarrow \alpha\cdot + R\cdot$	14.9	62	14.9	64
Hydrogen Elimination				
36-41. All reactions	12.8	38	12.8	41

The Arrhenius factor for the condensation of phenolic groups (reaction #57) is assumed a value of $10^{14.5}$ sec^{-1}. To match the amount of water observed at 500°C, the activation energy for this reaction is adjusted to be 50 Kcal/mole.

Simulation Results and Discussion

We present the computation results for 500°C and 600°C for the weight loss and the generation of various gases (figures (VII-38) through (VII-43)). Again, experimental data points are indicated by X marks on the figures. The dependence of the kinetics on temperature is much more

marked for this coal than for the previous one studied, the main reason being a lower proportion of the most reactive ethylene bridges (cf Table (VII-8)). From Table (VII-8) we also notice large amounts of side chains in this coal which translate into the correspondingly higher evolution of various hydrocarbon gases at 600^{o}C. The higher proportion of side chains than bridges also means that the tar/gas ratio will be somewhat lower, a phenomenon which is observed both experimentally and from the simulation output (figure (VII-44)).

The effect of the phenolic condensation reaction on the weight loss is shown in figure (VII-45). Phenolic condensation creates a new type of bridges, and therefore should reduce the formation of volatile fragments. In our pyrolysis experiments, the quantity of water generated cannot be accurately measured because response is very insensitive and non-linear on the gas chromatograph. Nevertheless, a crude estimate of 7.5 mg/gm sample indicates that this extent of phenolic condensation does not drastically reduce the weight loss at 500^{o}C. The effect is more severe for 600^{o}C.

FIGURE (VII-38)

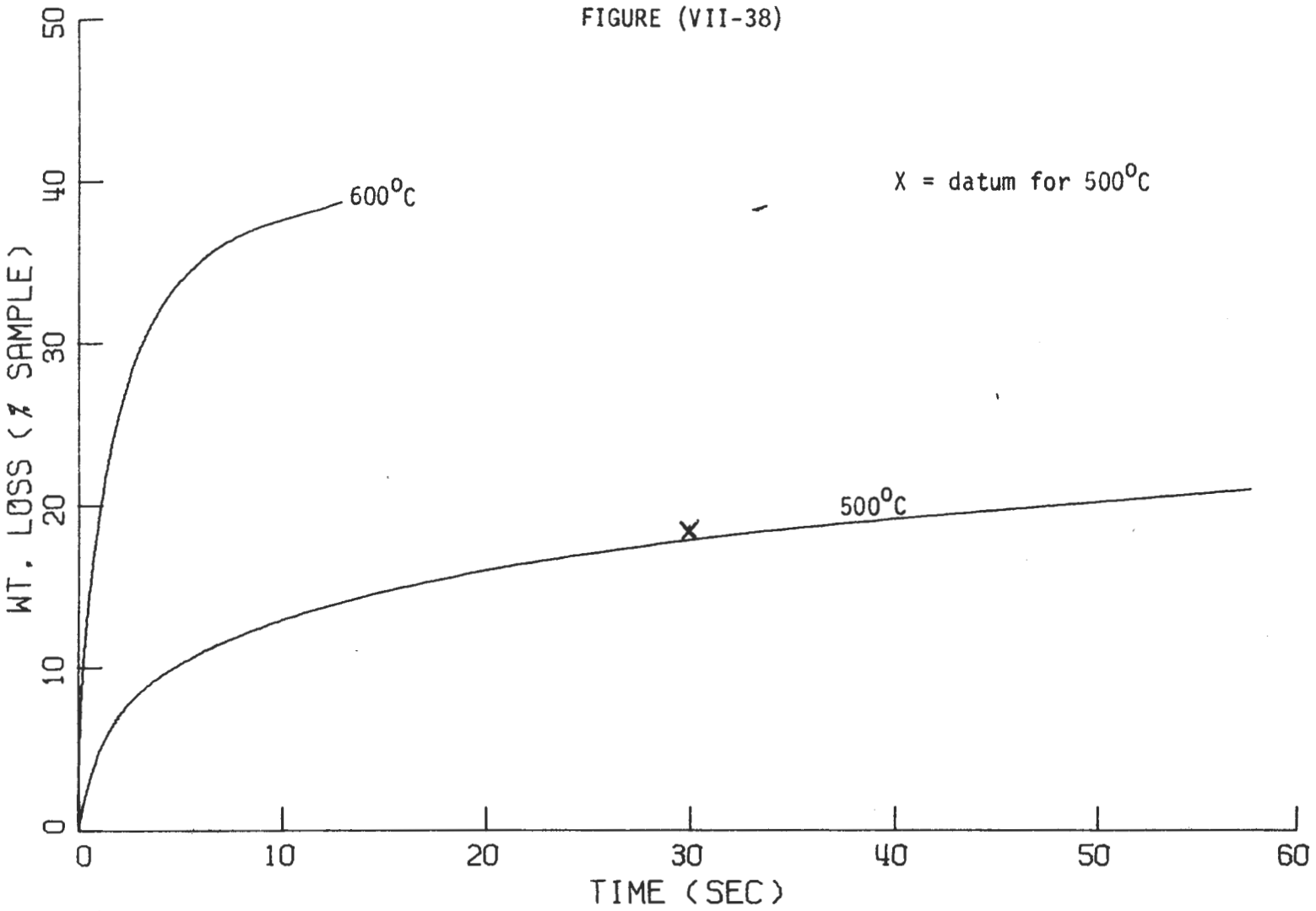

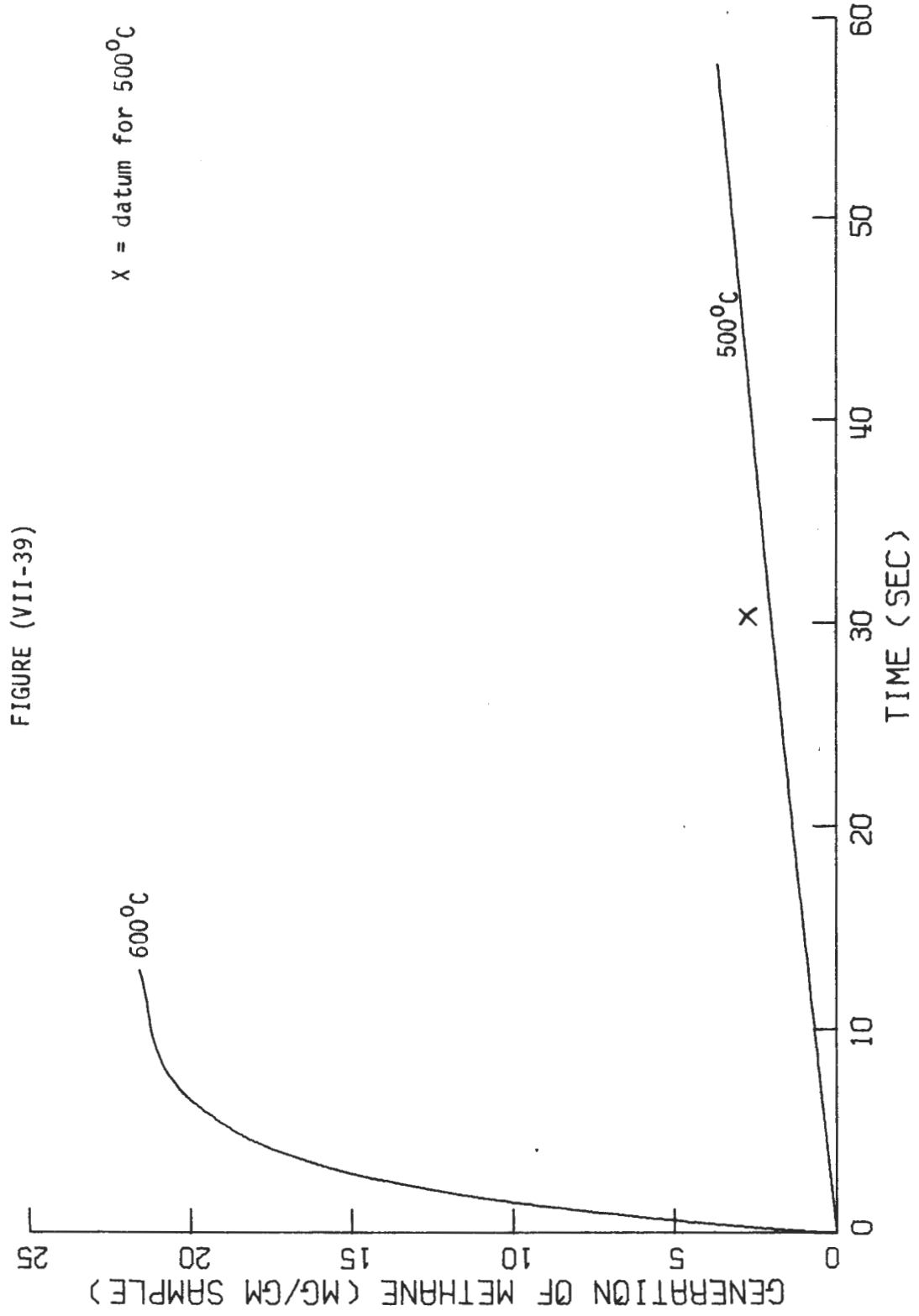

FIGURE (VII-39)

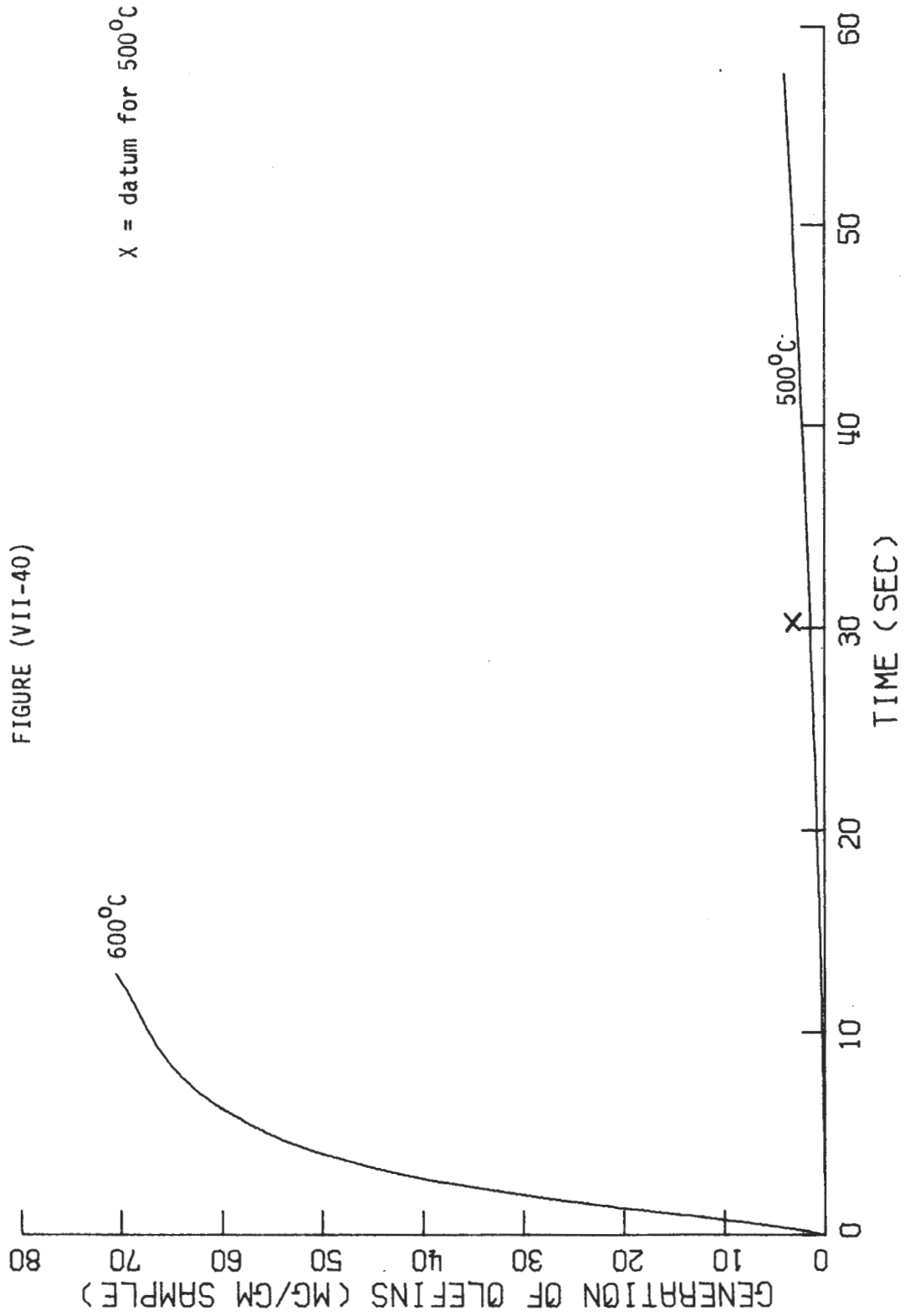

FIGURE (VII-40)

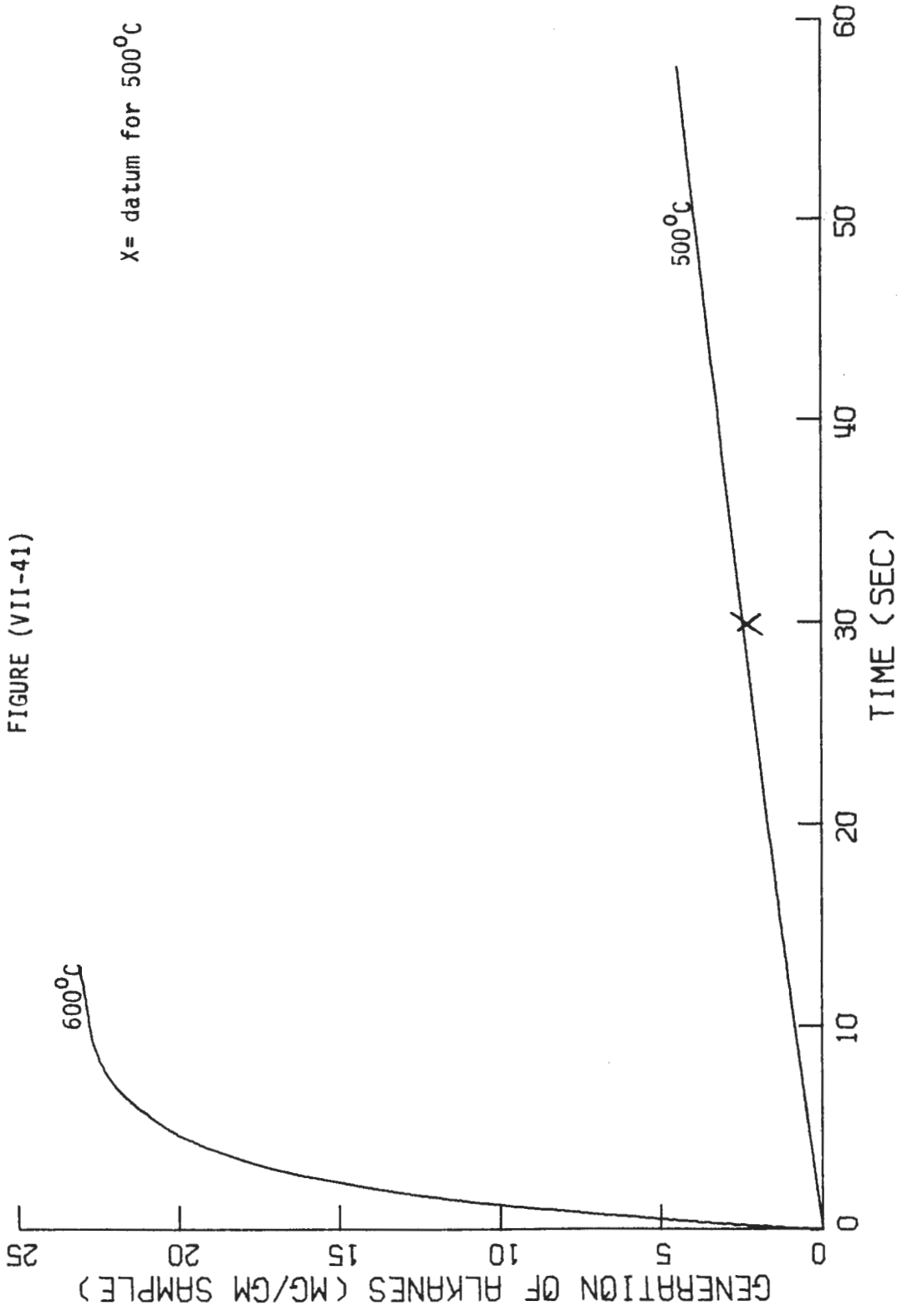

FIGURE (VII-41)

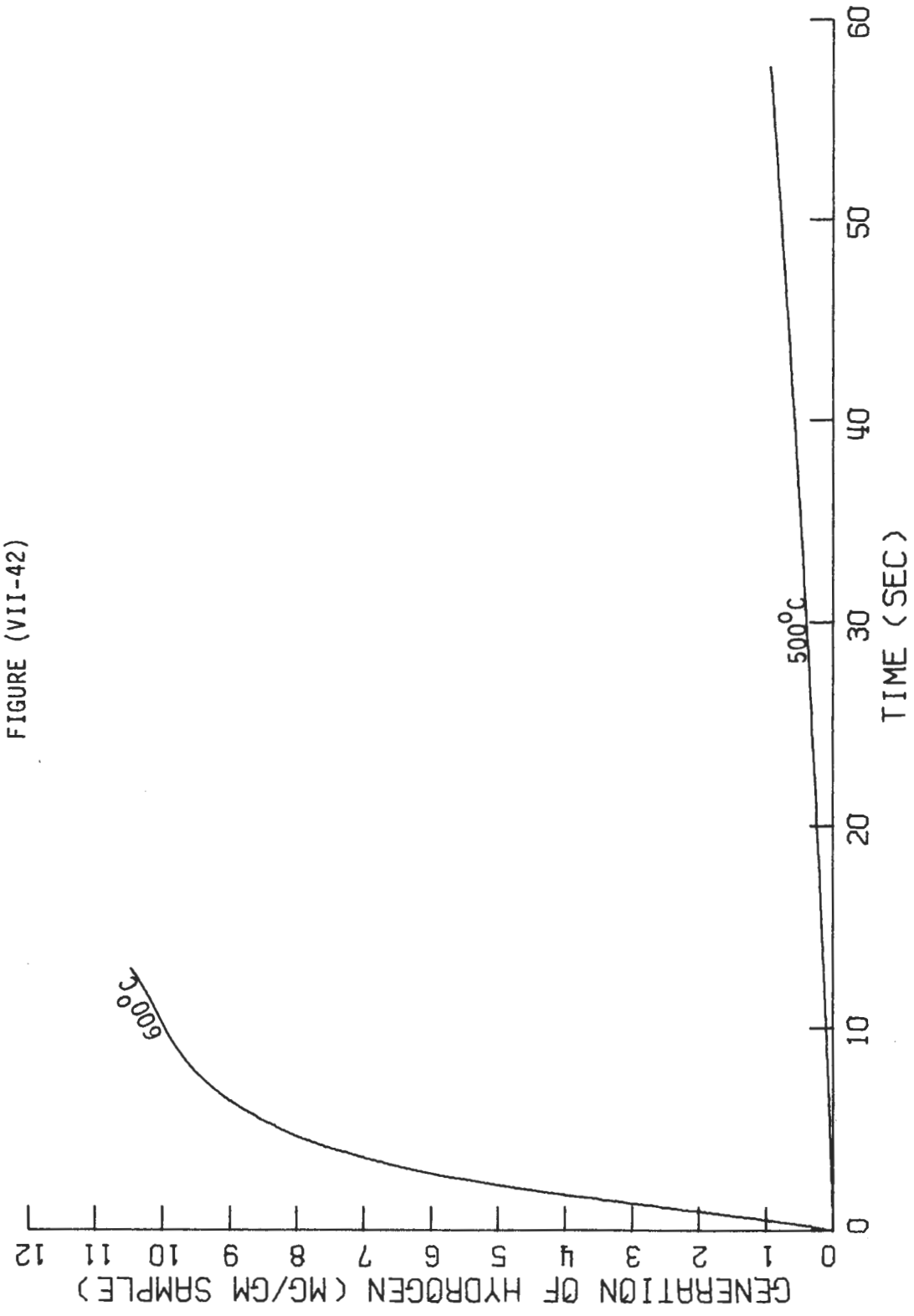

FIGURE (VII-42)

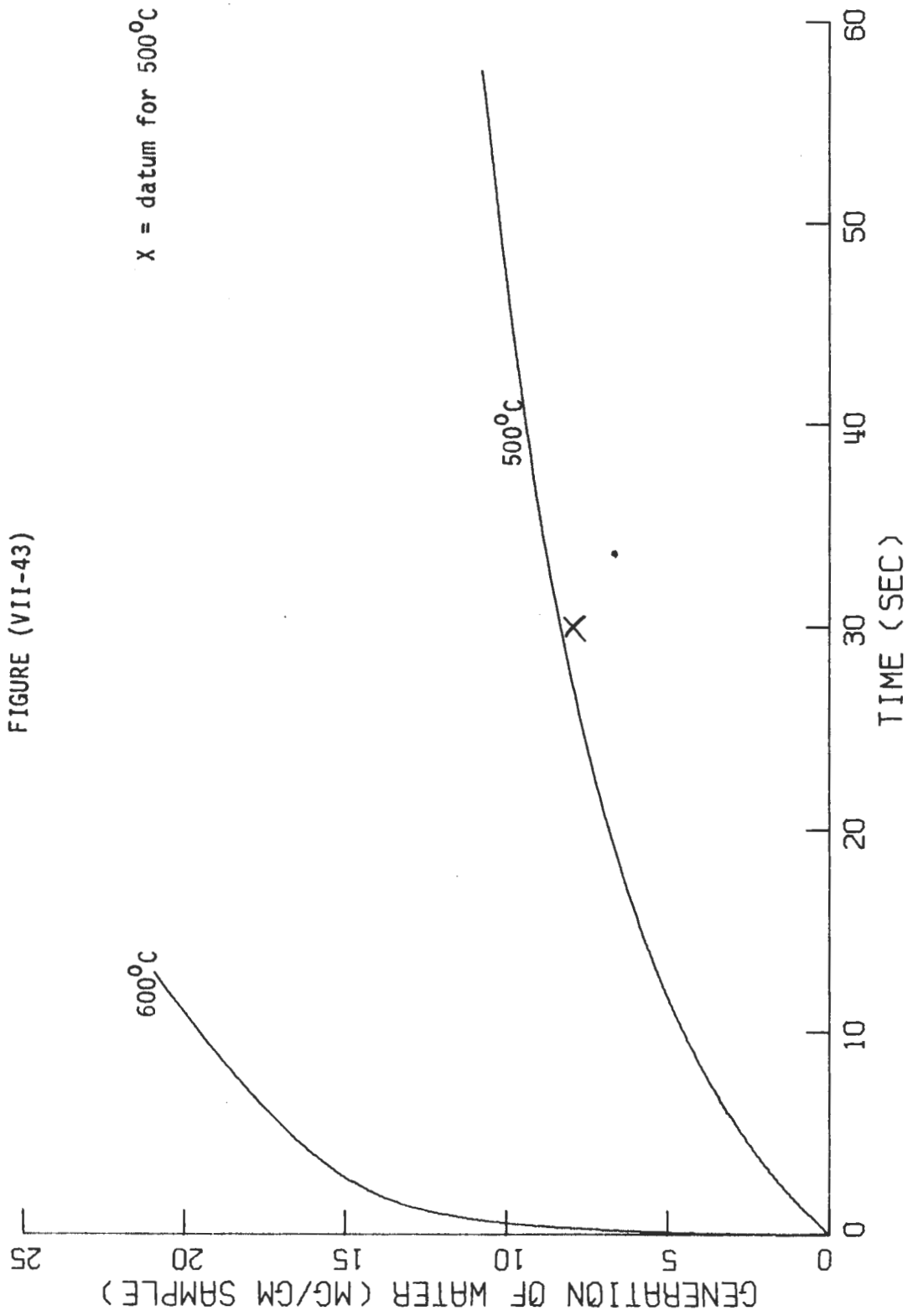

FIGURE (VII-43)

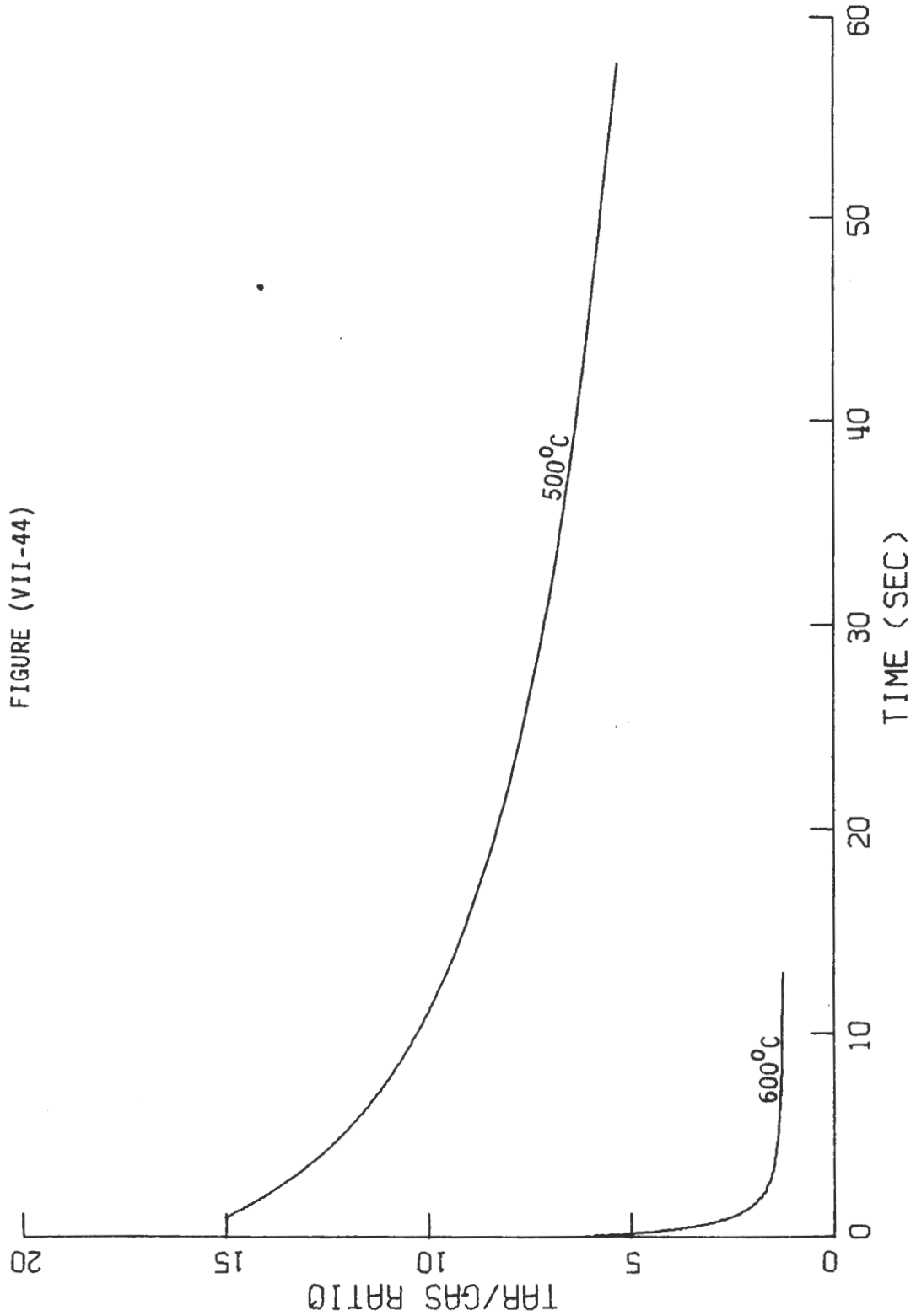

FIGURE (VII-44)

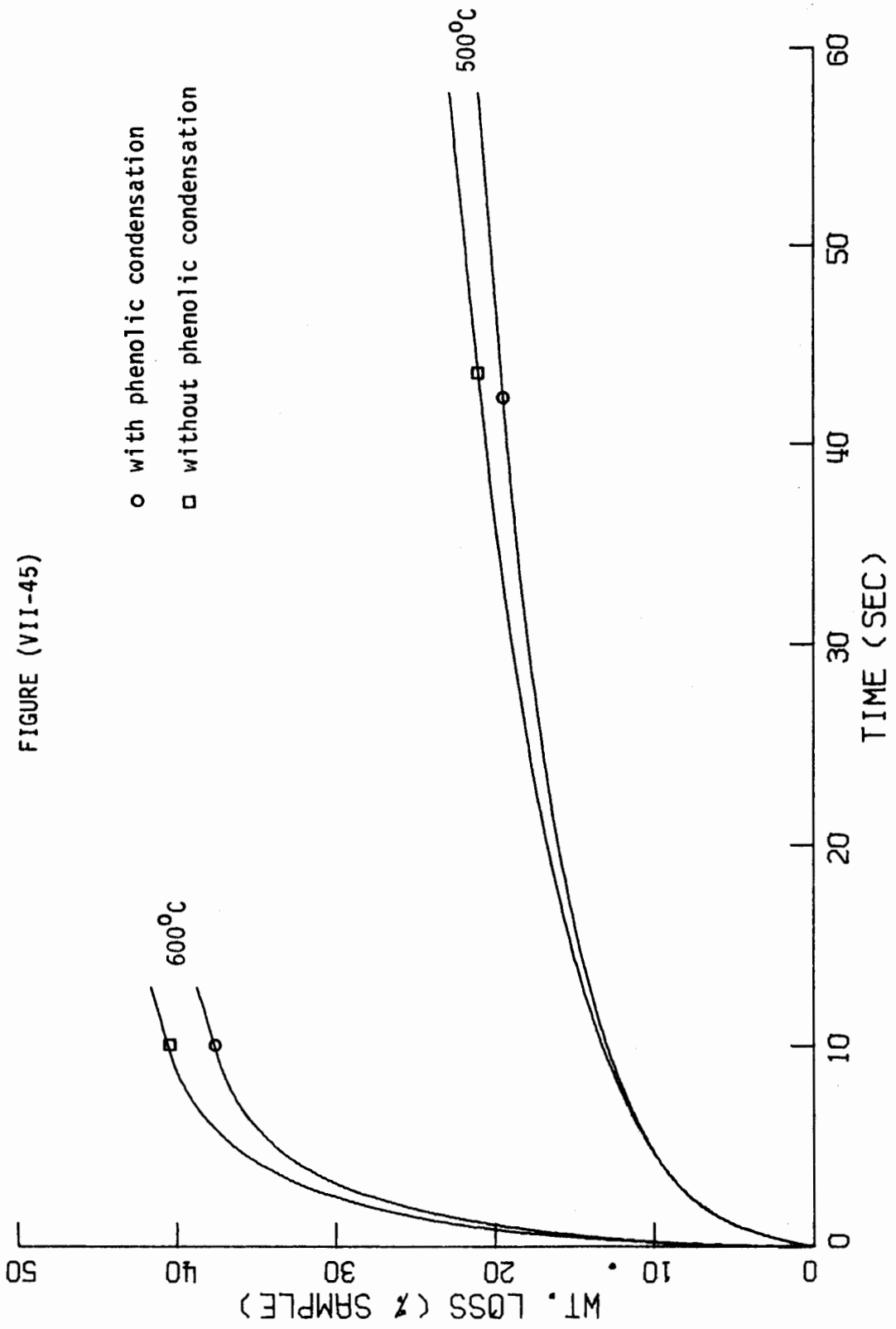

FIGURE (VII-45)

VIII. GENERAL CONCLUSIONS AND RECOMMENDATION FOR FURTHER WORK

General Conclusions

This research is a pioneering attempt to understand and describe the thermal behavior of coal on the most fundamental basis that is still practicable. Despite the substantial difficulty in the assignment of initial conditions and rate parameters, it is encouraging that our simulation results are predictive of the general patterns of pyrolysis behavior. The model itself embodies three vital elements as we show in the simple diagram in figure (VIII-1). Because of the detailed physicochemical processes that are incorporated, the level of sophistication of the model equations at this stage far exceeds that of the other elements. The value of the model as a quantitative, predictive tool, which constitutes the motivation of this work, depends much on the quality of new information that can be generated to improve our knowledge of both the structural and rate parameters. In this regard, a continuing experimental and theoretical research program is under way with the author's research group, and some plausible areas of investigation are discussed in the next section.

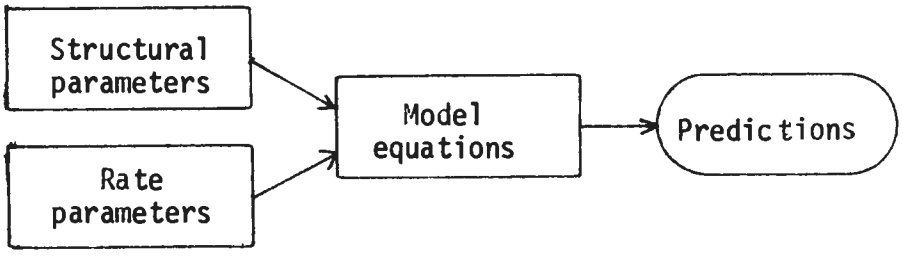

Figure (VIII-1) Simplified Diagram of the Three Elements of the Model

Recommendation for Future Work

Theoretical Areas

It appears at this point that improvement attempts that will further complicate the model equations may not be worthwhile until more experimental information is gathered and evaluated. Rather, systematic efforts to simplify the model and eliminate less sensitive parameters will be most interesting from the standpoint of using it as a predictive tool. The following strategy is suggested:

(1) Disregard those reactions that have little or no effects on the simulation results, and

(2) Check the simulation response of the various state variables for possible correlations and subsequent lumping.

Other areas of theoretical interest are best explored with a complementary experimental program and are discussed below.

Experimental Areas

In our previous case studies of pyrolysis simulation, the transport of volatile materials in the macropores has not been included in the computation. Although the mathematical formulation for incorporating macropore transport has been developed, evaluation of the key parameters for a particular coal awaits accurate weight loss kinetics data at various temperatures, pressures and particle sizes, and with different inert components. Such a scheme of measurements is suggested in Chapter VI and is considered an area of immediate interest. The effects of the external pressure and the particle size can then be implemented into the model.

So far the data available to us from pyrolysis experiments have been obtained for 500^{o}C with a heating time of 30 seconds or more. The following additional information will be helpful in better adjustment of the model parameters and in testing the model as a whole.

(1) The kinetics of tar evolution at shorter heating times and higher temperatures may be used to adjust the dissociation rate of the bridges.

(2) Similar measurements on the generation of alkanes and alkenes in the gases will give some indication of the dissociation rate of the chains.

(3) The elemental composition (H/C ratio) of the char, tar and gaseous components is an excellent tool of model testing.

(4) The evolution of hydrogen gas and water poses challenging experimental problems because of their poor response on the gas chromatograph. The amounts of hydrogen gas and water are related respectively to the extents of the hydrogen elimination and phenolic condensation. Both of these reactions tend to reduce the reactivity of the coal through the formation of unbreakable bridges. If the amounts are measured, the rate constants for these reactions may be adjusted accordingly.

(5) Information from C^{13}NMR will be valuable in the better assessment of structural parameters. Besides the aromaticity, C^{13}NMR has the potential to distinguish other forms of carbon atoms such as those in carbonyl groups.

(6) The thermal chemistry of the phenolic groups is evidently the least

understood among all the functional groups we consider in this work. Our speculation is that chemical water (not physical moisture) from pyrolysis invariably originates from the condensation of phenolic OH groups; and when this occurs, a certain bridge is formed between two clusters. The actual stoichiometry and rate have yet to be determined. Experimental pyrolysis studies with model phenolic compounds on this underexplored area of chemistry will be most beneficial in this regard.

APPENDIX I

TABULATION OF RATE CONSTANTS AND THEIR SOURCES

	Reaction	$\log_{10} A$ (in sec^{-1} or l/mole sec^{-1})	E Kcal/mole	E KJ/mole
	Dissociation			
1.	$b_1 \rightarrow \alpha\cdot + \Phi\cdot$	14.4	78.5	328
2.	$b_2 \rightarrow \alpha\cdot + \alpha\cdot$	14.4	56.8	237
3.	$b_3 \rightarrow \alpha\cdot + \beta_2\dot{}$	14.4	68.6	287
4.	$c_1 \rightarrow \alpha\cdot + CH_3\dot{}$	15.3	73.0	305
5.	$c_2 \rightarrow \alpha\cdot + R\cdot$	14.9	68.6	287
	Hydrogen abstraction			
6.	$b_3\dot{} + H_\alpha \rightarrow b_3 + \alpha\cdot$	8	15	62.7
7.	$CH_3\dot{} + H_\alpha \rightarrow CH_4 + \alpha\cdot$	8	10	41.8
8.	$R\cdot + H_\alpha \rightarrow RH + \alpha\cdot$	8	10	41.8
9.	$\Phi\cdot + H_\alpha \rightarrow \alpha\cdot$	8	10	41.8
10.	$H\cdot + H_\alpha \rightarrow H_2 + \alpha\cdot$	11	10	41.8
11.	$\beta_2\dot{} + H_\alpha \rightarrow c_2 + \alpha\cdot$	8	10	41.8
12.	$\beta_1\dot{} + H_\alpha \rightarrow c_1 + \alpha\cdot$	8	10	41.8
13.	$b_2\dot{} \rightarrow b_2 + \alpha\cdot$	8	15	62.7
14.	$CH_3\dot{} + c_1 \rightarrow CH_4 + \beta_1\dot{}$	8	10	41.8
15.	$H\cdot + c_1 \rightarrow H_2 + \beta_1\dot{}$	11	10	41.8
16.	$R\cdot + c_1 \rightarrow RH + \beta_1\dot{}$	8	10	41.8
17.	$\Phi\cdot + c_1 \rightarrow \beta_1\dot{}$	8	10	41.8
18.	$CH_3\dot{} + c_2 \rightarrow CH_4 + \beta_2\dot{}$	8	10	41.8

	Reaction	$\log_{10}$ A	E Kcal/mole	KJ/mole
19.	$H\cdot + c_2 \rightarrow H_2 + \beta_2\cdot$	11	10	41.8
20.	$R\cdot + c_2 \rightarrow RH + \beta_2\cdot$	8	10	41.8
21.	$\Phi\cdot + c_2 \rightarrow \beta_2\cdot$	8	10	41.8
22.	$CH_3\cdot + b_2 + H_\alpha \rightarrow CH_4 + b_2\cdot$	8	10	41.8
23.	$H\cdot + b_2 + H_\alpha \rightarrow H_2 + b_2\cdot$	11	10	41.8
24.	$R\cdot + b_2 + H_\alpha \rightarrow RH + b_2\cdot$	8	10	41.8
25.	$\Phi\cdot + b_2 + H_\alpha \rightarrow b_2\cdot$	8	10	41.8
26.	$\beta_1\cdot + b_2 + H_\alpha \rightarrow c_1 + b_2\cdot$	8	10	41.8
27.	$\beta_2\cdot + b_2 + H_\alpha \rightarrow c_2 + b_2\cdot$	8	10	41.8
28.	$b_3 + \alpha\cdot \rightarrow b_3\cdot + H_\alpha$	8	15	62.7
29.	$b_2 + \alpha\cdot \rightarrow b_2\cdot$	8	15	62.7
30.	$CH_3\cdot + H_\alpha + b_3 \rightarrow CH_4 + b_3\cdot$	8	10	41.8
31.	$H\cdot + H_\alpha + b_3 \rightarrow H_2 + b_3\cdot$	11	10	41.8
32.	$R\cdot + H_\alpha + b_3 \rightarrow RH + b_3\cdot$	8	10	41.8
33.	$\Phi\cdot + H_\alpha + b_3 \rightarrow b_3\cdot$	8	10	41.8
34.	$H_\alpha + \beta_1\cdot + b_3 \rightarrow c_1 + b_3\cdot$	8	10	41.8
35.	$H_\alpha + \beta_2\cdot + b_3 \rightarrow c_2 + b_3\cdot$	8	10	41.8
	Hydrogen elimination			
36.	$\beta_1\cdot + H_\alpha \rightarrow c_1{=} + H\cdot$	12.8	38	159
37.	$\beta_2\cdot + H_\alpha \rightarrow c_2{=} + H\cdot$	12.8	38	159
38.	$b_2\cdot + H_\alpha \rightarrow b_2{=} + H\cdot$	12.8	38	159
39.	$b_3\cdot \rightarrow b_3{=} + H\cdot$	12.8	38	159
40.	$\alpha\cdot + c_1 \rightarrow c_1{=} + H\cdot$	12.8	38	159
41.	$\alpha\cdot + c_2 \rightarrow c_2{=} + H\cdot$	12.8	38	159

	Reaction	$\log_{10}$ A	E Kcal/mole	KJ/mole
	β scission			
42.	$b_3^{\cdot} \rightarrow c_2= + \alpha\cdot$	14.0	50	209
43.	$\beta_2^{\cdot} \rightarrow \alpha\cdot + R=$	12.8	28	117
	Addition			
44.	$3H_\alpha + H\cdot \rightarrow CH_3^{\cdot}$	11	10	41.8
45.	$CH_3^{\cdot} + c_2= \rightarrow \alpha\cdot + c_2$	7	7	29.3
46.	$R\cdot + c_2= \rightarrow \alpha\cdot + c_2$	7	7	29.3
47.	$H\cdot + c_2= \rightarrow \alpha\cdot + c_2$	10	2	8.4
48.	$H\cdot + c_1= \rightarrow \alpha\cdot + c_1$	10	2	8.4
49.	$CH_3^{\cdot} + c_1= \rightarrow \alpha\cdot + c_2$	7	7	29.3
50.	$R\cdot + c_1= \rightarrow \alpha\cdot + c_2$	7	7	29.3
	Recombination			
51.	$\alpha\cdot + \alpha\cdot \rightarrow b_2$	8.0	0	0
52.	$\alpha\cdot + \beta_2^{\cdot} \rightarrow b_3$	8.5	0	0
53.	$\alpha\cdot + \beta_1^{\cdot} \rightarrow b_3$	8.5	0	0
54.	$\alpha\cdot + CH_3^{\cdot} \rightarrow c_1$	8.5	0	0
55.	$\alpha\cdot + R\cdot \rightarrow c_2$	8.5	0	0
56.	$\alpha\cdot + H\cdot \rightarrow H_\alpha$	11.0	0	0

With the exception of the addition reactions, all the rate parameters are obtained from data compiled by Benson and coworker [specifically (Benson, 1968) and (O'Neal, 1973)] for functional groups attached to a benzene ring. Thus, the rate assigned for reaction 2 represents actually the dissociation rate of bibenzyl, which is estimated from thermochemical kinetics. The inherent crudeness of some of these data, plus the fact the aromatic clusters in coal are not monosubstituted benzene rings would call for certain adjustments of these rate constants when simulation results are compared with experimental findings. However, such adjustments as may be required should not alter the order of magnitude of these parameters, or reflect any drastic change in the better known physical quantities such as bond energies. Specific comments for individual reactions follow:

Initiation:

1. O'Neal tabulated $\log_{10}A$ for reaction 2 as 14.4. The frequency factors for the dissociation of other bridges are assumed to be the same. The bond energy of the phenyl-benzyl linkage is 78.5 Kcal/mole and is equal to the activation energy.
2. Given in (O'Neal, 1973).
3. Frequency factor assumed same as 2. Bond energy assumed the same as c_2 in reaction 5.
4. Given in (O'Neal, 1973).
5. Given in (O'Neal, 1973).

Hydrogen Abstraction

6-35. The abstraction of hydrogen by a hydrogen atom has frequency factor of the order of $10^{11\pm0.5}$ l/mole-sec. For radical-molecule metathesis

reactions, the A factor lies between $10^{8.5+0.5}$ l/mole-sec. A value of $10^{8.0}$ is used for hydrogen abstraction by all radicals other than hydrogen atoms. For most reactive radicals, the activation energy of hydrogen abstraction has an order of 10 Kcal/mole. (See (Benson, 1968).) We assume that α radicals such as $\alpha\cdot$, $b_2^{\cdot}$, and $b_3^{\cdot}$ are stabilized, less reactive radicals which can only abstract α hydrogens with a correspondingly higher activation energy of 15 Kcal/mole.

Hydrogen elimination

36-41. These are in fact the same type of reaction and therefore have similar rates. Benson estimates the rate for

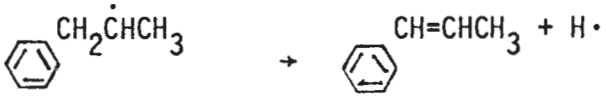

to be

$$10^{12.8}\, e^{-\frac{38}{RT}}\ \text{sec}^{-1}$$

42. The rate parameters are taken the same as that for

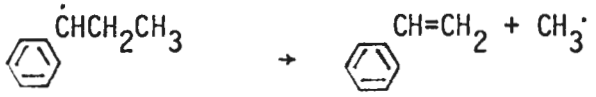

which Benson estimates to be

$$10^{14}\, e^{-\frac{50}{RT}}\ \text{sec}^{-1}$$

43. The Arrhenius factor is taken to be the same as reaction 36. The activation energy is derived from values of β-scission reactions of alkyl radicals, which has a typical value of 28 Kcal/mole. (Allara, 1973.)

Addition

44-50. The addition of alkyl radicals to an olefinic double bond has a frequency factor of about 10^7 l/mole-sec and an activation energy of around 7 Kcal/mole. This addition reaction is expected to be much less predominant than hydrogen abstraction because of a lower rate constant and a comparatively higher availability of hydrogen than double bonds. For the addition of hydrogen atoms, the frequency factor is of order 10^{10} l/mole-sec and activation energy 2 Kcal/mole. The addition or displacement reaction $\Phi CH_3 + H\cdot \rightarrow \Phi H + CH_3\cdot$ is assumed to have the same rate as hydrogen abstraction. In the pyrolysis of toluene at 680°C a constant ratio of 60% to 40% hydrogen and methane has been observed (Szwarc, 1948) which is not altered by an increase in temperature. The formation of methane in this reaction is primarily due to the displacement of the methyl groups by hydrogen atoms. The phenyl-methyl bond which has a bond energy of 103 Kcal/mole is believed to be stable at this temperature. This ratio of hydrogen to methane indicates comparable rate constants for the displacement and hydrogen abstraction reactions.

The concentration of methyl group can be obtained as the concentration of carbons multiplied by the probability that all its three substituents are hydrogen. We denote that concentration by

$$N_{CH_3} = C_\alpha f_3^3 = C_\alpha \left(\frac{H_\alpha}{3C_\alpha}\right)^3$$

Recombination

51-56. The corresponding dissociation rates of these recombination

reactions have been estimated from thermodynamics assuming that these reactions have activation energy zero and that they have the frequency factors indicated. (O'Neal, 1973). These sets of dissociation-recombination rate constants are therefore thermodynamically consistent.

APPENDIX II

COMPILING THE WORKING EQUATIONS FOR THE STATE VARIABLES

List of Variables in the equations

1. V_{II}
2. n_{CH_4}
3. n_{RH}
4. $n_{R=}$
5. n_{H_2}
6. $b_{1,I}$
7. $b_{2,I}$
8. $b_{3,I}$
9. $b_{2}^{\cdot},I$
10. $b_{3}^{\cdot},I$
11. $b_{2}^{=},I$
12. $b_{3}^{=},I$
13. $c_{1,I}$
14. $c_{2,I}$
15. $\beta_{1}^{\cdot},I$
16. $\beta_{2}^{\cdot},I$
17. $c_{1}^{=},I$
18. $c_{2}^{=},I$
19. $\alpha_{I}^{\cdot}$
20. $H_{\alpha,I}$
21. $\Phi_{I}^{\cdot}$
22. $CH_{3}^{\cdot}I$
23. $R^{\cdot}I$
24. $H_{I}^{\cdot}$
25. $b_{1,II}$
26. $b_{2,II}$
27. $b_{3,II}$
28. $b_{2}^{\cdot},II$
29. $b_{3}^{\cdot},II$
30. $b_{2}^{=},II$
31. $b_{3}^{=},II$
32. $c_{1,II}$
33. $c_{2,II}$
34. $\beta_{1}^{\cdot},II$
35. $\beta_{2}^{\cdot},II$
36. $c_{1}^{=},II$
37. $c_{2}^{=},II$
38. $\alpha_{II}^{\cdot}$
39. $H_{\alpha,II}$
40. $\Phi_{II}^{\cdot}$
41. $CH_{3}^{\cdot}II$
42. $R^{\cdot}II$
43. $H^{\cdot}II$
44. n_{H_2O}
45. OH_{I}
46. $b_{0,I}$
47. OH_{II}
48. $b_{0,II}$

List of the Differential Equations

$$\frac{dV_{II}}{dt} = - \mu r_b (P_1 + 2P_2) \frac{V_I}{V_{II}}$$

For the gases, i = 2 through 5

$$\frac{dn_i}{dt} = \sum_j \nu_{ij} r_{jI} V_I + \sum_j \nu_{ij} r_{jII} V_{II}$$

For the bridges in region I, i = 6 through 12

$$\frac{dc_i}{dt} = \sum_j \nu_{ij} r_j - \mu r_b P_2 (2 - \xi) \frac{c_i}{M} + \mu r_b (P_1 + 2P_2) \frac{c_{i+19}}{N_c}$$

For the functional groups in region I attached to aromatic clusters, i = 13 through 21

$$\frac{dc_i}{dt} = \sum_j \nu_{ij} r_j - \mu r_b c_i \left[\frac{P_1 (h_{aru} - 1)}{h_{aru} N_c - 2M} + \frac{P_2 (2h_{aru} - 3 + \xi)}{h_{aru} N_c - 2M} \right] + \mu r_b (P_1 + 2P_2) \frac{c_{i+19}}{N_c}$$

For the small alkyl radicals in region I, i = 22 through 24

$$\frac{dc_i}{dt} = \sum_j \nu_{ij} r_j$$

For all the species in region II, except small radicals, i = 25 through 40

$$\frac{dc_i}{dt} = \sum_j \nu_{ij} r_j$$

For the small radicals in region II, i = 41 through 43

$$\frac{dc_i}{dt} = \sum_j \nu_{ij} r_j + \frac{V_I c_i}{V_{II} N_c} \mu r_b (P_1 + 2P_2)$$

where

$$M = b_{1I} + b_{2I} + b_{3I} + b_{2I}' + b_{3I}' + b_{2I}'' + b_{3I}'' = \sum_{i=6}^{12} c_i$$

(where the reaction of phenolic groups creating a biphenyl bridge is considered, the concentration of bridges b_{0I} must be added to the value of M.)

$$\mu = \frac{M - 2\bar{\eta}}{M} \quad ; \quad \xi = \frac{M\mu}{M - \bar{\eta}}$$

$$\bar{\eta} = \frac{15M + \frac{3N_c}{2} \left[\left(\frac{3N_c}{2}\right)^2 + 45MN_c - 15M^2\right]^{\frac{1}{2}}}{30}$$

$$P_1 = \frac{2(1 - p)^2}{1 - (1 - p)^3 - 3p(1 - p)^4}$$

$$P_2 = \frac{4p(1 - p)^3}{1 - [(1 - p)^5 + 5p(1 - p)^4]}$$

$$p = \frac{M - \bar{n}}{\left(\frac{3N_c}{2}\right)}$$

The fixed parameters in these equations are:

h_{aru} = number of peripheral sites per cluster.

N_c = concentration of clusters, and

V_I = the volume of region I based on unit original volume of bulk phase.

The stoichiometric coefficients ν_{ij} and the rates r_j are those listed in Table IV - 1.

For coals with high oxygen contents the inclusion of phenolic group dehydration is necessary.

The additional differential equations are

44. $$\frac{dn_{H_2O}}{dt} = \nu_{H_2O,57} r_{57,I} V_I + \nu_{H_2O,57} r_{57,II} V_{II}$$

45. $$\frac{d[OH_I]}{dt} = \nu_{OH,57} r_{57,I} - \mu r_b [OH_I] \left[\frac{\bar{P}_1 (h_{aru} - 1)}{h_{aru} N_c - 2M} + \frac{P_2 (2h_{aru} - 5 + 2\xi)}{h_{aru} N_c - 2M} \right] +$$

$$\mu r_b (P_1 + P_2) \frac{[OH_{II}]}{N_c}$$

46. $$\frac{db_{0I}}{dt} = \nu_{b_0,57} r_{53,I} - \mu r_b P_2 (2 - \xi) \frac{b_{0I}}{M} + \mu r_b (P_1 + 2P_2) \frac{b_{0II}}{N_c}$$

47. $$\frac{d[OH_I]}{dt} = \nu_{OH,57} r_{57,II}$$

48. $$\frac{db_{0II}}{dt} = \nu_{b_0,57} r_{57,II}$$

The stoichiometry and rates of reaction 57 are described by equation (V- 24) in Chapter V.

REFERENCES

Allara, D. L., "A Compilation of Kinetic Parameters for the Thermal Degradation of n-alkane Molecules," Bell Laboratories Report, (1973)

Anthony, D. B. and Howard, J. R., "Coal Devolatilization and Hydrogasification," A review prepared for AIChE Journal, (December, 1975)

Anthony, D. B., Howard, J. B., Hottel, H. C., and Meisnner, H. P., "Rapid Devolatilization of Pulverized Coal," submitted for presentation at the 15th international symposium on Combustion, Tokyo, Japan, (1974)

Benson, S. W., "Thermochemical Kinetics," Wiley,(1968)

Brown, J. K., J. Chem. Soc. (London), 1955, p. 744

Chakrabartty, S. K. and Berkowitz, H., Fuel, 51, 44 (1972)

Chermin, H. A. G. and Van Krevelen, D. W., Fuel, 36, 85 (1957)

Dryden, I. G. C., "Chemistry of Coal Utilization," supplementary volume, Wiley, pp.232-295, (1963)

Feng, C. and Stewart, W. E., I. & E. C. Fundamentals, 12, 143 (1973)

Fitzer, E., Mueller, K., Schaefer, W., "Chemistry and Physics of Carbon," Vol. 7, p. 237, (1971)

Gan, H., Nandi, S. P. and Walker, P. L., Jr., Fuel, 51, 272 (1972)

Gear, C. W., "Numerical Initial Value Problems in Ordinary Differential Equations," Prentice Hall, (1971)

Hirsch, P. B., Proc. Conf: "Science in the Use of Coal," Inst. Fuel, London, p. A-29, (1958)

McCartney, J. T., O'Donnell, H. J. and Ergun, S., "Advances in Chemistry," Academic Press, Vol. 55, p. 261, (1966)

Nandi, S. P. and Walker, P. L., Jr., Fuel, 49, 309 (1970)

Nandi, S. P., Ramadass, V. and Walker, P. L., Jr., Carbon, 2, 199 (1964)

O'Neal, H. E. and Benson, S. W., "Free Radicals," Vol. 2, Wiley, pp. 275-359, (1973)

Szwarc, M., J. Chem. Phys., 16, 128 (1948)

Walker, P. L., Jr., Austin, L. G. and Nandi, S. P., "Chemistry and Physics of Carbon," Vol. 2, Marcel Dekker, p. 239, (1966)